Science and Technology Facilities Council

Technical Report
STFC-TR-2023-003

In-situ calorimetry sample can testing for performance and development

R Rushworth

September 2023

Enquiries concerning this report should be addressed to:

RAL Library
STFC Rutherford Appleton Laboratory
Harwell Oxford
Didcot
OX11 0QX

Tel: +44(0)1235 445577
email: library@stfc.ac.uk

Science and Technology Facilities Council reports are available online at:
https://epubs.stfc.ac.uk

Accessibility: a Microsoft Word version of this document (for use with assistive technology) may be available on request.

DOI: 10.5286/stfctr.2023003

ISSN 2753-5797

In-Situ Calorimetry Sample Can Testing for Performance and Development

University of Hull Industrial Placement Student

Rachel Rushworth

Supervisor

Dr. Mona Sarter

1st August 2022 – 28th July 2023

Science and Technology Facilities Council

ISIS Neutron and Muon Source

Contents

Abstract

Following on from previous developments and reviews, this report evaluates the performance of the in-situ calorimeter sample cans for both liquid and solid powder samples. The in-situ calorimeter stick has been designed for use on IRIS at the ISIS Neutron and Muon Source. The techniques used through both instruments are described within this report. The in-situ calorimeter was used in conjunction with a commercially available calorimeter, called the Mettler Toledo DSC1, and comparisons between the results obtained from both calorimeters are discussed. Before the characterisation tests could begin on the in-situ calorimeter, problem shooting was required to regain function of the setup. Once the issue was located and fixed, tests were completed to characterise the cans and to find the optimal experimental conditions for the current setup. Various tests, using different samples along with some trouble shooting and modifications to the existing method, were needed to observe transitions with the solid cans. The liquid cans were tested to benchmark the performance of the in-situ calorimeter with several samples and to provide a comparison to the solid sample cans. Through various sample tests, key features were highlighted as areas for future review and further development. These features are discussed throughout the testing of both the solid and liquid sample cans.

Abbreviations

CCR	Closed Cycle Refrigerator
DSC	Differential Scanning Calorimetry
GUI	General User Interface
INS	Inelastic Neutron Spectroscopy
IVC	Inner Vacuum Chamber
MD	Molecular Dynamics
QENS	Quasi-Elastic Neutron Spectroscopy
R	Reference
S	Sample
T	Top
B	Bottom
TOF	Time-Of-Flight

1. Aims of the Project

A sample stick for in-situ calorimetry scans during neutron experiments was designed, produced and has been undergoing testing for use on the IRIS instrument. The aim for the sample stick is to complete Differential Scanning Calorimetry (DSC) measurements in-situ with Quasi Elastic Neutron Spectroscopy (QENS) scans on IRIS. This would allow for temperature adjustments to be made during QENS scans based on the results of the DSC. The results from both measurements are, also, complementary as the temperature dependant phase changes and transitions seen through DSC are accompanied by changes in molecular dynamics, which are studied by QENS. Therefore, using both measurements give a more complete understanding of the sample material.

Previous evaluation by S. Postorino, focused on developing cans for liquid samples and improving the environment used during experiments. Through testing various types of linkers, Postorino found that the G-10 linkers gave the least thermal conduction between the cans and recognised the temperature gradient down the sample stick. The effect of the can environment on the measurements was, also, emphasised through testing separately under vacuum and with helium. Postorino's findings resulted in the installation of additional heaters and sensors on the cans so that each can has two heaters and sensors. It was also found that He aided in cooling the setup.[1]

The project was continued by J. Ponsonby as the new liquid cans required testing and the operation of the in-situ calorimeter was reviewed. Ponsonby found that the PID settings, which aid in controlling the temperature of the setup, were not optimal for the measurements made and that not only was the heating power on the cans limited but that the CCR had deficient heating and cooling ability. Due to this, the PID controls were adjusted, and an additional heater was added to the CCR. This allowed for the CCR to maintain constant heating rates as high as 10 K/min. During system characterisation, Ponsonby introduced the 'reference on bottom' arrangement, shown in Figure 6, and found this to be most effective when paired with a He environment. Through reviewing the liquid cans, scripts for both running the calorimeter and producing graphs of the results, including the heater current subtractions, were developed. Ponsonby, also, tested the cans in-situ with QENS scans to produce successful results showing that the liquid cans were functional.[2]

After the success of the liquid cans, cans were developed to test solid powder samples. Two types of cans were produced, shown in Figure 1, and these were initially tested by C. Twigg. The characterisation of the empty cans showed issues with the heater outputs on both types of cans and a temperature gradient across the sample stick continued to be present. Sample testing saw no solid-state transitions. However, using the hot setup, solid-liquid transitions were observed and highlighted the need to retune the PID settings. Due to COVID-19, Twigg's experimental work was restricted, and no in-beam experiments were carried out. Instead, Twigg developed a user-friendly GUI to run the in-situ calorimeter.[3]

The current aims for the project were to finalise the testing of the solid cans and to benchmark the liquid cans. Despite beamtime being granted for use on IRIS after writing a successful proposal, moderator development on the beamline saw the testing of the cans restricted to the ex-situ setup only. Due to previous anomalies found by Twigg, the solid cans were initially tested empty before sample testing. During empty can testing, issues with the setup arose and required problem shooting. Once the calorimeter setup was functional, solid samples were examined with aims to observe solid transitions, specifically glass transitions. Various solid and liquid samples were used to evaluate the functionality of the solid cans and to test the sensitivity of the liquid cans.

2. Introduction to the Facility

ISIS Neutron and Muon Source is a facility owned by the Science and Technology Facility Council (STFC) at the Rutherford Appleton Laboratory (RAL) located in Oxfordshire. At the ISIS Neutron and Muon Source, beams of neutrons and muons are produced and directed to the two Target Stations (TS1 and TS2) where the various instruments are housed. Using the beamline instruments, scientists can carry out their research in the physical and life sciences with various non-destructive techniques to study materials at the atomic level.[4]

3. Introduction to the Techniques

Differential Scanning Calorimetry (DSC)

Differential Scanning Calorimetry (DSC) is an analytical technique used to quantify enthalpy changes and analyse phase transitions, such as the glass transition, T_g, in liquid and solid samples. The principle behind the calorimeter is that the difference in heat required to equally raise the temperature of a sample (S) and reference (R) can be used to measure the changes in enthalpy of the sample. [2] This measurement is achieved through the comparison of the energy required to keep the sample and reference at the same temperature.

Therefore, this technique requires two identical containers called cans or cells, which are heated at a constant rate so that both cans are simultaneously at the same temperature. One cell contains the sample, and the other is left empty so that it can be used as a reference. These cells are mounted separately so that the cells can be heated independently with no heat flow between the sample and reference. [3]

A commercial DSC instrument was used for comparison to aid in the benchmarking of the in-situ DSC stick. The instrument chosen was the DSC1 and is commercially available through Mettler Toledo. The DSC1 is a thermal analysis instrument with an operating range from -150 to 700 °C. The ability to reach colder temperatures made the DSC1 a good choice of instrument to compare to the in-situ setup, which uses a cryostat for cooling. For the DSC1, to reach such low temperatures, liquid nitrogen is used. The DSC1 is fully automated and

uses a 34-position auto sampler to allow for multiple tests to be queued and ran. The sample and reference environment is internal and purged with argon gas.[5]

Quasi Elastic Neutron Spectroscopy (QENS)

The Quasi Elastic Neutron Spectroscopy (QENS) instrument that the in-situ DSC stick is designed for is called IRIS. IRIS is a time-of-flight (TOF) high resolution quasi-elastic and inelastic neutron scattering spectrometer, which can be found in TS1 at the ISIS Neutron and Muon Source. QENS is a special case of Inelastic Neutron Scattering (INS), which provides insight into the molecular dynamics (MD) of materials by measuring the change in energy of a neutron as it scatters from the sample. The energies of the scattered neutrons are analysed through Bragg reflections of crystal analysers to give information on the vibrational motions within the molecular structure of a sample. Such information is complimentary to that given by DSC as the changes in enthalpy caused by chemical and physical alterations are accompanied by variations in MD. Thus, allowing for a more complete understanding of a material's characteristics at varying temperatures.[2, 6]

In-situ DSC

An in-situ sample stick was developed for use on IRIS in order to perform QENS and DSC analysis simultaneously. [6, 7] The stick allows for accurate phase transition temperatures in samples to be determined in-situ. By taking both measurements simultaneously, the sample and environment used for DSC and QENS experiments are identical, and the temperatures chosen for the QENS scan can be adjusted depending on the findings during the DSC run. [2] Therefore, sample differences caused by performing multiple tests ex-situ are eliminated resulting in more accurate results. Also, the large sample volume required for QENS experiments results in the reduced effects of small contaminants within the sample on the DSC scans.

The solid sample cells have two different designs: annular and tapered. Both types of can include metal cores, two heaters and two sensors. The sensors and heaters are connected to the top and bottom of the can. The heaters are attached on the outside of the can and the sensors are placed inside slots in the metal cores within the can. The metal cores have been designed so that, when a sample-filled aluminium foil sachet is wrapped around the core and placed inside the can, the sachet would have good contact with the can.

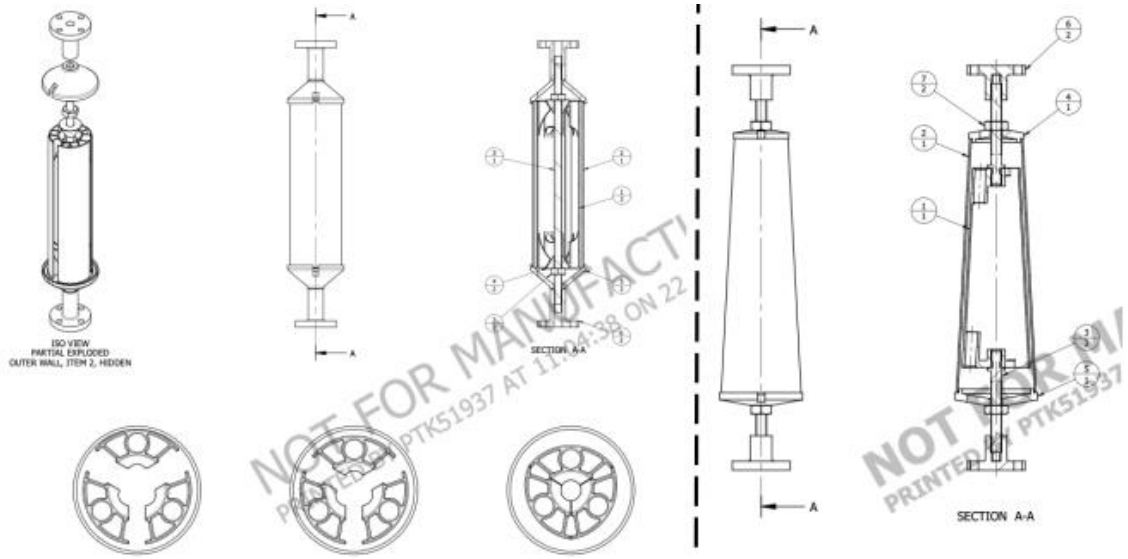

Figure 1: Can designs for the annular can with three points of view (left) and tapered can with two points of view (right). On the bottom left, the annular can cores can be seen in three stages of expansion and the gap between the cores and can wall is where the sample within a sachet is held. [3]

The liquid cans were designed to have a 2 ml sample space, two sensors and heaters, which are taped to the outside of the can at both ends. The slots, for the sensors to be placed into, are on the outside of the cans closer to the ends of the can than the heaters. The placement of these slots differs between the two types of liquid cans: either on the same face of the can or opposite sides, as shown in Figure 2.

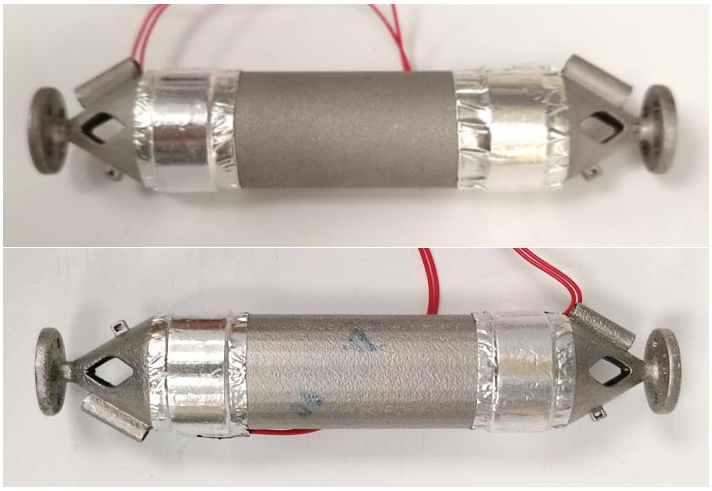

Figure 2: Original (top) and new (bottom) liquid can designs showing the different placements of the sensors.

The cans attach to the centre stick through linkers that screw onto metal rods, which run through each of the cans. Two cans are required on the centre stick for DSC runs. One can should be filled with the sample while the other can is used as a reference. The reference can is always attached to the centre stick below the sample can, as shown in Figure 6.

Notably, the cans and other metallic parts, such of the cores and screws, are made from aluminium as the metal has a high thermal conductivity and is neutron transparent as well as

being able to withstand high temperatures. By using a thermally conductive material, the sample held within the can will be heated without hinderance, as the heaters are positioned on the outside of the can, and the temperature gradient across the can is reduced. The neutron transparency of aluminium allows for the sample to be studied with QENS as the interaction of the neutrons with the aluminium does not obstruct the sample. The caps and linkers, on the other hand, are made from G-10 resin, which has a low thermal conductivity. This material was chosen to reduce the amount of thermal interference between the cans.[1]

The setup for the in-situ DSC includes a CCR setup, as shown in Figure 3, and is controlled by four Keithleys, a Eurotherm and two Lakeshores. The Eurotherm controls the CCR temperature while the can heaters are controlled through the Keithleys and Lakeshores. The Keithleys measure the output from the sensors on the cans and change the heater outputs accordingly and Lakeshores are used to control and measure the temperature of the heaters. Helium is a key part to the CCR setup as it is pumped into the CCR before runs to flush out any air from the inner vacuum chamber (IVC) and is used within runs to act as a thermal exchange medium.

Figure 3: The He canister and compressor (left), which are connected to the CCR (middle). The compressor pumps cold liquid He through the outer bin of the CCR. The He supply and scroll pump are attached at a three-way valve to the CCR. The scroll and turbo pumps (right) control the vacuums of the inner and outer vacuum chambers, respectively.

4. In-situ DSC Method

Solid Sample Can Preparation. Aluminium foil sachets were made for the annular can using either a net, as shown in Figure 4, or by cutting out a 150 mm by 75 mm rectangle. This rectangle was folded in half and closed by folding the edges twice to form a ‘TOSCA-style sachet’. For the tapered can, a stencil was used. The powder samples are held in sachets made of aluminium foil, a thermally conductive and neutron transparent material, to avoid sample leakage as the cans are unsealed. The sachet mass was recorded and filled with the powdered sample before the sachet was folded closed, and a rolling pin was rolled over to evenly distribute the sample. The full sachet was weighed and rolled into a cylinder to be inserted into the respective can so that it sat flush to the inner wall of the can. The inner cores of the can and inner metal rod were inserted into the hollow part of the cylindrical

sachet. The cores were expanded by screwing the bolts down the rod as shown in Figure 5. [8]

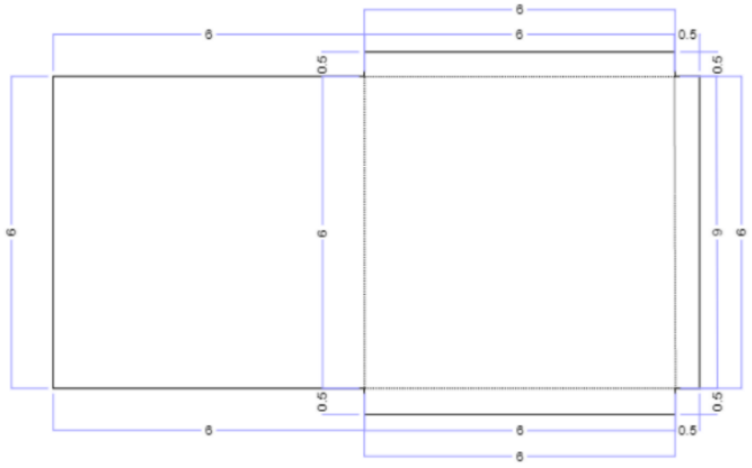

Figure 4: Net for the aluminium foil sample sachet designed for the Annular can. Units are in cm. [3]

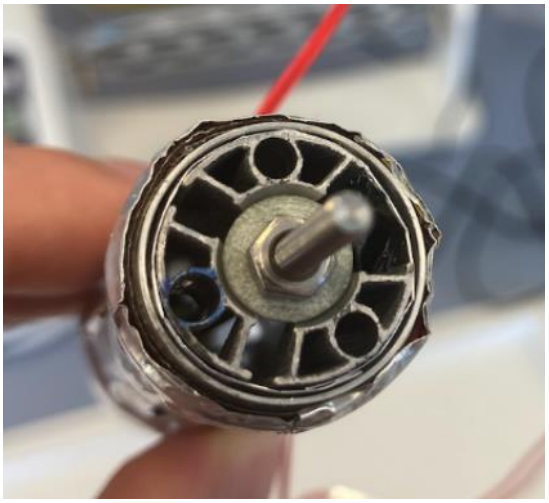

Figure 5: The filled sample sachet placed into the assembled Annular sample can. [3]

Liquid Sample Can Preparation. Indium seals were prepared by pressing indium wire into groves at both ends of the can. The linker was screwed onto the bottom of the can with the indium seal in place. Liquid sample was pipetted into the hole at the top of the can until the sample space was completely filled and the top linker was screwed into place with indium underneath. [8]

Assembly of the sample stick. Sensors (Cernox for cold setup [20 K to 300 K] or Pt-100 for hot setup [70 K to 470 K]) were placed into the slots of the sample and reference cans. The cans were attached to the sample stick in the ‘reference on bottom’ arrangement, and the sensors and heaters were connected to the stick by plugging in the corresponding wires.[2, 8]

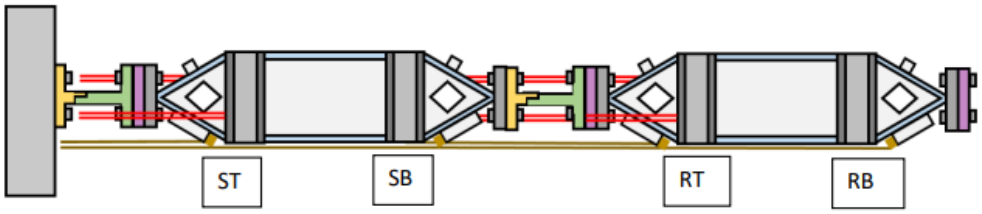

Figure 6: Diagram of the liquid cans after assembly to the stick in the 'reference on bottom' arrangement. Once in the upright position, the sample can (left) will sit above the reference can (right). The linkers are colour coded to represent the material used: aluminium (yellow for the screw linkers and purple for the flat linkers) and G-10 (green). The heater positions are shown at the top (T) and bottom (B) of both the sample (S) and reference (R) cans.[3]

Setting up the cryostat. The CCR and He canister were connected to the cryostat, and the He flow was opened. The fully constructed stick was inserted into the IVC tube, aligned by dropping screws into the upper plate and connected to the CCR via plugs and cables. The IVC was purged and filled three times by flushing the chamber with He gas, re-pressurising the IVC to 500 mbar and evacuating again to 10 mbar. The pressure was put to 50 mbar for running the cold setup tests and 30 mbar for hot setup tests. [8]

Changing Lakeshore settings. The lakeshore settings were changed to accommodate for the sensors by changing each sensor setting to either 'NTC RTD (Cernox)' or 'PTC RTD (Platinum)' . For cold setup, the 'Curve' settings were changed to the corresponding sensor/heater value shown in Table 1. For hot setup the 'Curve' settings were changed to '06 PT-100'.[8]

Table 1: Corresponding Block and Sensor/Heater Curve settings for the Cernox sensors to be inputted on the Lakeshores.

Block	Sensor/Heater
Reference Top	X104355
Reference Bottom	X104270
Sample Top	X104354
Sample Bottom	X104325

Using the GUI. The setup ('calor_offline') was selected in IBEX. [9] The temperature range (K), CCR offset (10, 15 or 20 K), heating rate (0.5, 1, or 5 K/min), heater output (low, medium, or high) and sensor setup (hot or cold) was put into the New Run tab on the GUI, which was loaded using the g.load_script("C:\scripts\Cal_GUI.py") command. The experiment was named and sent to run.[3, 8]

Using scripts. The previously written script ('Joel_High_Temp.py') was edited in WordPad to input current run parameters, such as temperature range and rate. This was saved and loaded into the Scripting page of IBEX using the 'g.load_script("C:/Scripts/Joel_High_Temp.py")' command. The run was started by calling upon the first defined line of the script ('calor_high()').[2, 8]

5. Materials

PVC powder (250 g), toluene (250 ml), sucrose (250 g), fructose (10 g) and lactose powder (1 kg) were purchased from Sigma Aldrich and stored at room temperature. Once opened, the sample containers were sealed with parafilm to prevent air moisture contamination. The same lab standard parafilm was used for DSC testing.

Everyday Brew teabags from teapigs were used to prepare black tea solutions. The hibiscus tea used in solution was Tesco's brand Red Berries Infusion flavoured tea. Twinings Pure Peppermint teabags were also used.

The milk sample was taken from a carton of skimmed longlife UHT milk (1 L) from Co-op and stored in a 5 °C fridge.

Pro Plus branded caffeine tablets were purchased from Tesco. Each tablet contains 50 mg of anhydrous caffeine as the active ingredient and also contains sorbitol.

6. Commercial DSC Method

Various samples, both solid and liquid, were tested with the Mettler Toledo DSC1 to examine phase changes and to find samples that display clear transitions. As well as either heating or cooling, two general methods were used to try to observe transitions, both of which used heat-cool cycles. The results of the commercial tests would later provide a guide for the experimental parameters used for the testing of the in-situ DSC cans.

General Method

Sample loading. Samples were loaded into aluminium pans, weighed, and hermetically sealed. For samples reaching boiling, the lid of the pan was pierced so that no pressure can build up inside the pan.

Setting up tests. To set up and evaluate runs, the Mettler Toledo DSC1 is accompanied by STARe software.[10] Using the DSC1 GUI, the temperatures and rates used for the experiment were set and the sample mass was logged. As the tests required temperature ranges, dynamic segments were set in the methods tab of the DSC1 GUI. Each segment included the starting and end temperatures and the rate of heating or cooling. Either multiple dynamic segments were set to heat, cool, and reheat within one experiment or one dynamic segment was used per experiment and multiple experiments were completed using one sample. Notably, the units used by the software for temperature and mass are °C and mg, respectively.

Solid Samples

Sample preparation. The solid samples were bought as powders with the exception of parafilm, which was cut into small pieces, and sucrose, which was ground into a powder.

Powder sample tests:

Table 2: Experimental details for the solid sample tests.

Sample	Mass / mg	Starting Temperature / K	End Temperature / K	Heating Rate / K/min	Cooling Rate / K/min
Sucrose powder	13.76	273	473	5	10
Sucrose powder	13.04	273	473	5	100
Lactose powder	5.53	443	473	5	10
Lactose powder	7.72	273	473	5	100
PVC powder	3.78	373	473	5	10
PVC powder	4.11	203	473	5	10
Parafilm	11.65	243	373	5	-

Liquid Samples

Solution preparation. All solutions were made with distilled water (50 mL, 318 K):

The sugar solutions were prepared by dissolving sugar samples (~10 g) individually.

To prepare the caffeine solution, one caffeine tablet was ground into a powder and dissolved.

Tea solutions were prepared by steeping tea bags for 1.5 hours.

Liquid sample tests:

Table 3: Experimental details for the liquid sample tests.

Sample	Mass / mg	Starting Temperature / K	End Temperature / K	Heating Rate / K/min	Cooling Rate / K/min
Sugar solutions	~38	223	423	5	10
Caffeine solution	32.36	223	423	5	10
Tea solutions	~32	223	423	5	10
Toluene	27.53	153	213	5	-
Skimmed milk	27.07	193	303	5	10

7. Commercial DSC Solid Sample Tests

Solid samples were tested using a commercial DSC to produce results for comparison with the in-situ DSC solid cans. By testing initially with the Mettler Toledo DSC1, the points of interest, including melting and boiling, were studied and transitions such as glass transitions were found. These commercial runs would provide a reference as to what to expect from in-situ results and allow for a comparison between the methods.

Sucrose

Due to the crystallinity of the sugars, the DSC tests needed to include a heat-cool cycle in order to see the glass transitions. During the first dynamic section, the sugar is melted so that it can be quickly cooled in the second dynamic section. By cooling the melted sugar at the fastest rate possible, an amorphous solid will be formed as the molecules cannot rearrange themselves back into the previous ordered structure.

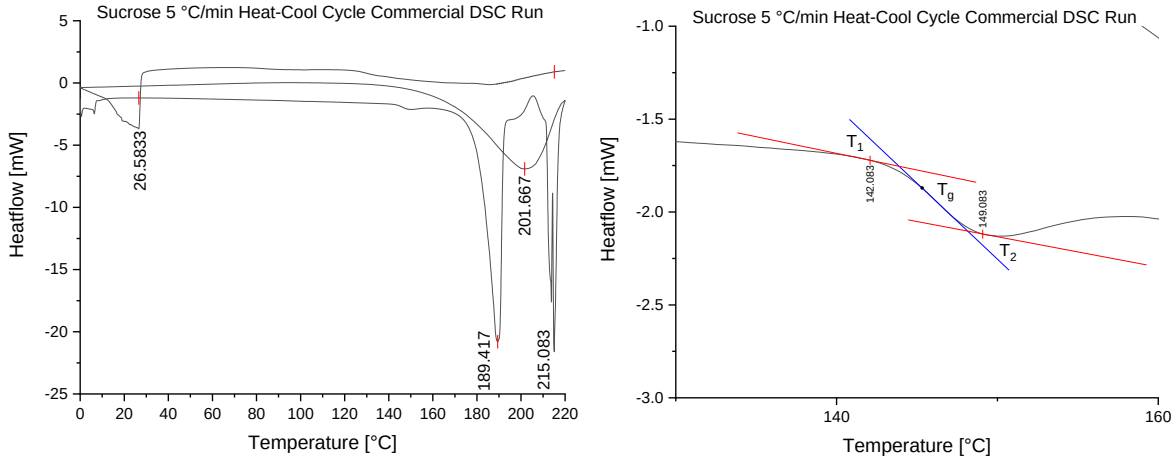

Figure 7: Ex-situ sucrose results (left) using the Mettler Toledo DSC1. The first dynamic segment was set to a temperature range of 273 to 473 K with a ramping rate of 5 K/min. The second dynamic segment was set to a temperature range of 473 to 273 K at a rate of 100 K/min. The last dynamic segment was set to a temperature range of 273 to 473 K at 5 K /min. The melting point is shown to be at 462.42 ± 0.25 K.
The sucrose results were scaled in to 403 to 433 K (right) and show a transition at 419 ± 1 K determined using the Quick Peak gadget in Origin and ASTM D 3418 method, which calculates the mean value between T_1 and T_2, and confirmed by the bisector method, which is the point where the bisector of the angle between two tangents intersects the curve.[11]

Sucrose has been known to have a T_g of 333 K and a melt within a temperature range of 433 to 465 K.[12] The transition, shown in Figure 7, at 419 ± 1 K is not close to previously reported T_g values. This early endothermic transition has been previously observed in crystalline sucrose and shows bond deterioration in the sucrose molecule before melting.[12] The melt, observed in Figure 7Figure 7, at 462.42 ± 0.25 K is in line with previously reported values and is followed by sample degradation. This degradation is responsible for the broad peak at 474.87 ± 0.25 K during the cooling segment. The peak at 299.58 ± 0.25 K during the second heating is an artefact of the DSC as the instrument reheats from the lowest set temperature. Therefore, the sucrose sample examined had a crystalline structure, suggested by the early transition and melting temperature, and should be run below 473 K to avoid sample degradation.

Lactose

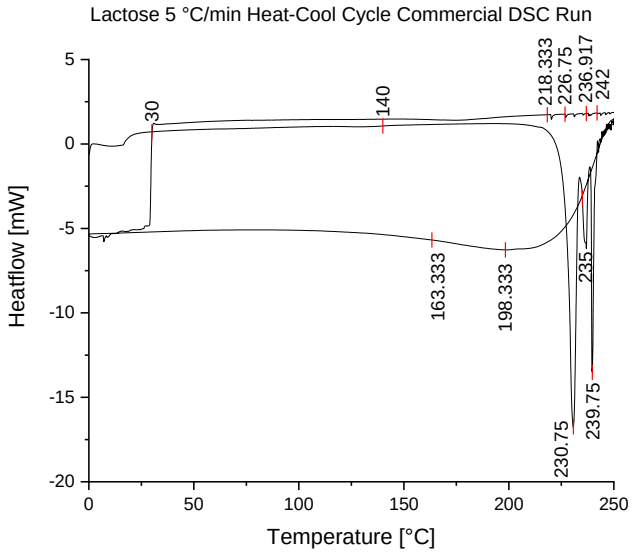

Figure 8: Commercial results (left) for lactose using the Mettler Toledo DSC1. The first dynamic segment was set to a temperature range of 273 to 523 K with a ramping rate of 5 K/min. The second dynamic segment was set to a temperature range of 523 to 273 K at a rate of 100 K/min. The last dynamic segment was set to a temperature range of 273 to 523 K at 5 K /min. The melting point is shown to be at 503.75 ± 0.25 K.

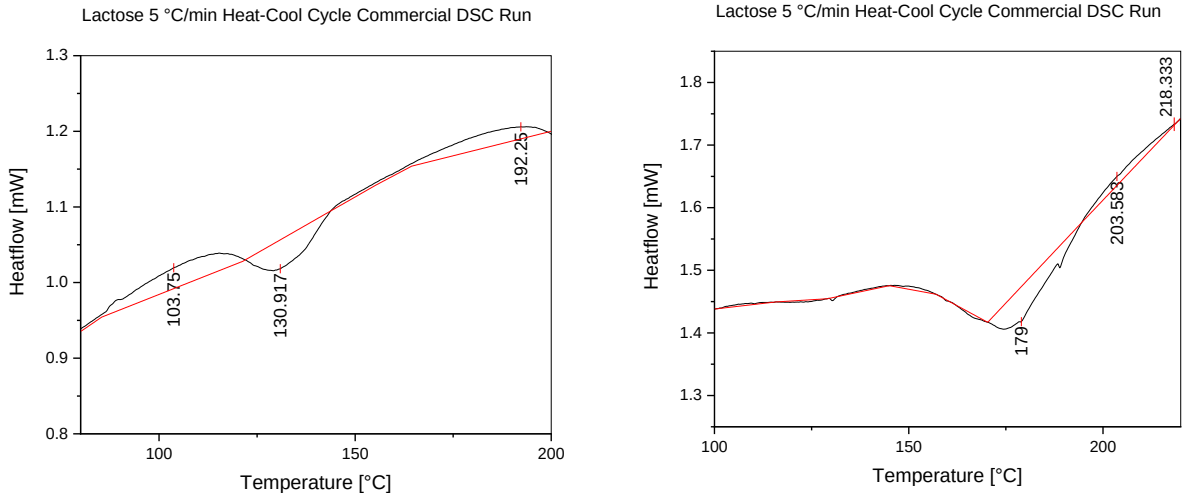

Figure 8. 1: The ex-situ lactose results scaled in to 353 to 473 K (left) and show a transition at 404 ± 1 K during the first heating segment determined using the Quick Peak gadget in Origin.
Ex-situ lactose results (right) scaled in to 373 to 493 K showing a transition at 452 ± 1 K during the second heating segment determined using the Quick Peak gadget in Origin.

Lactose has previously been reported to have a glass transition at around 374 K.[13] Slight depressions, shown in Figure 8.1, were seen at 404 ± 1 K in the initial heating and 452 ± 1 K in the second heating. These temperatures are not aligned with the stated T_g value. These depressions could be due to decomposition within the sample suggested, in Figure 8*Figure 8*, by the peak at 508.00 ± 0.25 K onwards. The melt was observed, in Figure 8, at 503.75 ± 0.25 K, which is lower than previous results for β-lactose that shows a melt at 513 K.[14] The lower observed melting temperature was as a result of water being present in the sample. Decomposition of the sample significantly impacted the second melt, as the water within the

sugar boiled causing an increase of pressure within the sample pan, resulting in the sample leaking and the appearance of multiple minor peaks in the temperature region of melting and decomposing as the remaining sample further decomposed.

PVC

Polymers are well known to display glass transitions with PVC obtaining low temperature transitions in previous literature.[15] PVC was initially run from 273 to 523 K at 5 K/min to observe the T_g and the max temperature before thermal degradation. A heat-cool cycle was then used to study the properties of PVC whilst cooling and reheating.

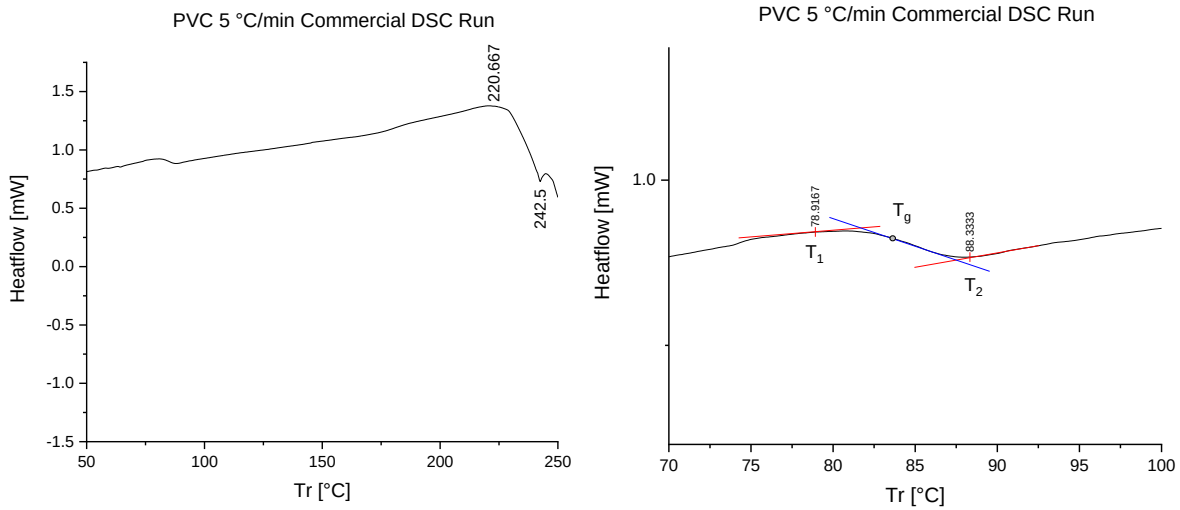

Figure 9: Commercial PVC results (left) run from 273 to 523 K at 5 K/ min using the Mettler Toledo DSC1.The sample was shown to have a cold crystallisation temperature of 493.70 ± 0.25 K before showing decomposition at 518.50 ± 0.25 K. The commercial DSC results (right) for PVC scaled in to 343 to 373 K showing a transition at 357 ± 1 K determined using the Quick Peak gadget in Origin and the ASTM D 3418 method and confirmed using the bisector method.

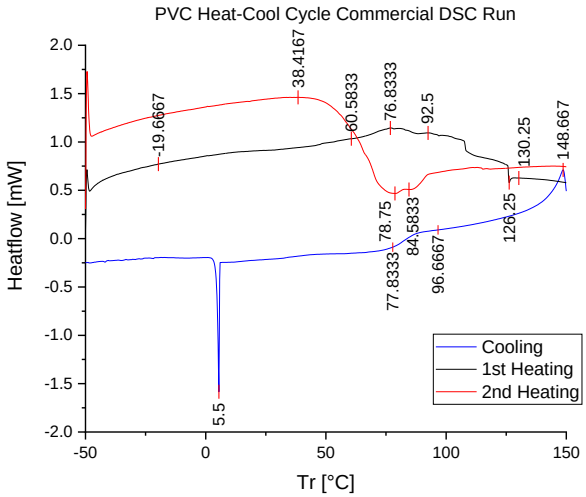

Figure 9. 1: Commercial PVC results using the Mettler Toledo DSC1. Three runs were used to complete a heat-cool cycle: first the sample was heated from 223 to 423 K at 5 K /min before cooling back down to 223 K at 10 K

/min in the second run. The third run reheated the sample back to 423 K at 5 K /min. Decomposition is shown to occur above 333 K. During the cooling run, peaks at 278.50 ± 0.25 K and 421.67 ± 0.25 K are seen.

From the commercial DSC tests, the PVC powder was observed to have a clear transition of 357 ± 1 K, as seen in Figure 9. This value is somewhat close to previously reported temperatures of around 343 K and, in Figure 9, decomposition was seen after 493 ± 1 K, which is a lower temperature than reported in literature.[15] This could be due to the use of different experimental methods as a higher starting temperature was used and the test was run at a slower rate. In Figure 9.1, the thermal sensitivity of the PVC was shown as discontinuities occur during the first heating segment after 333 ± 1 K, which are caused by enthalpy relaxation and stress relief. When cooling, an exothermic peak was observed at 421.67 ± 0.25 K before a transition between 369.67 ± 0.25 K and 350.83 ± 0.25 K. A sharp endothermic peak at 278.50 ± 0.25 K, correlating to the freezing of PVC, was also seen.

Parafilm

Parafilm is made up of paraffin wax and polyolefins and is a soft, self-sealant thermoplastic that displays irreversible thinning when stretched.[16] As a thick film, it was necessary to cut the parafilm into small pieces in order to fit the sample into the DSC pan.

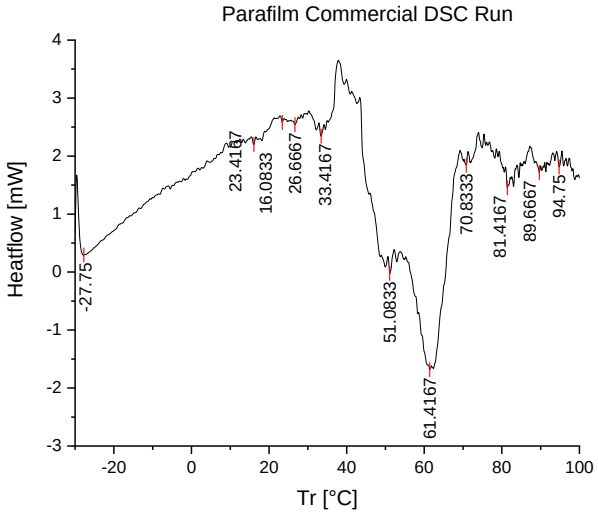

Figure 10: Commercial results for parafilm run from 243 to 373 K at 5 K/min using the Mettler Toledo DSC1. The melting of the parafilm can be seen between 318 K and 339 K.

Paraffin wax has a melting point around 323 K and a solid-solid transition around 303 K according to literature.[17] This is in line with the commercial DSC run as peaks at 306.42 ± 0.25 K and 324.08 ± 0.25 K were observed, as shown in Figure 10. The further peaks are due to the presence of polyolefins within the parafilm and their thermal degradation. These could also be as a result of the inconsistent size and thickness of the pieces of parafilm as larger and thicker pieces require more thermal energy to melt.

8. Commercial DSC Liquid Sample Tests

Similarly to the solid samples, liquids were initially tested with the Mettler Toledo DSC1. The results from the commercial tests provided a reference to compare the in-situ liquid cans to. The observed changes of state confirm the temperature range required for in-situ DSC tests as, due to the cans being sealed, boiling points need to be avoided as to not increase the pressure within the cans. The lids of the sample pans for the commercial DSC tests were pierced so that the pressure could be released from inside the pans during the runs. This leads to potential shifts in the temperature at which transitions occur due to the difference in pressure. The samples tested were non-toxic, thus, the unsealed samples were not a health and safety risk. As the aim of benchmarking the liquid cans was added towards the end of the project, sample availability was a potential issue. Therefore, samples were chosen that were readily available or already in the facility labs.

Caffeine Solution

The solution of caffeine in water was run in a heat-cool cycle to confirm the boiling point of the solution so that the in-situ DSC tests can be run below this temperature. No peaks were observed after the initial heating segment, confirming that the solution had boiled and evaporated out of the pieced pan lid. Therefore, only the first heating segment is shown in the results. The full heat-cool cycle can be found in Appendix B.

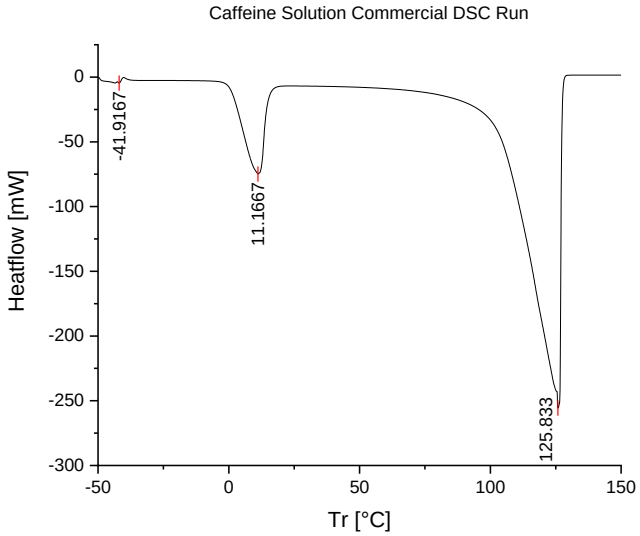

Figure 11: Commercial DSC1 caffeine solution results from 223 to 423 K using a rate of 5 K/min showing a melt at 284.17 ± 0.25 K and boiling at 398.83 ± 0.25 K .

The caffeine-water solution produced two clear endothermic peaks at 284.17 ± 0.25 K and 398.83 ± 0.25 K, as shown in Figure 11, corresponding to the melting and boiling of the solution. As water is known to have a melting point of 273 K and a boiling point around 383 K, the results could suggest that caffeine increases the temperature at which the phase changes of water occur. [11] This shift in boiling point is could be due to the boiling point elevation effect as the caffeine particles decrease the vapor pressure of the water.[18] The increase in melting temperature is the result of caffeine broadening the peak. Melting begins around 273 ± 1 K, as expected for water, but does not reach the peak temperature until

284.17 ± 0.25 K as the caffeine particles melt at a higher temperature.[19] The shift at 232.92 ± 0.25 K is expected to be an artefact of the DSC1 as the system begins to ramp up to temperature at the required rate.

Milk

A sample of skimmed milk was run in a heat-cool cycle well below the boiling temperature. This was to study the effect of freezing and reheating on the melting temperature of the recrystalised milk.

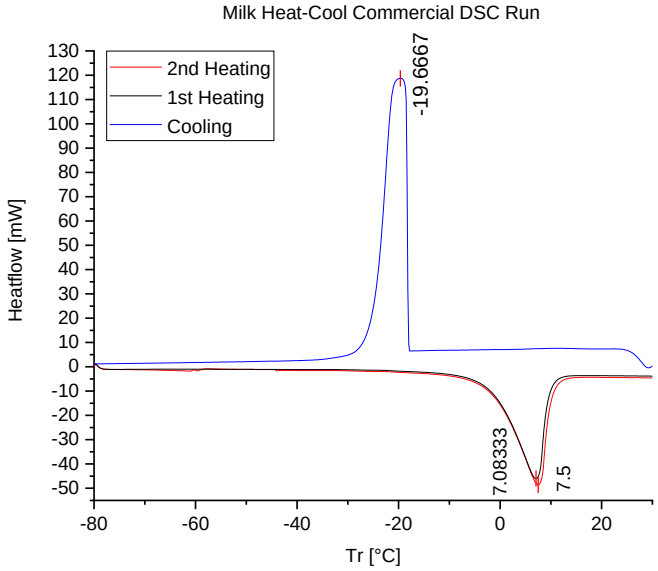

Figure 12: Commercial DSC results of milk using the Mettler Toledo DSC1. Data were collected in the temperature range -193 to 303 K using a heating rate of 5 K/min and shows melting around 280.29 ± 0.25 K and recrystallisation at 254.67 ± 0.25 K.

From the commercial DSC results, the melting point of milk was observed to be around 280.29 ± 0.25 K during both the initial and second heating runs, as shown in Figure 12. This shows that reheating the sample has little to no effect on the melting temperature, which increased by ~0.4 K after freezing. The milk recrystallized at 254.67 ± 0.25 K to give a substantial peak of ~110 mW.

Toluene

Toluene is a highly volatile solvent, which caused difficulty when sample loading the DSC pans as little liquid can be held in the crucible. To find the melting point of toluene, the sample was run from 123 K to 213 K at 5 K/min in an unpierced commercial DSC pan. Despite the sealed pan, a large amount of the sample did evaporate before sealing.

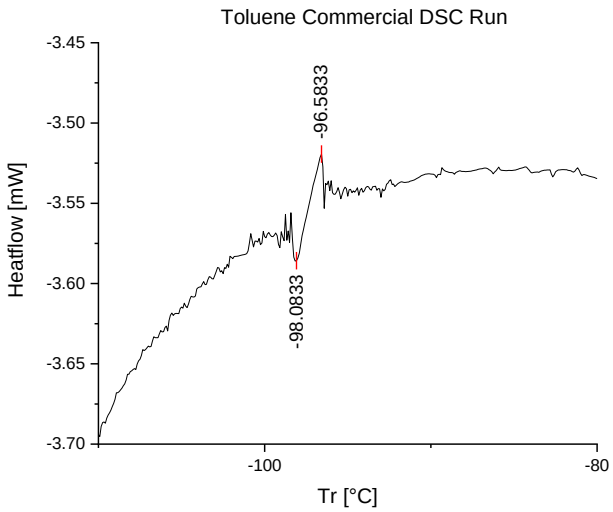

Figure 13: Commercial DSC results for toluene using the Mettler Toledo DSC1. Data were collected in the temperature range 123 K to 213 K using a heating rate of 5 K/min and shows a melt around 176 K.

Due to the small amount of toluene remaining in the DSC pan, the total signal, shown in Figure 13, is ~0.1 mW. However, this signal is seen to be around 176 ± 1 K, which is in line with previous literature, which states that toluene has a melting temperature of 174 K.[20] The small signal, also, resulted in clearer artefacts from the sample pan itself, shown by the oscillations of the baseline, as the difference of signal height between the sample and the pan was reduced.

Tea Solutions

The tea solutions were run in heat-cool cycles to study the effects of various teas on the transitions of water and to confirm the boiling points of the solutions. After the initial heating segment, no peaks were observed as the samples had evaporated through the pierced lid. Therefore, only the first segment is displayed in the results and the full results can be found in Appendix B.

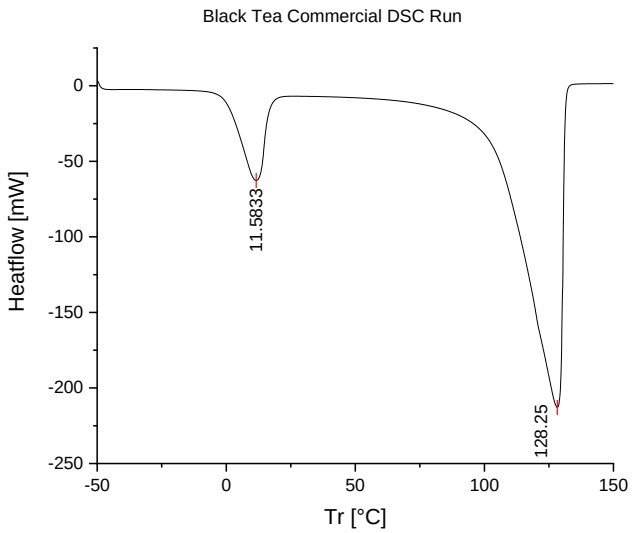

Figure 14: Commercial DSC black tea solution results using the Mettler Toledo DSC1. Data were collected in the temperature range 223 to 423 K using a heating rate of 5 K/min and shows water melting at 284.58 ± 0.25 K and boiling at 401.25 ± 0.25 K .

Figure 14 shows that the melting and boiling point of water shifted significantly with the addition of black tea. Water is known to have a melting point of 273 K and a boiling point around 383 K. [11] However, the black tea solution shows a melting point of 284.58 ± 0.25 K and a boiling point of 401.25 ± 0.25 K. This shift in temperature is likely due to the high caffeine content within black tea. This can be seen by comparison with the caffeine solution, Figure 11, as both solutions have similar melting and boiling temperatures. The black tea particles decrease the vapour pressure of the water resulting in a higher boiling point and the particles melt at a higher temperature than water. Therefore, the melting point increases as the peak broadens.

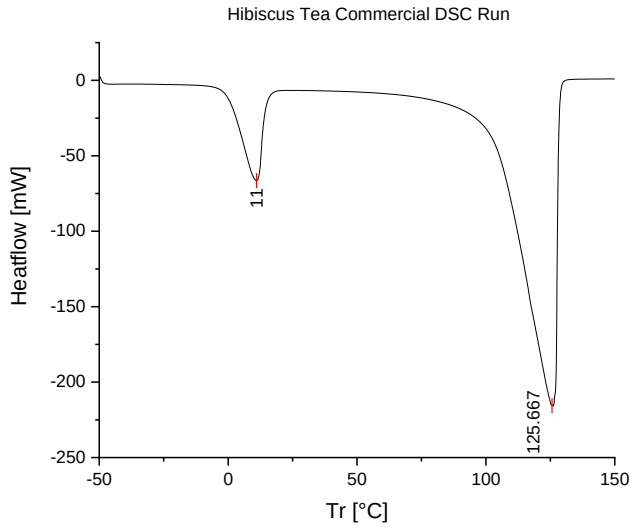

Figure 15: Commercial DSC hibiscus tea solution results using the Mettler Toledo DSC1. Data were collected in the temperature range 223 to 423 K using a heating rate of 5 K/min and shows water melting at 284.00 ± 0.25 K and boiling at 398.67 ± 0.25 K .

Similarly to the black tea solution, Figure 14, the hibiscus tea raised the phase change temperatures of the water within the solution. The melting point, shown in Figure 15, of the hibiscus tea was 284 ± 0.25 K and the boiling point was 398.67 ± 0.25 K. However, hibiscus tea is known to contain no caffeine so the shift in temperature is as a result of other thermally resistant molecules within the tea, such as flavonoids and anthocyanins.[21, 22]

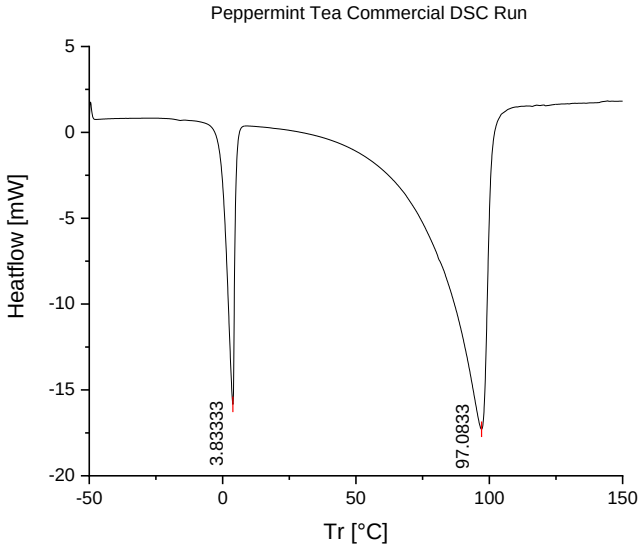

Figure 16: Commercial DSC peppermint tea solution results using the Mettler Toledo DSC1. Data were collected in the temperature range 223 to 423 K using a heating rate of 5 K/min and shows water melting at 276.83 ± 0.25 K and boiling at 370.08 ± 0.25 K.

Pure peppermint tea, similarly, to hibiscus tea contains no caffeine naturally.[23] The phase transitions of water with peppermint tea were observed to not be so greatly affected like the other teas. The melting and boiling points, as shown in Figure 16, were found to be at 276.83 ± 0.25 K and 370.08 ± 0.25 K, respectively. This lack of change is due to the main component of the peppermint tea being menthol, which has a low melting point (175 K). [24] Therefore, there are no effects on the melting temperature of water. The broadening of the boiling peak is due to the low boiling point of methanol (338 K). [24]

Sugar Solutions

Sugar samples were chosen to be tested due to the outcome of the liquid can tests with recrystallized sucrose, Figure 52, displaying a broadened melting peak for the water retained in the sucrose. Also, the s the availability of the sugars was favourable. Notably, the sugar solutions were run in heat-cool cycles and after the initial heating segment, no peaks were observed as the samples had evaporated through the pierced lid. Therefore, only the first segment is displayed in the results. The full heat-cool cycle can be found in Appendix B.

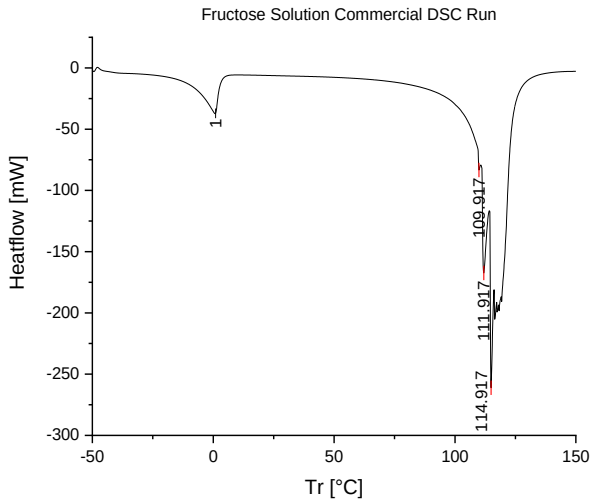

Figure 17: Commercial DSC fructose solution results using the Mettler Toledo DSC1. Data were collected in the temperature range 223 to 423 K using a heating rate of 5 K/min and shows water melting at 274.00 ± 0.25 K and boiling at 382.92 ± 0.25 K . Extra peaks are caused by melting fructose around 388 K.

The melting temperature of the fructose solution can be seen at 274.00 ± 0.25 K, in Figure 17, before the solution boiled to produce staggered peaks from 382.92 ± 0.25 K. The melting peak temperature shows no effect from the dissolved fructose on the melting point of the water. However, some peak broadening can be seen as a result of hinderance from the sugar. The multiple peaks after 373 K suggest that the water boiled at 382.92 ± 0.25 K, and the fructose melted at 387.92 ± 0.25 K before decomposing. Solid fructose exhibits melting temperatures of 364 – 458 K depending on the structural properties of the sugar. [25] Therefore, the observed melting of the fructose itself is within the given literature range.

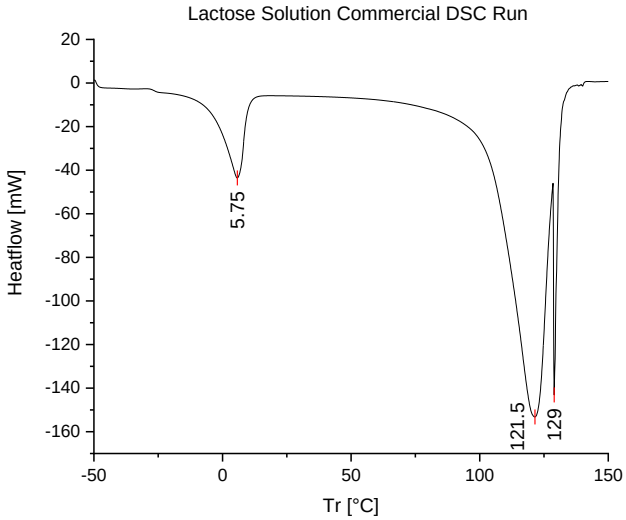

Figure 18: Commercial DSC lactose solution results using the Mettler Toledo DSC1. Data were collected in the temperature range 223 to 423 K using a heating rate of 5 K/min and shows water melting at 278.75 ± 0.25 K and boiling around 394.50 ± 0.25 K . Extra peaks are caused by lactose melting at 402.00 ± 0.25 K.

The lactose solution results, Figure 18, shows the melting point of water had increased slightly in temperature from 273 K to 278.75 ± 0.25 K with the addition of the more thermally resistant sugar. The broad boiling peak at 394.50 ± 0.25 K suggests that the water boiled at a higher temperature due to a decrease in vapour pressure, caused by the large lactose molecules, resulting in boiling point elevation. The sharp peak at 402.00 ± 0.25 K shows a reduction in melting temperature for the damp lactose remaining from the solution.

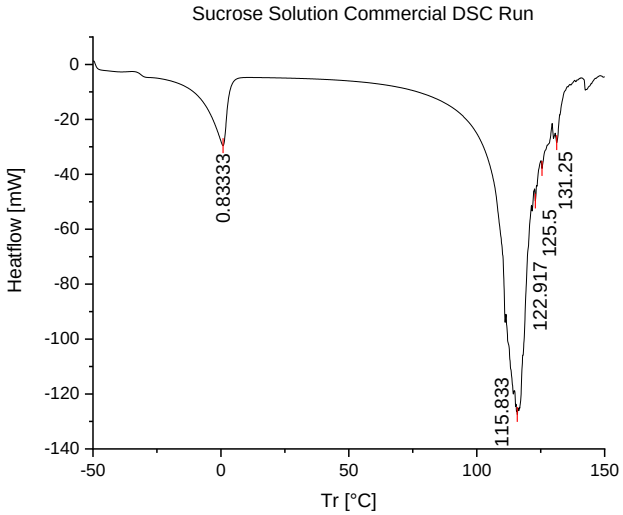

Figure 19: Commercial DSC sucrose solution results using the Mettler Toledo DSC1. Data were collected in the temperature range 223 to 423 K using a heating rate of 5 K/min and shows water melting at 273.83 ± 0.25 K and boiling around 428.83 ± 0.25 K . Extra peaks are caused by melting sucrose from 395.917 to 404.250 K.

In Figure 19, the melting point of water appears to be less effected by the presence of sucrose with a peak temperature of 273.83 ± 0.25 K and only slight broadening beforehand. The boiling point, however, was increased. The water in the solution boiled at 388.83 K due to elevation caused by the presence of sucrose. The further peaks suggest that after majority of the water boiled, the sucrose decomposed.

9. Empty DSC Sample Can Testing

Annular Cans

Empty Annular can runs were carried out on the in-situ DSC to test for the functionality of the sample stick and to determine the background current subtractions. Cold conditions (Cernox sensors, temperature range of 20 – 300 K, low heater output with a CCR offset of 10 K) were used to check for an anomalous peak at 210 K, which was previously observed in the initial testing of the solid cans.[3]

The first runs (1704 to 1707) raised issues with the communication between IBEX and the Keithleys as the data for the heater currents outputted during the run were not saved by IBEX, thus no results are shown in this report. This required the Keithleys to be power cycled and emphasised the importance of loading the configuration (calor_offline_setup) before the GUI.

Further testing (runs 1709 to 1723) showed the heaters on the cans trip resulting in inconclusive data, as shown in Figure 20, Figure 21 and Appendix C. During the runs, the heater tripping could be seen through IBEX as the Log Plotter showed the temperature reading dropped and the heater status in the Synoptic flagged an error. Within the results, the output either remained at 0 A or spiked to plot multiple spiralled lines as the heater tripped, as shown in Figure 20 and Figure 21. From these runs, it appeared that the heaters, when in cold setup, were more stable at high heater output with a CCR offset of 15 K. To further the stability of the heaters and prevent them from burning out quickly, the current output was lowered from 1 to 0.35 A (run 1715 to 1739). The ref_bot heater consistently tripped upon heating to 100 K throughout these runs.

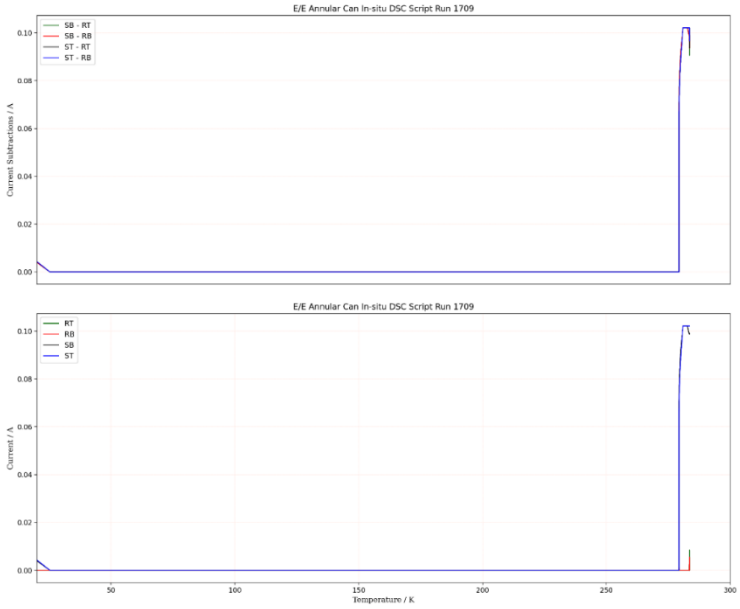

Figure 20: Results from the in-situ DSC setup testing of the empty annular cans with low heater output. The GUI run was from 20 - 300 K at 0.5 K/min with a CCR offset of 10 K.

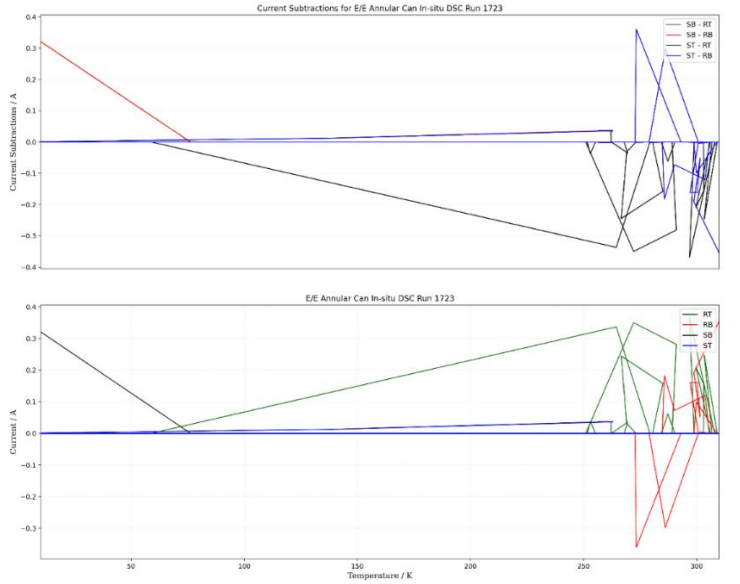

Figure 21: Results from the ex-situ calorimeter setup testing of the empty annular cans with low heater output. The GUI run was from 20 - 300 K at 5 K/min with a CCR offset of 15 K.

To locate the source of the heater issues, the setup, stick, and cans were checked. The heaters were replaced multiple times due to burn out, and both can types were tested. Throughout these checks, the reference bottom heater continued to trip. The heaters were swapped top to bottom and then sample to reference. Despite the swaps, the reference bottom heater tripped and produced inconsistent results, such as Figure 21, suggesting that there was a fault with the reference Lakeshore. This Lakeshore was replaced, and further testing confirmed this fault as the heater no longer tripped during runs (1755 onwards), as shown in Figure 22. Testing continued with the replacement Lakeshore, while the faulty console was sent for reconfiguration, and resulted in the heaters burning out at a significantly reduced rate.

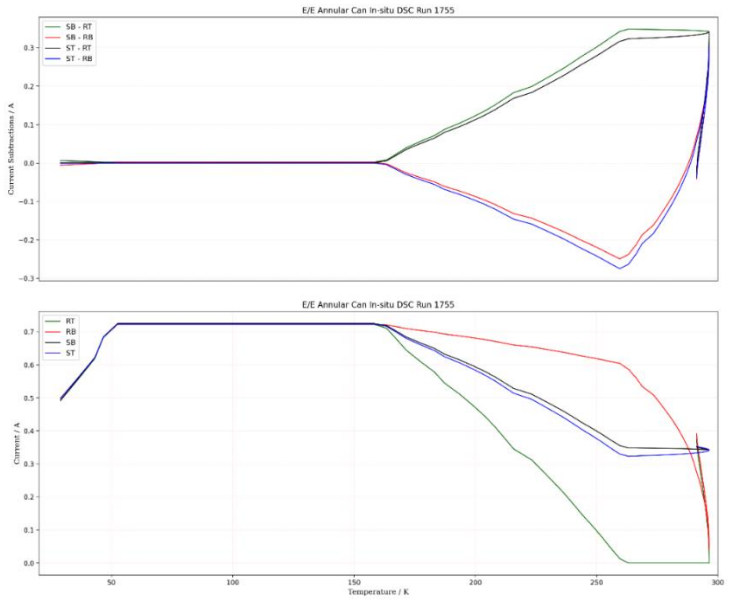

Figure 22: Results from the ex-situ calorimeter setup testing of the empty annular cans with high heater output. The GUI run was from 20 - 300 K at 2 K/min with a CCR offset of 10 K.

However, more problems were highlighted after fixing the tripping heater issue. When ramping down to 20 K, results (1756 onwards) show a consistent peak at 100 K, seen in Figure 23. The peak is thought to be caused by the inconsistent CCR cooling rate due to the CCR pausing to allow the can temperatures to come within range of the CCR temperature. This issue will be picked up in the future by the cryogenics team and initial work towards determining the cause of these results can be found in Appendix D.

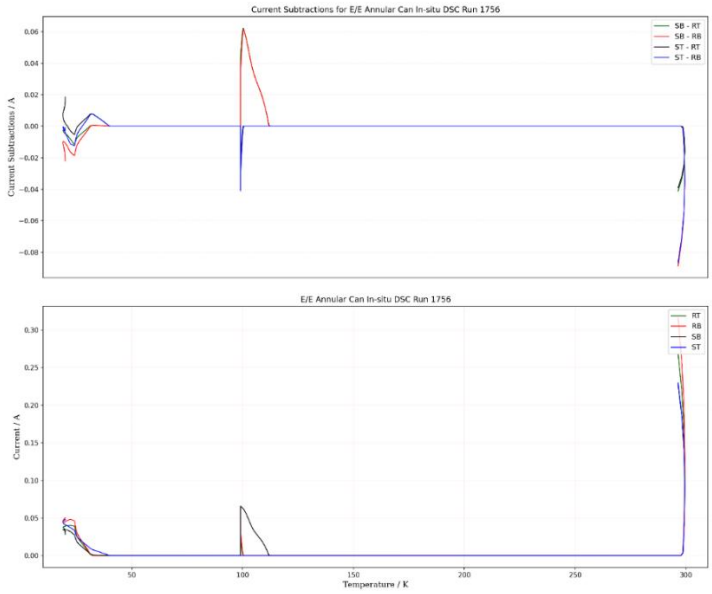

Figure 23: Results from the ex-situ calorimeter setup testing of the empty annular cans with high heater output. The log purge was from 300 - 20 K at 100 K/min (to allow for cooling as fast as possible) with a CCR offset of 10 K.

Due to the cooling issue, focus was placed onto testing the empty cans during heating ramps to examine the effects of the test conditions on the results to obtain the optimal experimental settings in the cold setup (20 – 300 K). Testing continued with the annular cans and the heater output, rate and CCR offset were changed in each test.

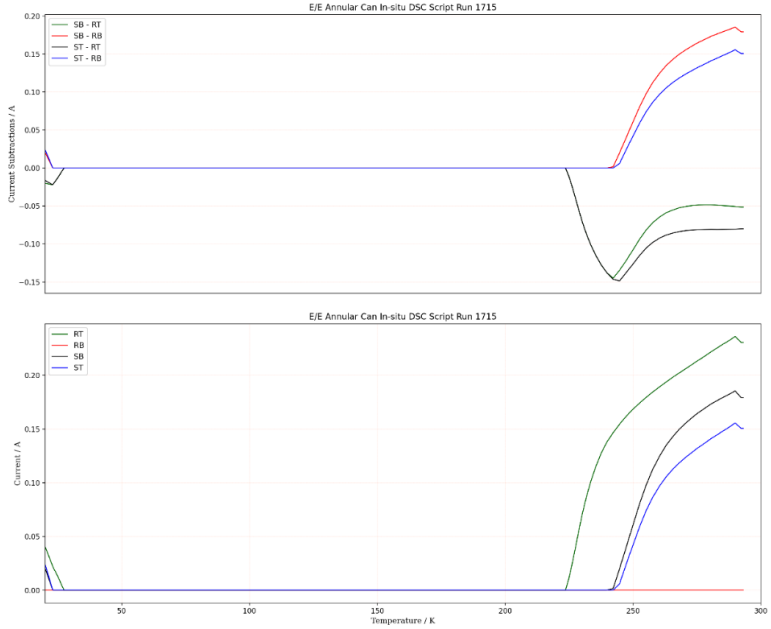

Figure 24: Results from the ex-situ calorimeter setup testing of the empty annular cans with medium heater output. The GUI run was from 20 - 300 K at 5 K/min with a CCR offset of 20 K.

In Figure 24, the annular cans were run with medium heater output with a CCR offset of 20 K. This resulted in the heaters outputting only after 225 K barring the reference bottom heater, which did not engage during the heating ramp. This lack of heater contribution is due to the reliance on the CCR to heat the setup while remaining 20 K below the heater temperatures. After 225 K, the CCR cannot produce enough heat to remain at the required rate, so the can heaters engage despite the most bottom heater (RB), which is still heated enough by the setup. Thus, the CCR offset was reduced to 10 K to check for any significant effect on the can heaters.

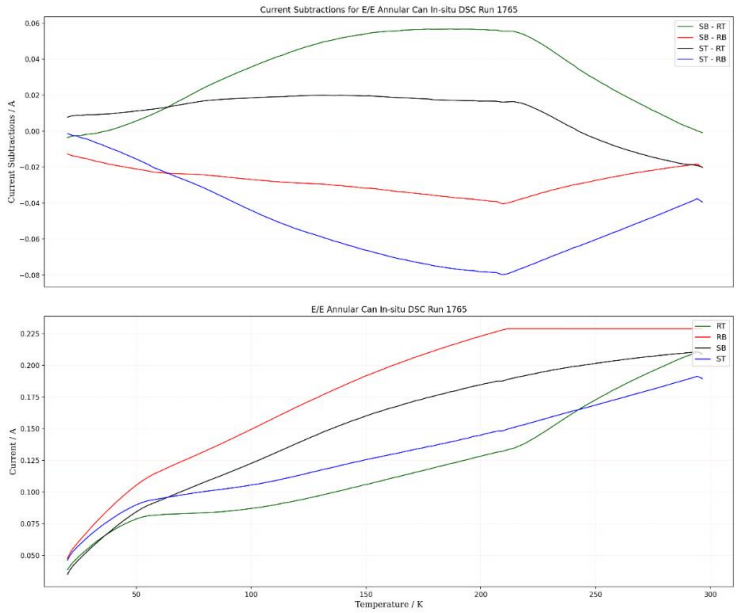

Figure 25: Results from the ex-situ calorimeter setup testing of the empty annular cans with medium heater output. The GUI run was from 20 - 300 K at 5 K/min with a CCR offset of 10 K.

At a lower CCR offset of 10 K, the heaters engaged throughout the heating ramp, as shown in Figure 25. The output by the heaters generally increased as the temperature increased, as expected, omitting the shift around 210 K and the initial heating to 50 K as the heaters are outputting against the CCR. After 210 K, the reference can heaters outputted differently to the sample heaters. The reference top can heater output increases whereas the bottom heaters remained constant. This shows that the top heater was outputting in order to heat both ends of the can, so the heater output was set to high in the next run to encourage the reference bottom heater to heat independently.

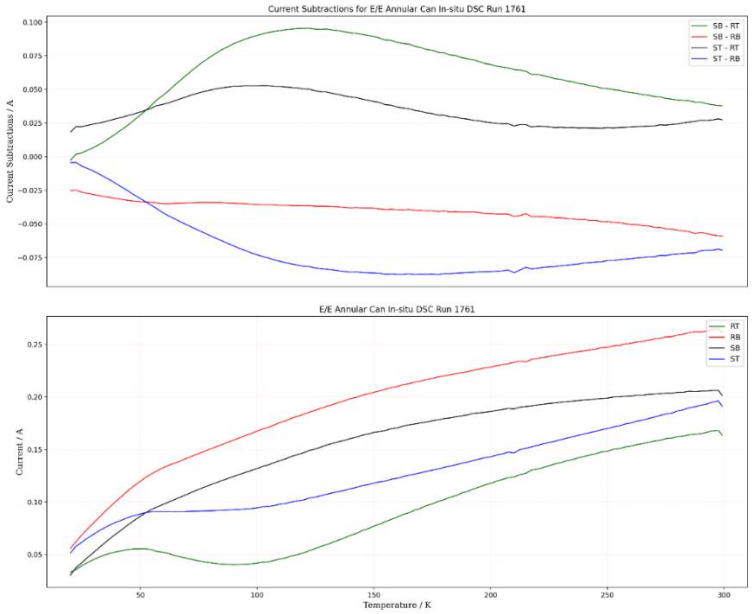

Figure 26: Results from the ex-situ calorimeter setup testing of the empty annular cans with high heater output. The GUI run was from 20 - 300 K at 5 K/min with a CCR offset of 10 K.

During the high heater output run, the reference heater outputted more consistently with the other heaters, as shown in Figure 26. The top and bottom heaters of each can heated in parallel with each other so that the difference in the heating of the reference and sample cans could be observed to show the effect of depth within the CCR to the heating on the DSC stick. In the first stage of heating, from 20 to 100 K, there was a larger difference between the top of the cans and the bottom of the cans than the medium output test with the bottom heaters outputting more than the top. This caused the top heaters to output less at 100 K in order to remain at the heating rate as the bottom heaters caused the top to overheat. Despite the initial heating, for cold setup experiments, the optimal settings were found to use high heater output and a CCR offset of 10 K as each heater functions individually.

Using high heater outputs and a CCR offset of 10 K, the ramping rate was changed to study the effect of slower rates on the heater outputs during cold setup tests.

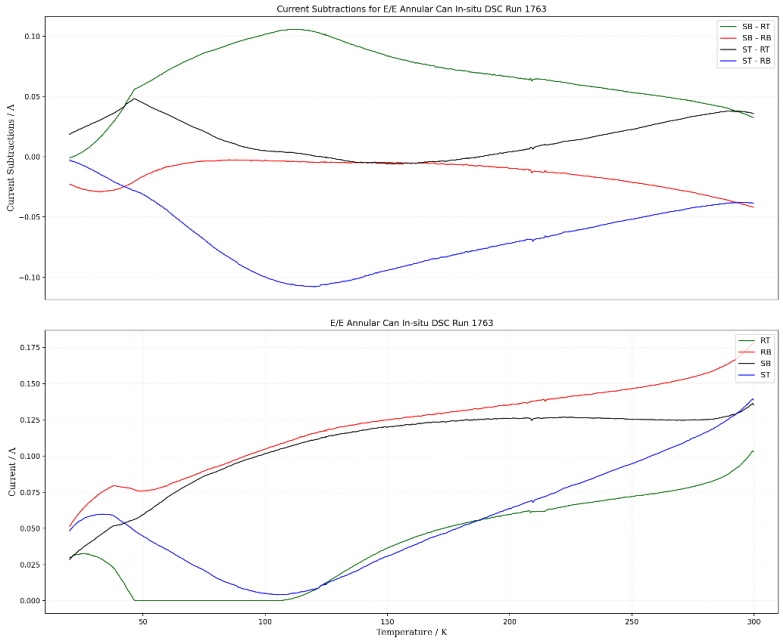

Figure 27: Results from the ex-situ calorimeter setup testing of the empty annular cans with high heater output. The GUI run was from 20 - 300 K at 1 K/min with a CCR offset of 10 K.

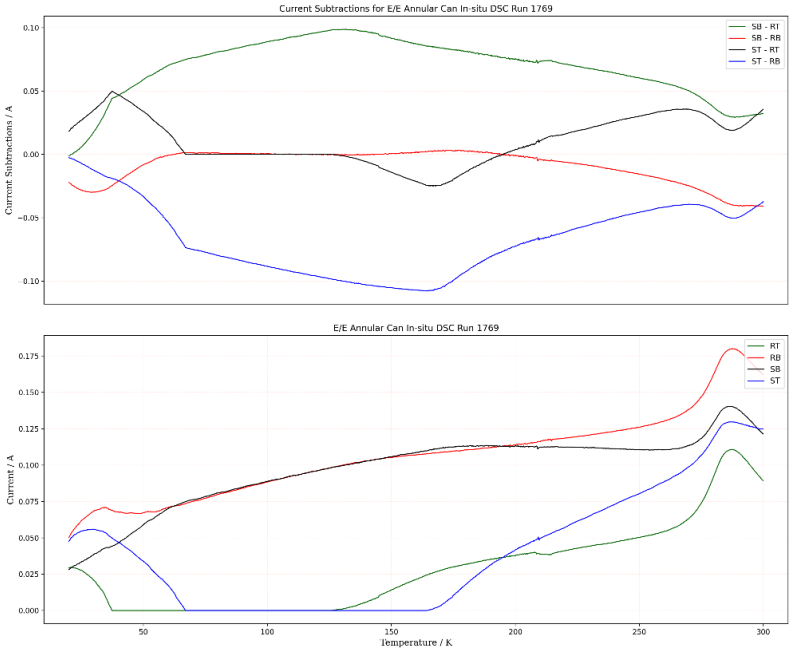

Figure 28: Results from the ex-situ calorimeter setup testing of the empty annular cans with high heater output. The GUI run was from 20 - 300 K at 0.5 K/min with a CCR offset of 10 K.

Runs using slower rates of 1 and 0.5 K/min gave worse results, shown in Figure 27 and Figure 28. During the slow rate runs, all the heater outputs reduce around 50 K whereas in the 5 K/min run, Figure 26, only the top heaters on the sample and reference can drop in output. It can been seen that as the rate decreases, this drop in heater output becomes more drastic. The 0.5 K/min run, Figure 28, shows that both the top heaters output 0 A from

around 60 to 130 K with the reference heater outputting less at slightly colder temperatures than the sample heater. At 1 K/min, Figure 27, only the top reference heater decreases to 0 A. Therefore, the heating rate of the annular cans may be limited to 5 K/min.

The annular cans were tested in hot setup (70 – 470 K) using different experimental settings. The heater output and CCR offset were changed in each test to observe the effects of each different setting. The rate was kept to 5 K/min due to the outcome of the cold setup tests, Figure 27 and Figure 28.

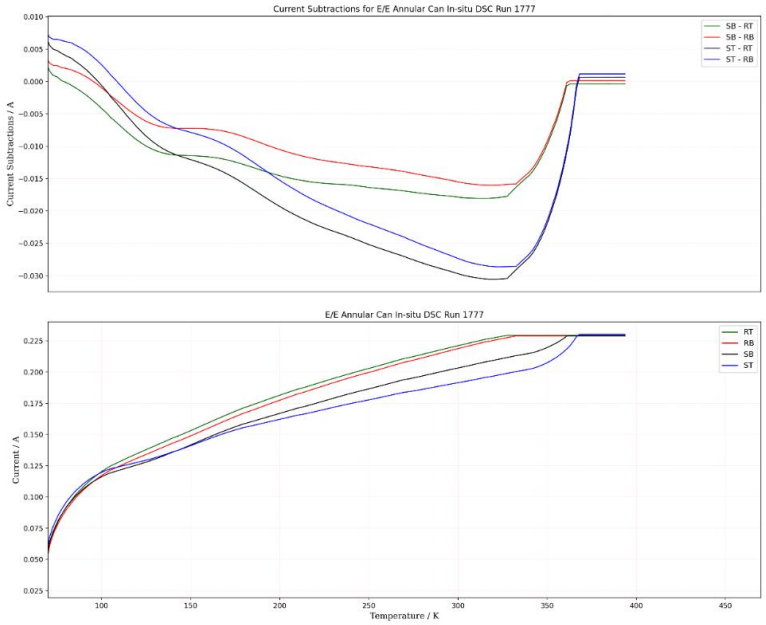

Figure 29: Results from the ex-situ calorimeter setup testing of the empty annular cans with medium heater output. The GUI run was from 70 - 470 K at 5 K/min with a CCR offset of 10 K.

In Figure 29, medium heater output in the hot setup resulted in the run not finishing as the max temperature (470 K) was not reached by the cans. This was due to the limited current the heaters can produce at this output and the inability of the reduced heaters to heat passed the CCR, which should be heated to a maximum of 290 K. It was also observed that the CCR overheated due to the smaller temperature offset between the heaters and the CCR. Therefore, the next run needed a larger CCR offset and high heater output.

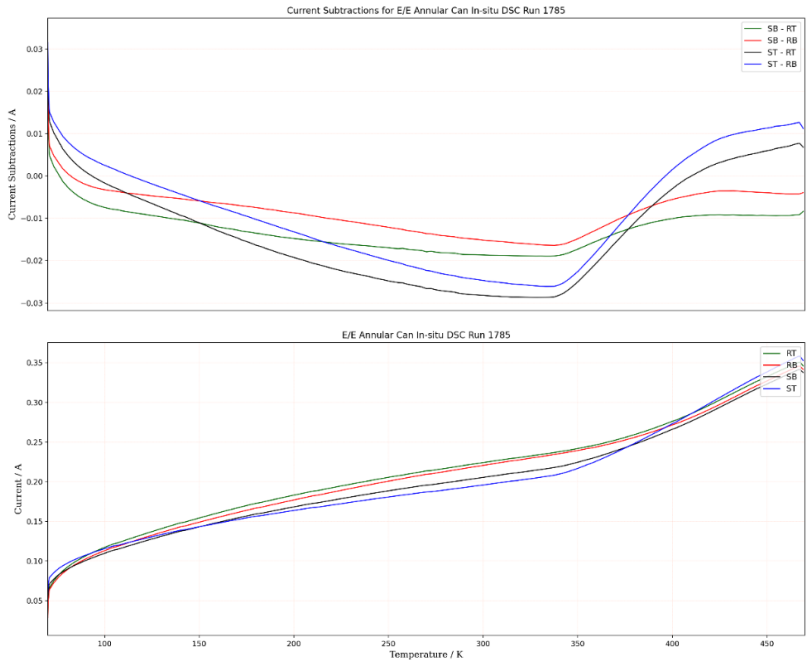

Figure 30: Results from the ex-situ calorimeter setup testing of the empty annular cans with high heater output. The GUI run was from 70 - 470 K at 5 K/min with a CCR offset of 15 K.

With the heater output set to high, the cans where able to reach the end temperature of the run, as shown in Figure 30. The heating of the cans was also similar between the top and bottom of the cans as well as between the sample and reference can. The greatest difference in heating was by the top sample heater after 325 K. However, this appeared to be as a result of heater position within the CCR as the sample bottom heater did not reduce its output and continued to heat in a similar manner to the reference can heaters.

After repeating previous tests on the liquid cans, Figure 50, the annular cans were run using scripts, shown in Appendix E, to test the function of the current GUI.[2, 3] The script used for the empty annular can test was the same as the toluene script and the same parameters were used for clear comparison between the liquid and annular cans.

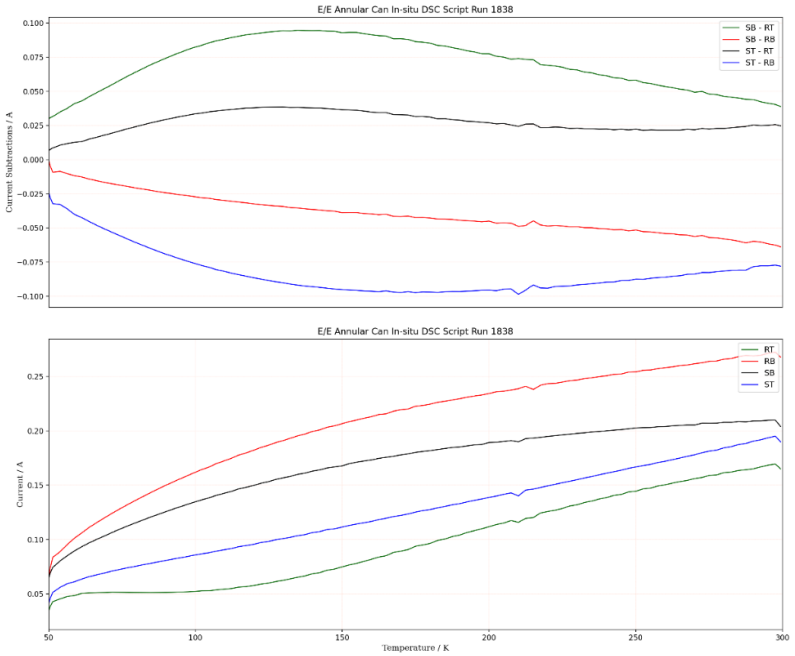

Figure 31: Results from the ex-situ calorimeter setup testing of the empty annular cans with high heater output. The script run was from 40 - 300 K at 5 K/min with a CCR offset of 10 K.

By comparing the script run, Figure 31, to a similar GUI run, such as Figure 26, it is shown that the script run produces more linear heater outputs. The decrease in heater outputs around 50 K in the GUI tests, are greatly reduced when using a script with a slight decrease in output by the reference top heater only. However, a shift, which was seen previously, around 210 K is more significant in the script run. [3]

Tapered Cans

Using the annular can results as a guideline, the tapered cans were tested with the same experimental settings to examine the effect of the cans' orientation and to compare with the annular cans. As the position of the cans within the CCR was seen to effect the individual heater outputs, in the testing of the empty Annular Cans, it was thought that the tapered cans would produce improved results as the different widths of the tapered cans, as shown in Figure 1, would have different thermal behaviour due to the wider side requiring more energy to heat to the same temperature as the smaller side. Tests using different CCR offsets, outputs and setups were completed as well as flipping the tapered cans around so that the wider side was facing up or down. Also, due to the heaters burning out during the annular can tests, the max temperature of future hot setup runs was limited to 400 K.

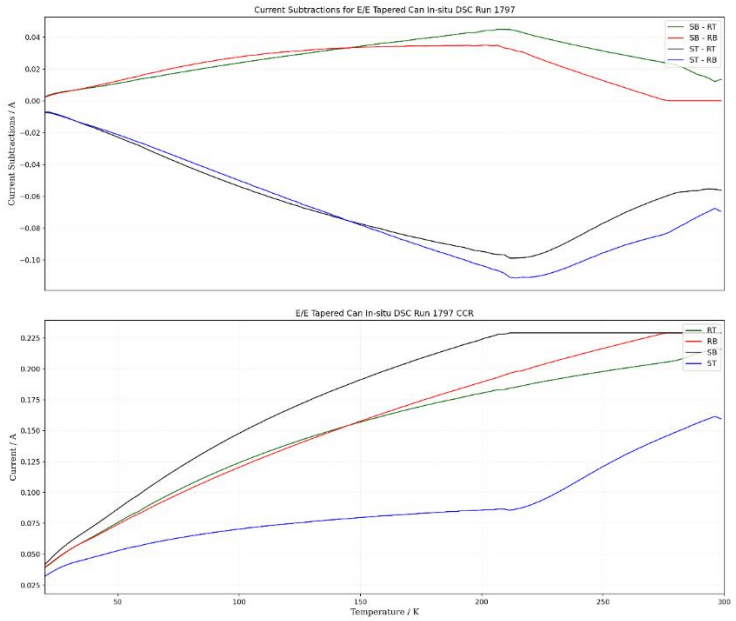

Figure 32: Results from the ex-situ calorimeter setup testing of the empty tapered cans with the wider side down and using medium heater output. The GUI run was from 20 - 300 K at 5 K/min with a CCR offset of 10 K.

In Figure 32, the medium output run with a smaller CCR offset displayed a similar heating pattern to the equivalent annular test, Figure 25. During the tapered can run, the sample top heater compensated for the sample bottom heater, whereas the reference can heaters exhibited the same behaviour during the annular can test. By comparing the current subtractions for the tapered can run with the annular, the tapered cans display worse current subtractions as the output subtractions are at a larger scale (0.04 to -0.10 A). Therefore, the current outputs, which should subtract to be as close to 0 A as possible, are shown to be affected by the tapered shape of the can as well as the position of the heaters within the CCR. The heaters further down into the CCR are generally required to output more to heat against the CCR temperature resulting in higher reference heater outputs. [3] The wider side of the tapered can also requires more heater output than the smaller side to maintain equal temperature due to the larger volume, which can be seen by the higher outputs of RB and SB.

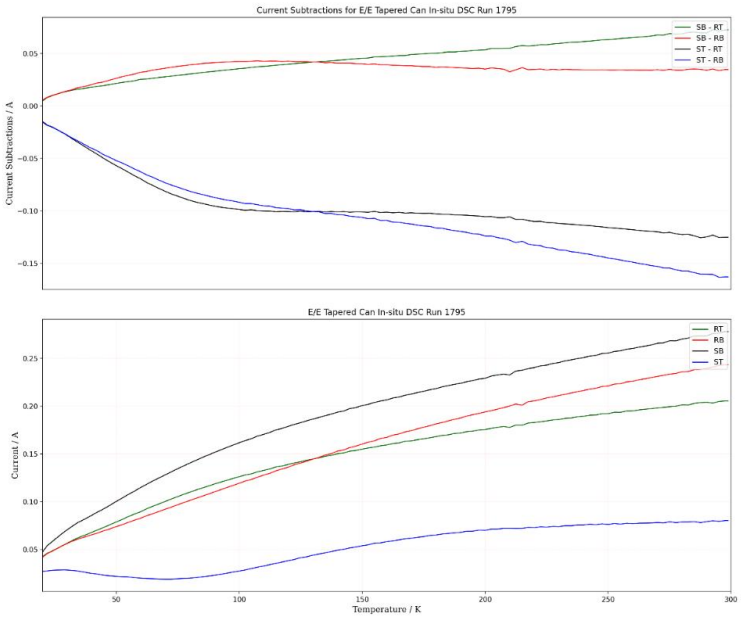

Figure 33: Results from the ex-situ calorimeter setup testing of the empty tapered cans with the wider side down and using high heater output. The GUI run was from 20 - 300 K at 5 K/min with a CCR offset of 10 K.

At high heater output, the sample top heater outputs significantly less than the other heaters and the bottom heater outputs the most, as seen in Figure 33. The pattern of the heater outputs is similar to the reference can in the equivalent test of the annular cans, Figure 26. Therefore, the high output is again the more optimal heater setting during cold setup runs. Upon initial comparison of the tapered and annular runs, the current subtractions are more linear for the tapered cans, which is desirable. However, the scale of the subtractions is larger meaning there is a greater difference between the highest and lowest heater outputs so the tapered can performs worse than the annular at high output.

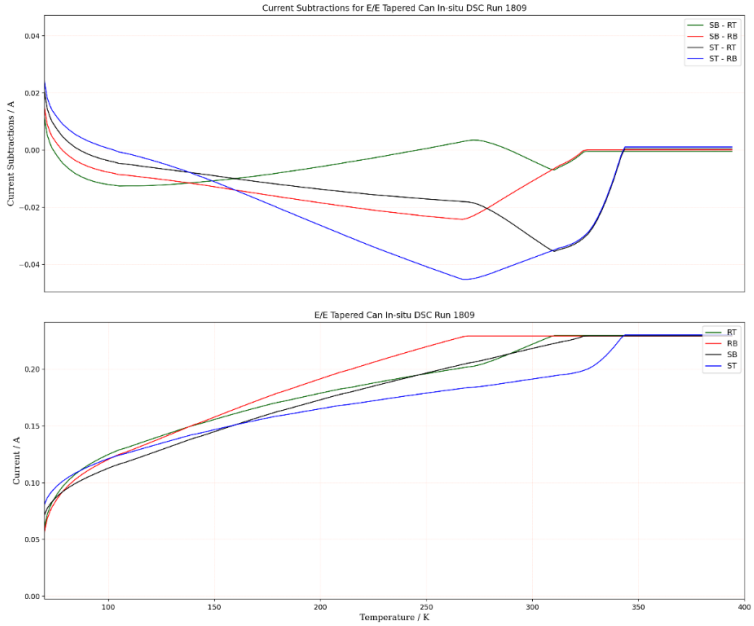

Figure 34: Results from the ex-situ calorimeter setup testing of the empty tapered cans with the wider side down and using medium heater output. The GUI run was from 70 - 400 K at 5 K/min with a CCR offset of 15 K.

Similarly to the medium output annular can test, the tapered can run did not reach the maximum run temperature as the heaters reached their maximum outputs and could not compete with the CCR temperature, as shown in Figure 34. The heating of the tapered can in comparison with the annular, Figure 29, is not as steady with the heaters reaching their max output at lower temperatures suggesting that the tapered can design is unfavourable to the annular.

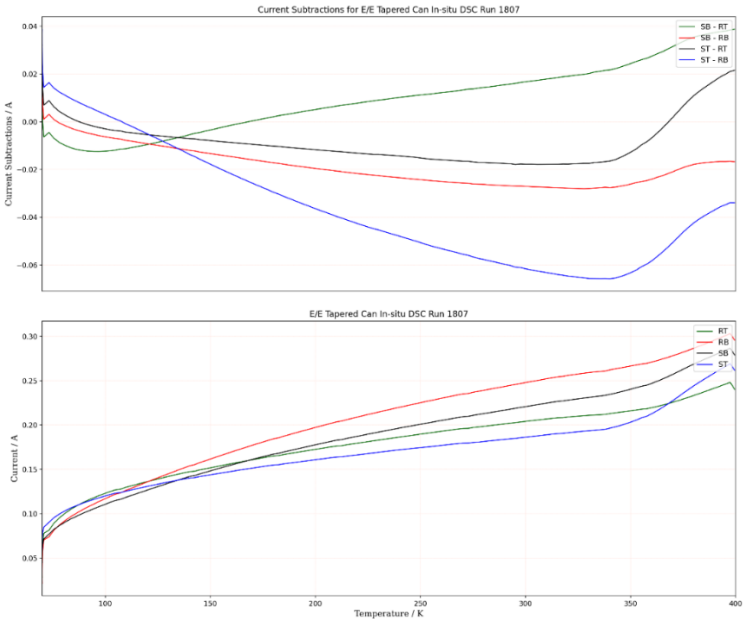

Figure 35: Results from the ex-situ calorimeter setup testing of the empty tapered cans with the wider side down and using high heater output. The GUI run was from 70 - 400 K at 5 K/min with a CCR offset of 15 K.

In Figure 35, it can be seen that the heaters all output over the temperature increase in an expected manor. However, there is a larger difference between the heater outputs than the annular test, Figure 30, and the comparisons between the heaters, through the current subtraction graphs, shows that the heaters on the tapered cans have a larger difference in outputs than the annular cans.

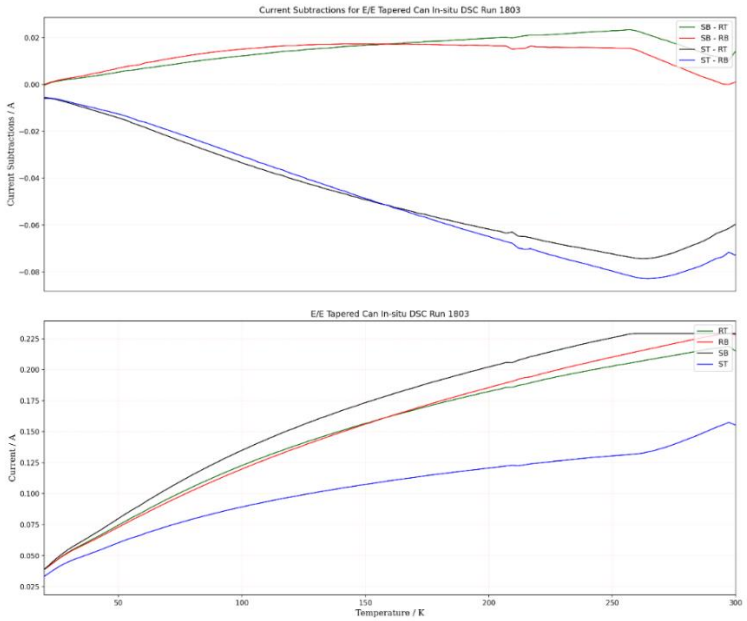

Figure 36: Results from the ex-situ calorimeter setup testing of the empty tapered cans with the wider side up and using medium heater output. The GUI run was from 20 - 300 K at 5 K/min with a CCR offset of 10 K.

The cold, medium output test with the wider side up, Figure 36, shows that the heater outputted more consistently than the wide side down run, Figure 32. This can be seen as the reference heaters and the bottom sample heater produce more similar outputs when the wide side is orientated upwards. The sample top heater, in the wide side up run, outputs more after 270 K to compensate for the sample bottom heater similarly to the wide side down run. However, with the wider side up, this change in output occurs at a higher temperature and has a more subtle shift.

In comparison to the equivalent annular test, Figure 25, the individual heaters outputted more steadily during the tapered can run and the sample bottom heater compromised for the top heater at a higher temperature (~260 K) than the reference heaters compromised during the annular run (~220 K). However, the tapered can current subtractions show an increasing difference between the top and bottom sample heaters as the temperature increases with a significant difference around 260 K. This is a greater difference in heater outputs than seen in the annular run.

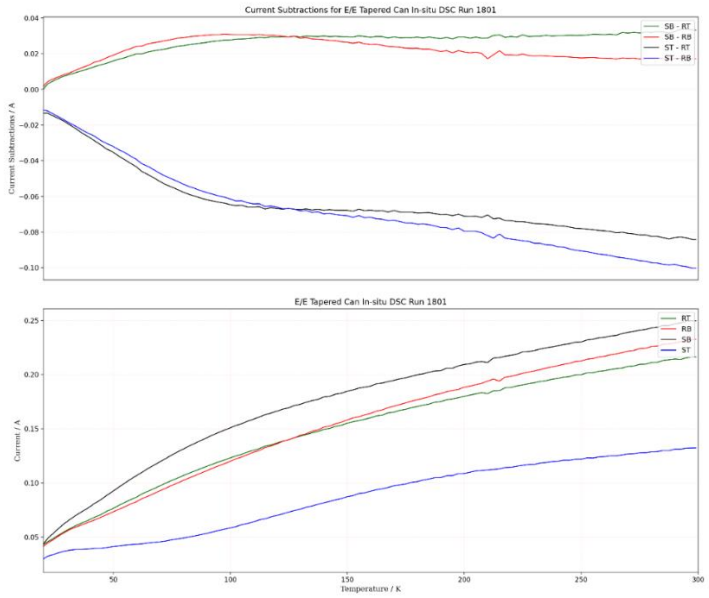

Figure 37: Results from the ex-situ calorimeter setup testing of the empty tapered cans with the wider side up and using high heater output. The GUI run was from 20 - 300 K at 5 K/min with a CCR offset of 10 K.

In Figure 37, the cold, high output run with the wider side up, the heater outputs are similar to the wide side down results, Figure 33. The wide up run displays the same output pattern as the wide down test but, with the wider side up, the heaters output more as the temperature increases. This is shown, through comparing Figure 37 with Figure 33, by the increased line gradients. Despite the higher heater outputs during the wider side up run, the currents subtracted to give a smaller scale than the wide side down run. This shows that the heaters outputted more consistently when the wider side was orientated upwards.

Compared to the annular can equivalent run, Figure 26, the current subtractions of the tapered can give a slightly larger scale and show a larger difference in current subtractions. The wide side up run, however, gave the more linear subtractions as the heaters outputted more steadily over the temperature range.

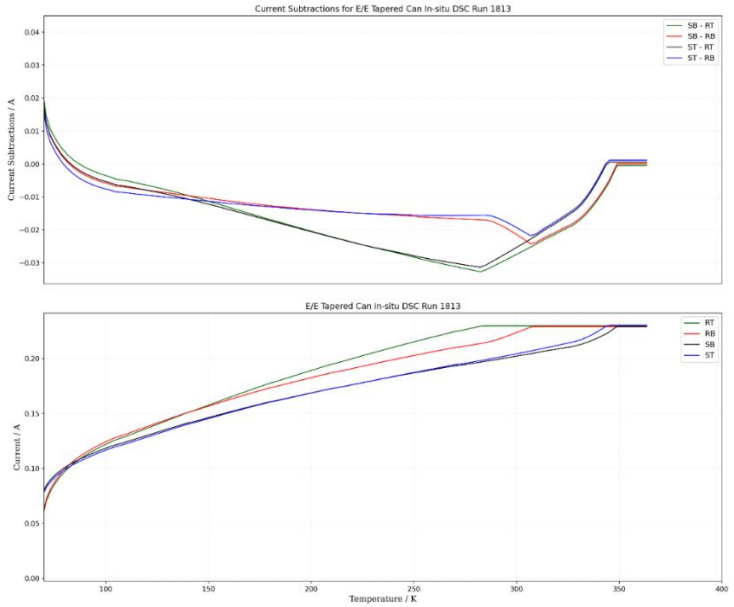

Figure 38: Results from the ex-situ calorimeter setup testing of the empty tapered cans with the wider side up and using medium heater output. The GUI run was from 70 - 400 K at 5 K/min with a CCR offset of 15 K.

The hot setup run using medium output with the wider side up, Figure 38, again did not reach the maximum set temperature similarly to the wide down run, Figure 34. Despite this, the wide up test shows the heater outputs of the sample and reference cans pair up with the sample can heaters outputting almost the same amount of current. The bottom reference heater, in the wide up test, was observed to compensate for the top heater around 270 K before all heaters, again, reach max output.

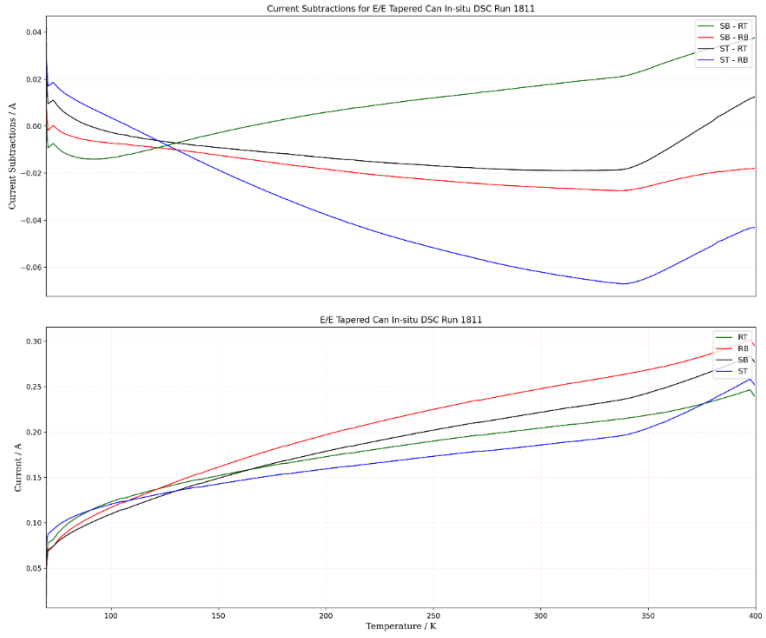

Figure 39: Results from the ex-situ calorimeter setup testing of the empty tapered cans with the wider side up and using high heater output. The GUI run was from 70 - 400 K at 5 K/min with a CCR offset of 15 K.

The high output runs, Figure 39 and Figure 35, produced very similar heater output results. The current subtractions of the wide side up run, Figure 39, show that the subtractions, after a shift around 340 K, produce more steady heater outputs over the increasing temperature. The subtractions for the wide side up and down runs have the same scale and show that the direct subtractions of the tops and bottoms of the cans (ST-RT and SB-RB) are closer to 0 A for the wide side up run. Therefore, the orientation does not differ the results significantly when using high heater outputs, however, the runs with the wider side up produce slightly better results.

In comparison to the high output hot run using the annular cans, Figure 30, the tapered can still shows a greater difference in heater outputs when orientated with the wider side up. This is made clear by the larger scale for the current subtractions. The difference between heater outputs also increases as temperature increases during the tapered run whereas the annular can run shows less deviation across the temperature range. Therefore, the annular cans design was proven to produce the most favourable results during the empty tests.

Liquid Cans

The liquid cans were run empty using the same script as the toluene test, as shown in Figure 51 in the Liquid DSC Can Testing of Toluene, to characterise the cans and to provide a comparison to the solid annular cans. The annular cans were focussed on as they produced better results than the tapered cans during the empty runs. As the liquid cans have previously been tested and performed well, the empty liquid can run would give insight into any differences between the solid and liquid cans that could hinder the solid can performance.[2]

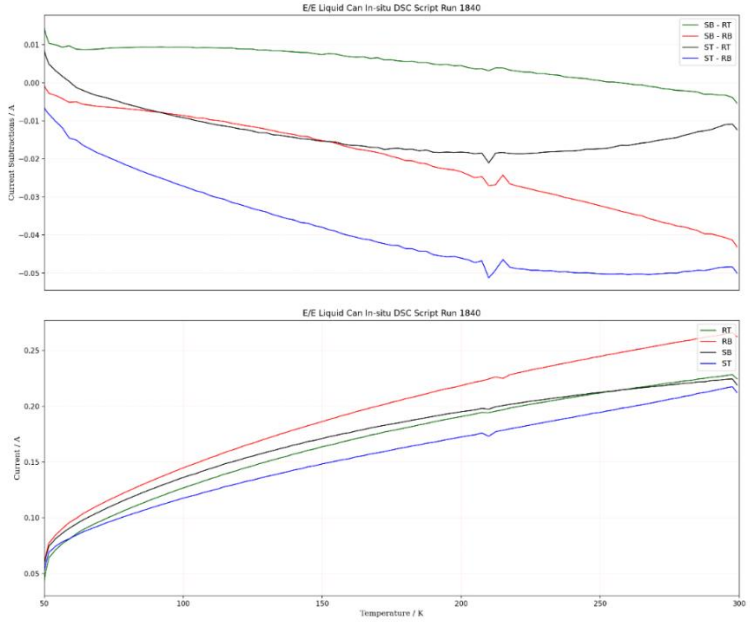

Figure 40: Results from the ex-situ calorimeter setup testing of the empty, original liquid cans with high heater output. The script run was from 40 - 300 K at 5 K/min with a CCR offset of 10 K.

The liquid cans show a steady increase in heater output as the temperature increases in Figure 40. However, an anomalous peak around 210 K, which has been previously

observed, is present and more significant in the outputs of the RB and ST heaters. [2, 3] In comparison with the annular can run using the same script, Figure 31, the heaters on the liquid cans output in a more consistent way than the annular can heaters. The difference in the outputs as the temperature increases is less in the liquid can run than the annular. This results in a smaller scale for the liquid can current subtractions and a more linear current pattern. A potential reason for this difference was the sensor position relative to the heaters as the liquid can sensors are placed further away from the heaters. However, during the testing of PVC, the annular can heaters were moved, and results showed no improvement.

10. Powder DSC Can Testing

The testing of the solid cans aimed to observe solid phase transitions. Various samples were tested with both the annular and tapered cans with focus on powder sample testing. However, during the powder tests, sample leakage and potential low sensitivity had proven to be problematic. Therefore, sensitivity testing continued using parafilm and different sachet types.

Sucrose

Sucrose had previously shown a transition at 419 ± 1 K, Figure 7, and literature states that a glass transition around 333 K exists. The sugar was tested in the annular and tapered cans in attempt to view the observed transition at 419 ± 1 K.

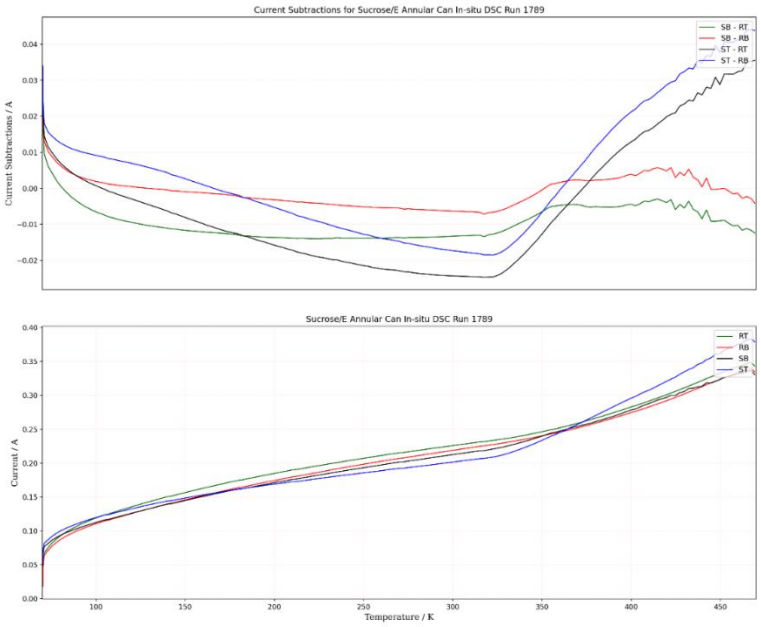

Figure 41: Results from the ex-situ calorimeter setup testing of the annular cans containing sucrose (1.70 g) with high heater output. The GUI run was from 70 - 470 K at 5 K/min with a CCR offset of 15 K.

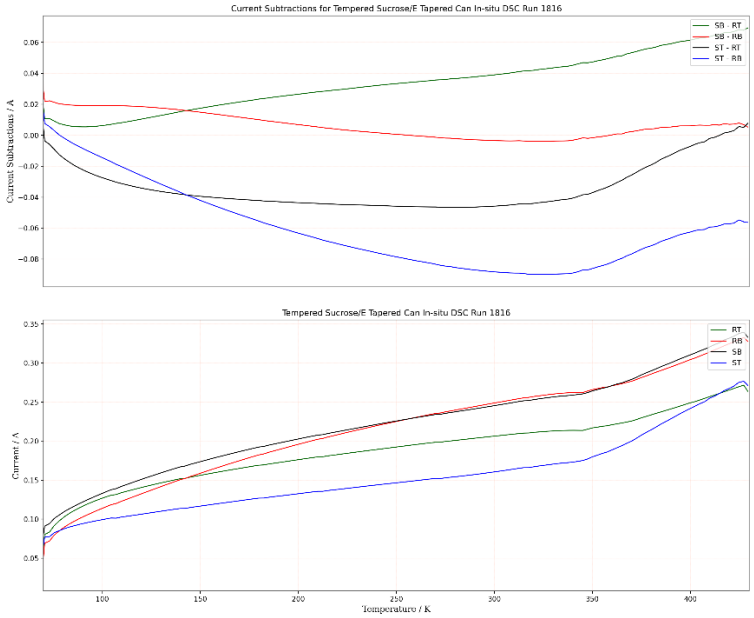

Figure 42: Results from the ex-situ calorimeter setup testing of the tapered cans containing sucrose (1.10 g) at high heater output with the wider side orientated downwards. The GUI run was from 70 - 430 K at 5 K/min with a CCR offset of 15 K.

The annular test with sucrose, Figure 41, shows interaction from the sample after 400 K. This interaction is clear in the current subtractions and can be confirmed to be real as it only affects the sample heaters. Comparison to the empty can run, Figure 30, also solidifies that the interaction is real as such peaks were not previously observed. Any transition between 300 and 350 K could not be confirmed due to the increase in the sample top current. This increase obscures any transitions and is confirmed by the empty run to be an artefact of the can. Also, during the run, the sucrose sample melted. However, due to the unsealed can design, the sample leaked resulting in no melting peak being observed.

To avoid the sample leaking and to try to observe the transitions of sucrose, the maximum temperature was lowered below the melting point and the tapered cans were tested. One proposed solution to containing samples within the tapered cans as they melt was to use silicon rubber O-rings to block the wider end of the sample space within the can. The tapered cans were better candidates for sealing as the solid metal core was more suited for the O-rings than the multiple cores used in the annular cans. Empty sachet and seal tests were conducted to check for any thermal interaction from the O-rings. Shown in Appendix C, runs at 5 K/min and using high heater output, suggested that the O-ring seals did not have a significant affect but at slower rates, interactions appear. Therefore, runs with the seals were restricted to the faster heating rate. However, the tapered can run, Figure 42, did not show any transitions from the sucrose.

To test if this could be a sensitivity issue, the melting sucrose was measured. This required the sample to be contained within the sample space of the can, so the liquid cans were used later in testing, as shown in Figure 53, as these cans can be fully sealed.

Lactose

Lactose was shown to have transitions at 404 ± 1 K and 452 ± 1 K, shown in Figure 8. This second transition was at too high a temperature for the cans as the max temperature needed to be limited to 450 K to avoid the can heaters burning out. The maximum heater

temperature could be raised from 400 K to 450 K as, after the Lakeshore was fixed, further testing with increasing maximum temperatures showed that the heaters could withstand the raised temperature, as shown in Figure 42 and Figure 43.

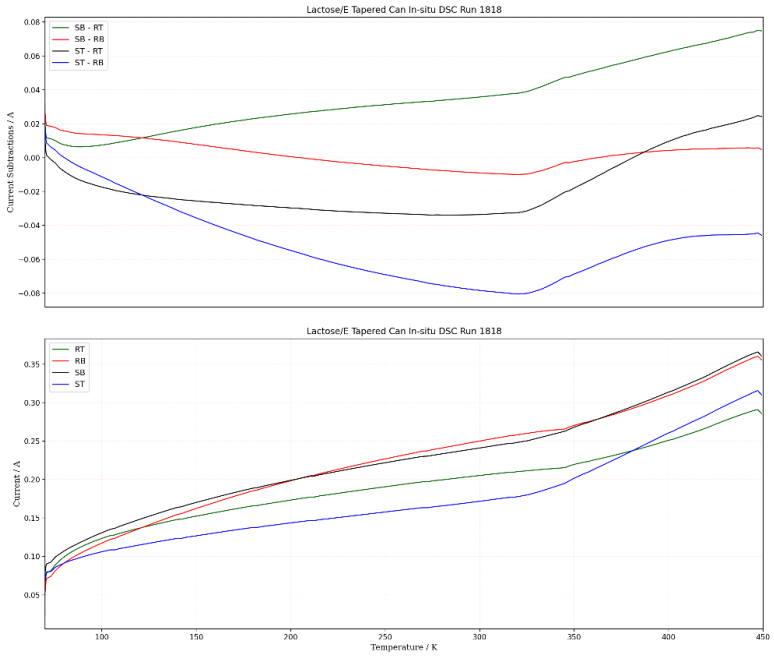

Figure 43: Results from the ex-situ calorimeter setup testing of the tapered cans containing lactose (0.67 g) at high heater output with the wider side orientated downwards. The GUI run was from 70 - 450 K at 5 K/min with a CCR offset of 15 K.

The transition around 400 K was subtle, Figure 8, and could not be seen in the lactose test using the tapered cans, Figure 43. As the melting point of lactose (503.75 ± 0.25 K) is higher than the heaters maximum temperature, the phase transition could not be tested for. Therefore, both the solid lactose sample was not used in further testing.

Issues with sample loading arose as less sample can fit into the tapered cans due to the solid metal core. This resulted in less thermal contact between the sample and can as, in order to place the sample sachet within the can, small gaps had to remain between the sachet and can. Thus, the tapered can tests no longer continued with the powder samples. However, the sample loading for the annular cans had more potential for viewing transitions as the cores can be expanded, as shown in Figure 1. By expanding the cores, the sample sachet is pressed against the inner can wall to allow for better thermal contact so testing continued with the annular cans.

PVC

During the testing of PVC, the can heaters were moved to the centre of the cans to examine the effects of heater position in relation to the sensors. This was suggested after comparing the liquid and solid cans to find any differences in the designs that could impact the function of the cans, Figure 1 and Figure 2. The script, shown in Appendix E, was edited to run at high temperatures and used for the PVC runs to test the script with a sample. The sachet used to hold the sample within the can was, also, changed to hold more powder to see if an increased amount of sample would produce a visible transition.

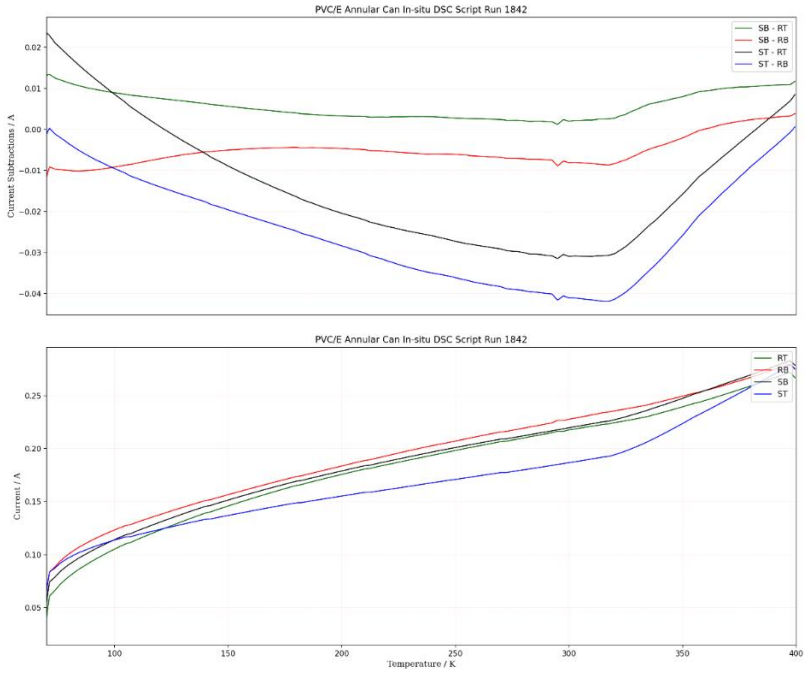

Figure 44: Results from the ex-situ calorimeter setup testing of the annular cans containing PVC (1.28 g) with high heater output. The script run was from 70 - 400 K at 5 K/min with a CCR offset of 10 K.

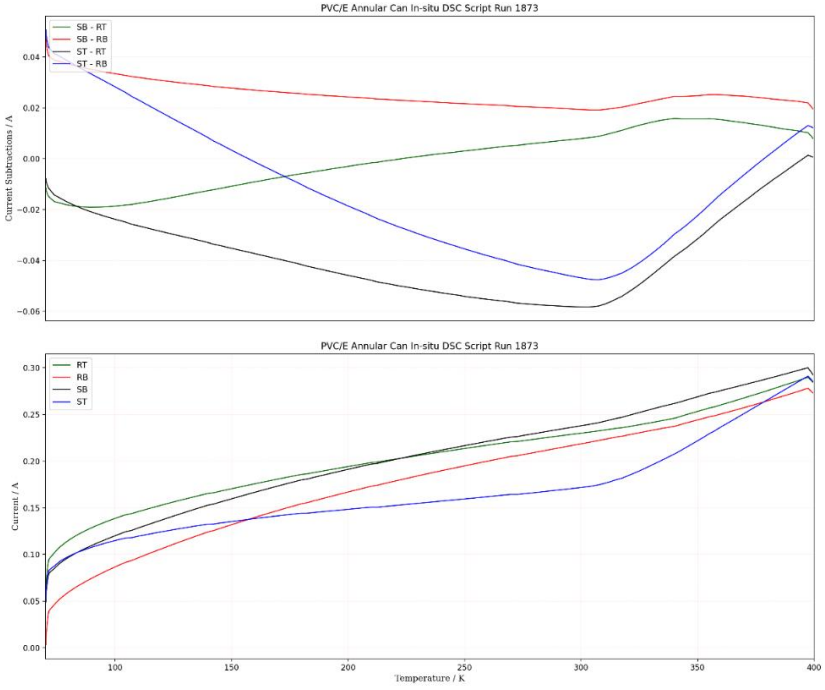

Figure 45: Results from the ex-situ calorimeter setup testing of the annular cans containing PVC (1.98 g) after moving the heaters to the centre of the can. The script run was from 70 - 400 K at 5 K/min with a CCR offset of 10 K and high heater output.

In Figure 44, the testing of PVC did not show the transition at 356.65 ± 0.25 K previously seen in the commercial DSC run, Figure 9. Visual inspection of the PVC powder after the in-

situ test confirmed that a transition did occur as the sample changed from a loose white powder to a pale pink brittle solid. As the transition was not observed with the cans, the heater position relative to the sensors was questioned and compared to the liquid cans, which had a larger distance between the heaters and sensors. Therefore, the heaters were moved to the centre of the can. After moving the heaters, in Figure 45, the transition was still not observed showing that the sensors were not overwhelmed by the heaters.

As the issue was unresolved by moving the heaters, the type of sachet holding the sample was changed. By using a 'TOSCA-style' sachet, an increased amount of sample could be held within the can from below 2 g to over a little over 3 g. With more sample filling the sample space, the aim was to increase the thermal contact between the can wall the sample as less empty space would remain between the sachet and the can.

The temperature of the run was also increased by 10 K after studying the log purges of the previous runs potentially showed the beginning of a shift caused by the sample at 400 K, as shown in Figure 66 in Appendix D. This shift was suspected to correspond the shift between 350.83 ± 0.25 K and 369.67 ± 0.25 K in the commercial DSC test, Figure 9.

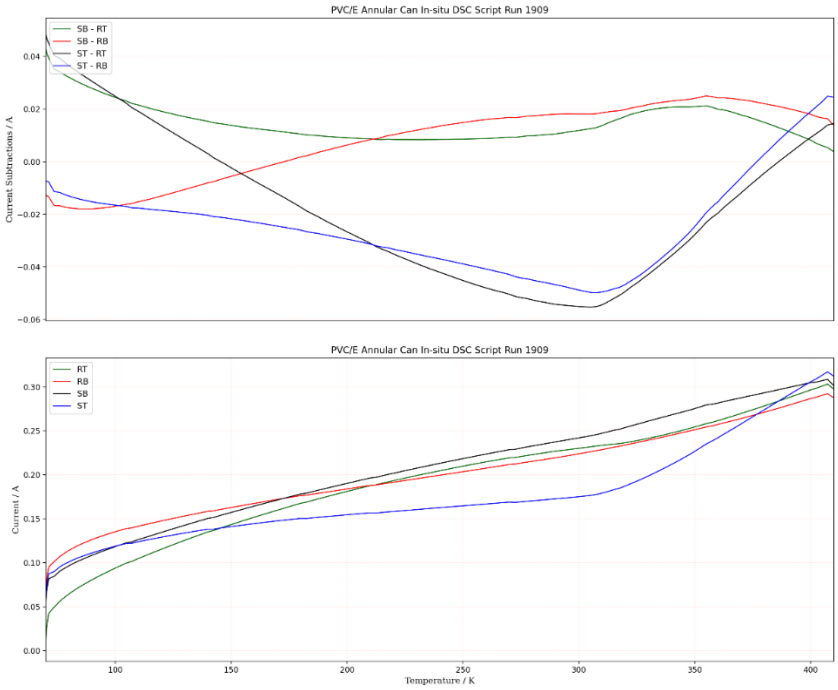

Figure 46: Results from the ex-situ calorimeter setup testing of the annular cans containing PVC (3.04 g) in a 'TOSCA-style sachet' with high heater output. The script run was from 70 - 410 K at 5 K/min with a CCR offset of 10 K.

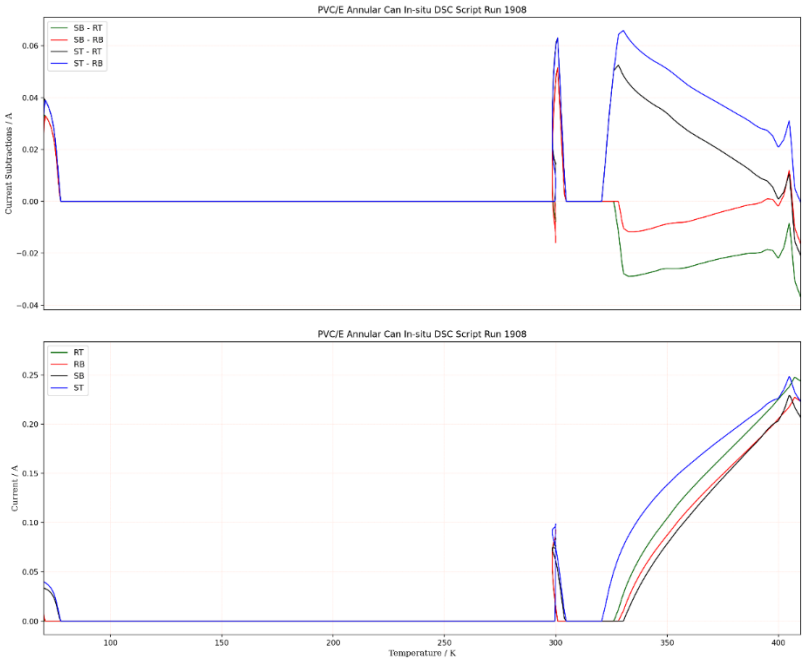

Figure 47: Results from the ex-situ calorimeter setup testing of the annular cans containing PVC (3.04 g) in a 'TOSCA-style sachet'. The log purge was from 410 - 70 K at 5 K/min with a CCR offset of 10 K and high heater output.

The heating ramp to 410 K, Figure 46, showed a potential interaction with the PVC around 355 K, which is in line with the commercial DSC shift in Figure 9. This interaction appears to affect the bottom sample heater the most, suggesting that the shift is real and that the powder had sunk to the bottom of the sample space. However, this is such a small interaction, with the most obvious current subtraction (SB-RB) giving a signal less than 0.005 A, that it is difficult to confirm.

However, in the log purge, Figure 47, a clear interaction with only the sample heaters around 400 K can be seen, which is suspected to correlate to the shift between 350.83 ± 0.25 K and 369.67 ± 0.25 K in the commercial DSC test, Figure 9. The increase in the shift temperature between the commercial and in-situ DSC tests could be due to the large difference in sample volume (around 3 g for in-situ and 0.004 g for the commercial DSC) and the sample environment, as the cans are unsealed unlike the DSC1 pans.

This peak, in Figure 47, is more resolved than previous purge results, Figure 66 in Appendix D. This suggests that an increased sample volume did improve the thermal contact between the sample and the can to provide a better signal. However, the peak at 278.50 ± 0.25 K seen in the commercial DSC results, Figure 9, cannot be seen, despite the large signal of this peak, as an artefact of the in-situ DSC around 300 K potentially blocks the peak. This signal was confirmed to be an artefact as the reference heaters are impacted and throughout the testing of the cans, this peak was consistent in the hot setup runs, shown in Appendix D.

Parafilm

As poor sensitivity due to a lack of thermal contact was an area of concern, parafilm was tested with and without a sachet. This aimed to test if the sachet had a significant impact on the contact between the sample and the can. The tapered can was, also, tested to compare the functionality of the different can designs. Parafilm, being an elastic film, could be

wrapped around the cores to fill the sample space as much as possible without leaking out of the can. When melted, parafilm is more viscous than the previously test sugars, so the melted sample leaking was not as much of a concern.

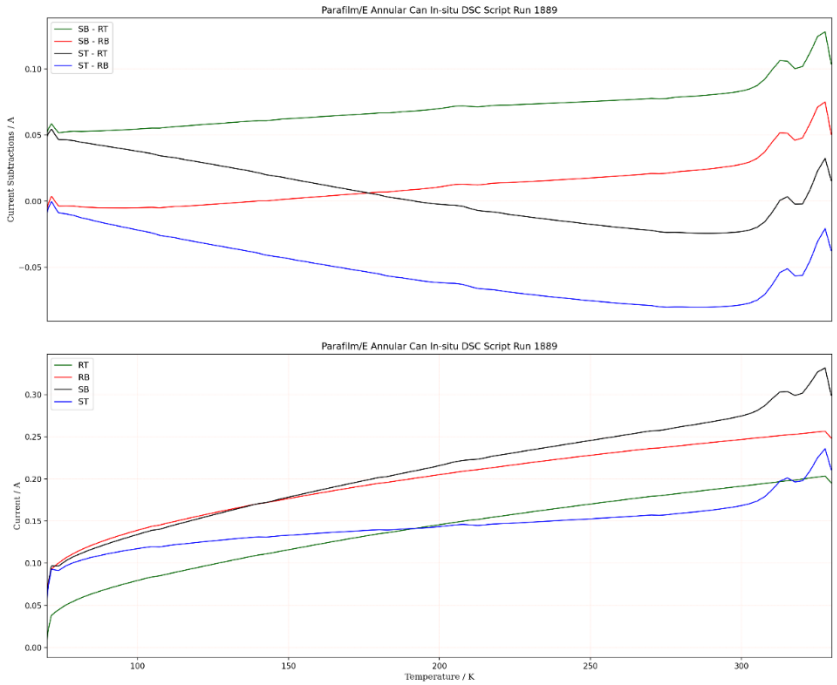

Figure 48: Results from the ex-situ calorimeter setup testing of the annular cans containing parafilm (4.76 g), without a sachet, with high heater output. The script run was from 70 - 330 K at 5 K/min with a CCR offset of 10 K.

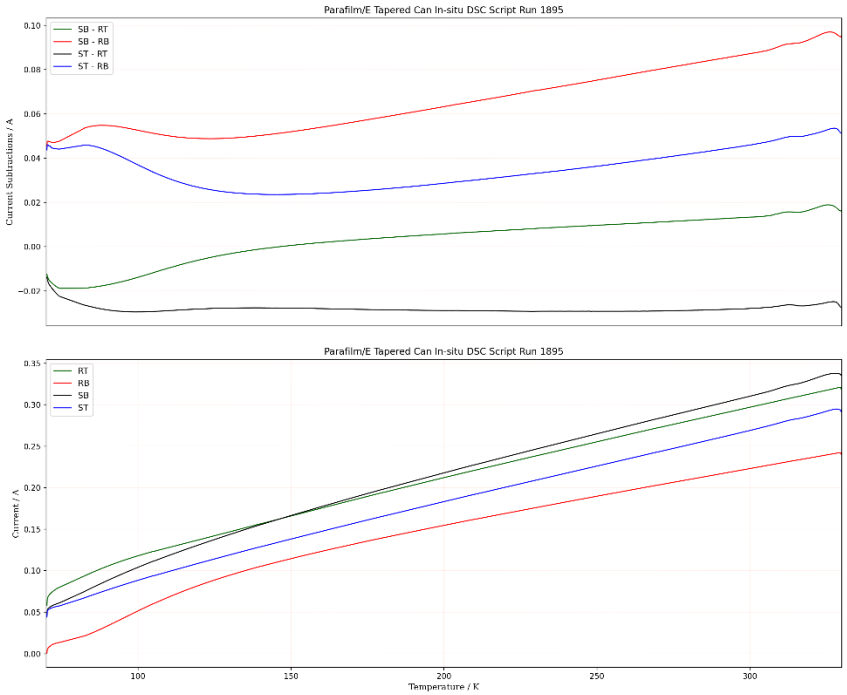

Figure 49: Results from the ex-situ calorimeter setup testing of the tapered cans (wide side down) containing parafilm (4.56 g), without a sachet but with an O-ring seal, with high heater output. The script run was from 70 - 330 K at 5 K/min with a CCR offset of 10 K.

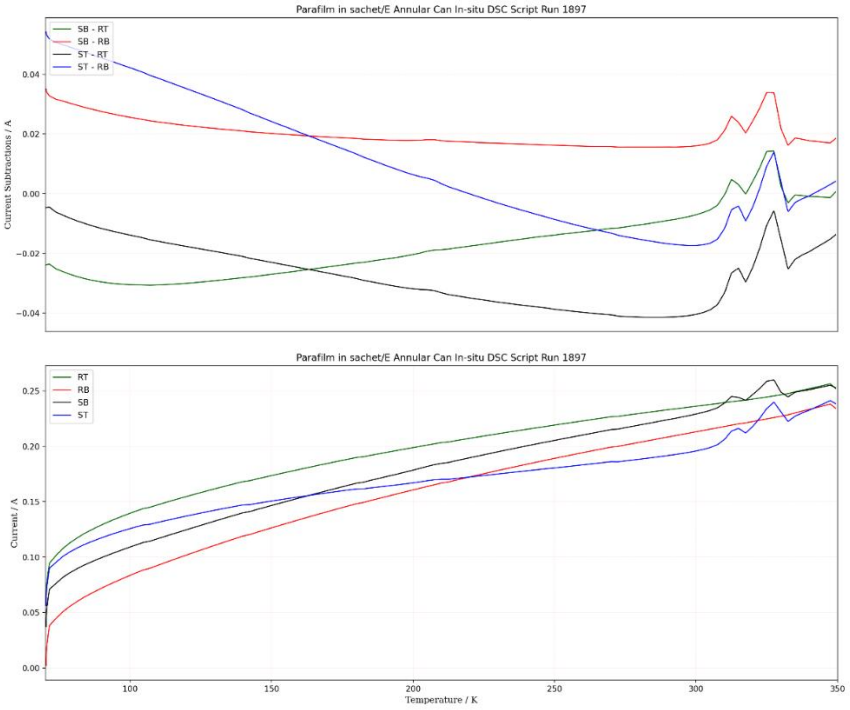

Figure 50: Results from the ex-situ calorimeter setup testing of the annular cans containing parafilm (2.34 g) in sachet with high heater output. The script run was from 70 - 350 K at 5 K/min with a CCR offset of 10 K. The max temperature was increased from 330 K to 350 K to observe the full peak.

In the commercial results for parafilm, the melting can be seen, in Figure 10, between 318 K and 339 K. The two major melting peaks could be seen in all results, Figure 48 - 50. By comparing the peak heights, the tapered can, Figure 49, clearly gave the poorest sensitivity despite containing a similar amount of parafilm to the equivalent annular can test, Figure 48. The peaks heights for the annular tests with and without a sachet initially show little difference in the current subtractions. However, the individual heater outputs show more clearly that, without a sachet, an increased signal was obtained. The current subtractions reflect this as the sachet run resulted in a smaller scale (0.04 to -0.04 A versus 0.1 to -0.05 A) and gave a major peak height, around 325 K, that was less than the run without a sachet.

However, the aluminium sachet itself cannot be concluded to be the cause of the decreased sensitivity as the amount of sample in the sachet run was significantly less than the runs without. Instead, the sachet's restriction of the sample mass and shape, due to the rigidity of the aluminium sachet, is more likely to be the cause of such issue. This emphasised the importance of the metal cores in the sample's interaction with the heaters and sensors on the can as, in the run without a sachet, the cores expanded to push the parafilm directly against the can wall as well as around the cores, in which the sensors sit. With the sachet, the parafilm was pushed against the can wall but not around the cores as the sachet restricted the parafilm's movement during the expansion of the cores.

The peak heights from the in-situ DSC tests when compared to the commercial DSC test, also, give an indication of the potential difference in sensitivity between the two instruments. The commercial test, Figure 10, resulted in a total peak height (from the base of the minor shoulder peak to the top of the major peak) of around 4.7 mW. In the in-situ test, Figure 48, the same peak had a height of around 1.2 A (7.2×10^4 mW). This gives an estimated ratio of around 1.5×10^4 mW resulting in the smaller peaks, which can be seen with the commercial DSC, not being observed using the in-situ DSC. This is due to the in-situ DSC requiring more power than the commercial DSC meaning that smaller peaks will be lost in the background current. However, comparing the base of the same peak gives a similar peak width of around 26 K, showing that the in-situ DSC produces similar temperature readings to the commercial DSC despite the difference in peak height.

11. Liquid DSC Can Testing

During the testing of the liquid cans, both the can designs were run to find determine whether the sensor position would have a significant effect on the results. Tests using the script and GUI were, also, run to test the function of the GUI. The benchmarking of the cans focussed mainly on water-based samples with differences in melting point temperatures. The deviation from the melting point of water varied between each dissolved sample and allowed for the temperature sensitivity of the in-situ DSC cans to be evaluated.

Toluene

As toluene had been previously tested, it was used to check the function of the setup.[2] This was required due to the technical issues experienced with the setup and the difficulty of observing transitions with the solid cans. The toluene tests, also, would test the GUI through comparison with the script runs.

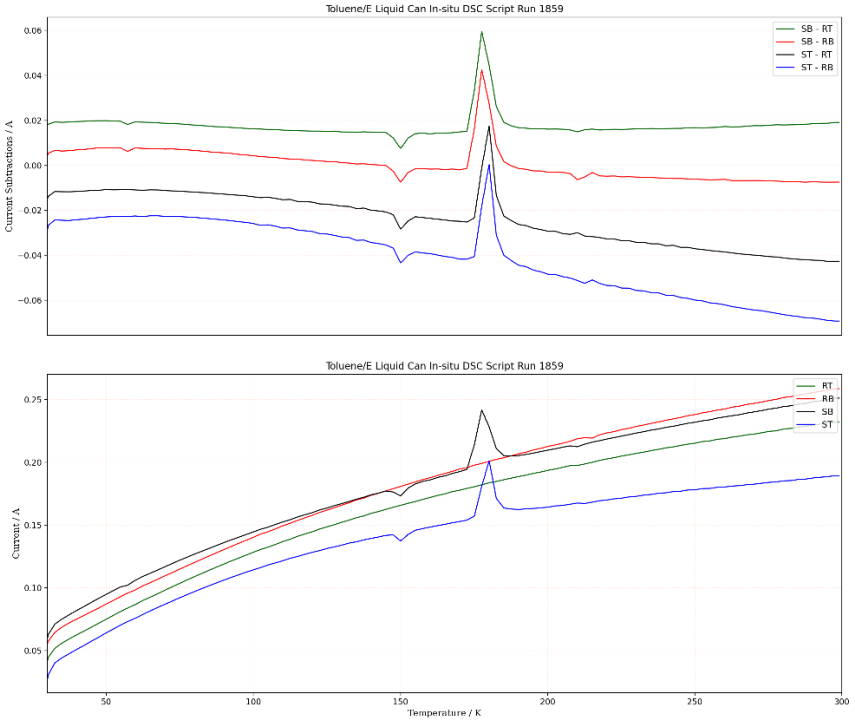

Figure 51: Results from the ex-situ calorimeter setup testing of the original liquid cans containing toluene (2.51 g) with high heater output. The script run was from 40 - 300 K at 5 K/min with a CCR offset of 10 K.

The toluene test, which was run with the original script as shown by Figure 67 in Appendix E, reproduced the results previously seen.[2] In Figure 51, results show the cold crystallisation and melt around 150 K and 176 K respectively, which is in line with the previously seen melt in Figure 13. The shift around 210 K corresponds to the prementioned anomalous peak.[3] Therefore, the setup was functional as peaks could be observed as done so in the past.

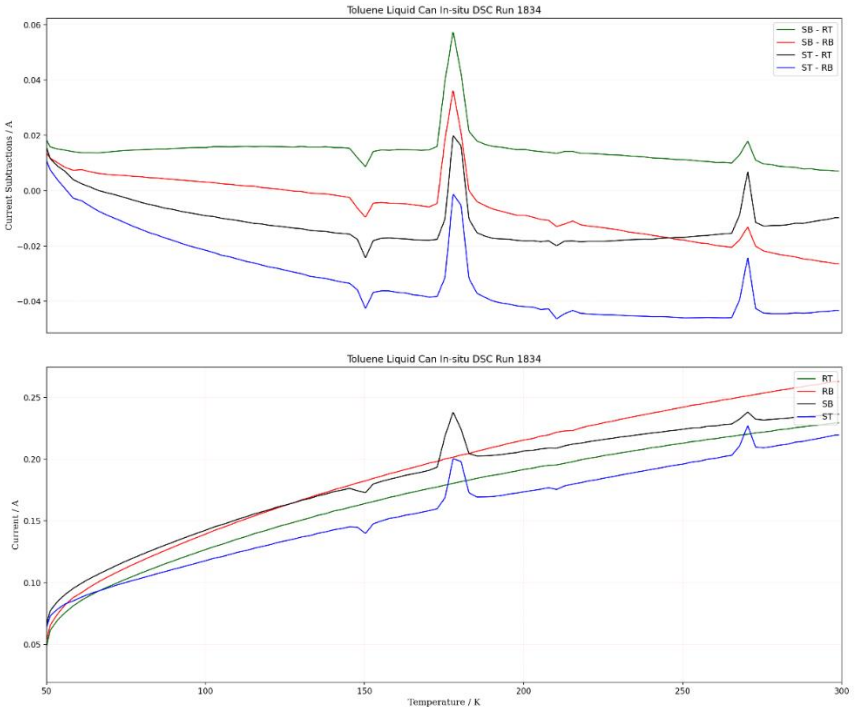

Figure 52: Results from the ex-situ calorimeter setup testing of the original liquid cans containing toluene (2.63 g) with high heater output. The GUI run was from 40 - 300 K at 5 K/min with a CCR offset of 10 K.

The GUI run, Figure 52, showed the same peaks as the script run, Figure 51, barring the extra peak around 270 K, which is due to a trace amount of water remaining in the can after cleaning. Therefore, the GUI was proven to be functional. It should be noted, however, that the heater outputs throughout the two runs behaved slightly differently resulting in decreasing gradient seen in the SB-RB current subtraction and the increasing spacing between current subtractions from 50 K to 100 K.

Recrystalised Sucrose

To test for the melting point of solid sucrose the liquid cans were used as these are designed to be fully sealed. In order to test solid sucrose, the sugar needed to be dissolved in water and recrystalised within the liquid can. This could, also, provide an alternative method for testing solid samples.

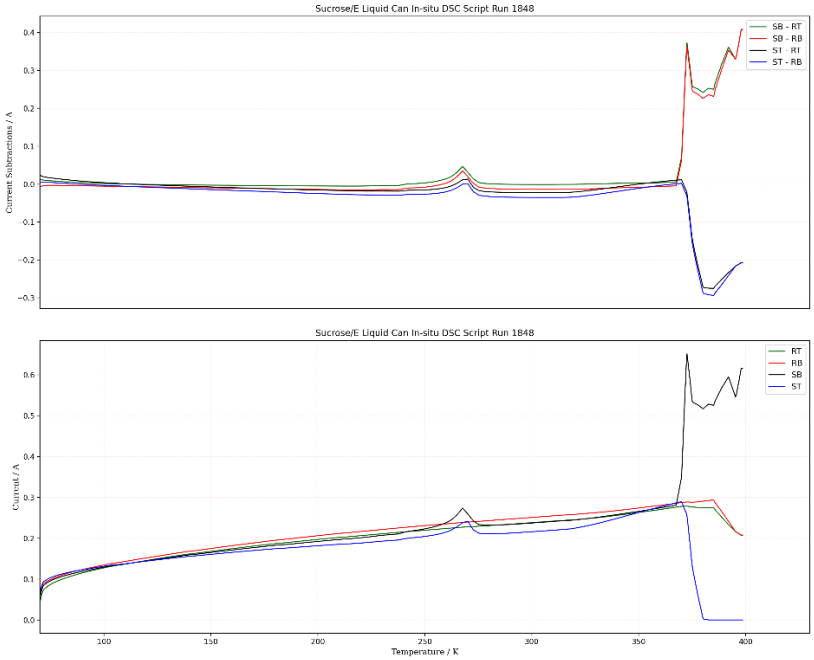

Figure 53: Results from the ex-situ calorimeter setup testing of the original liquid cans containing recrystallised sucrose (2.13 g) with high heater output. The script run was from 70 - 350 K at 5 K/min with a CCR offset of 15 K.

In Figure 53, exothermic peaks can be seen around 270 K and 370 K followed by peaks closer to 400 K. The first peak corresponds to ice melting while the peak at 370 K shows water boiling. Thus, showing that the recrystallised sugar had not fully dried, so water remained trapped inside the can. The boiling caused build-up of pressure inside the can as the temperature increased resulting in the drop in output from the top sample heater (SB) as the indium seal was blown out and the sample leaked.

Caffeine Solution

A solution of caffeine was tested in both types of liquid can, shown in Figure 2, to compare the effects of the different sensor placements on the cans. In the commercial DSC test, Figure 11, peak temperatures of 284.17 ± 0.25 K and 398.83 ± 0.25 K were found to correspond to the melting and boiling of the water in the solution. Therefore, the test was run using the cold setup (20 K to 300 K) to keep well below the boiling point of the solution.

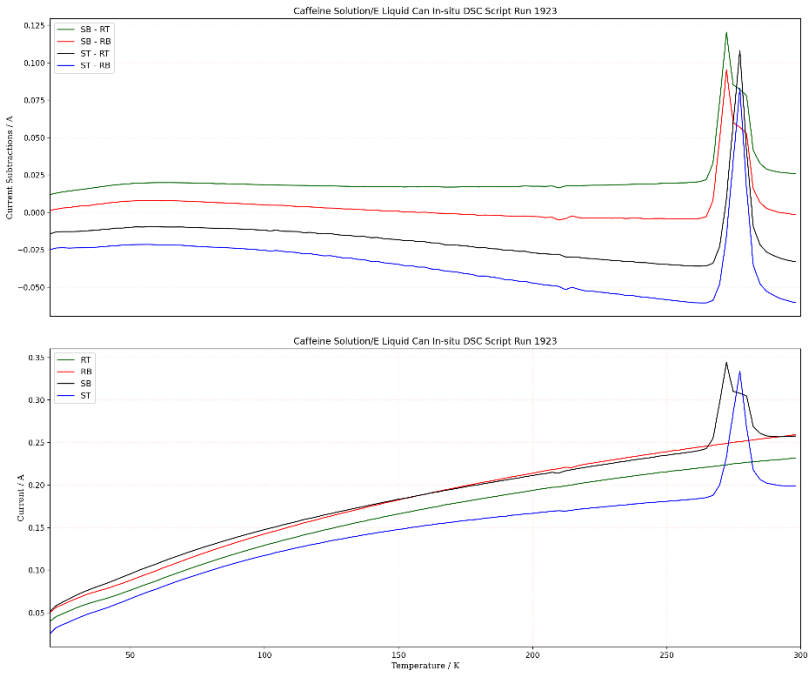

Figure 54: Results from the ex-situ calorimeter setup testing of the original liquid cans containing caffeine solution (2.40 g) with high heater output. The script run was from 20 - 300 K at 5 K/min with a CCR offset of 10 K.

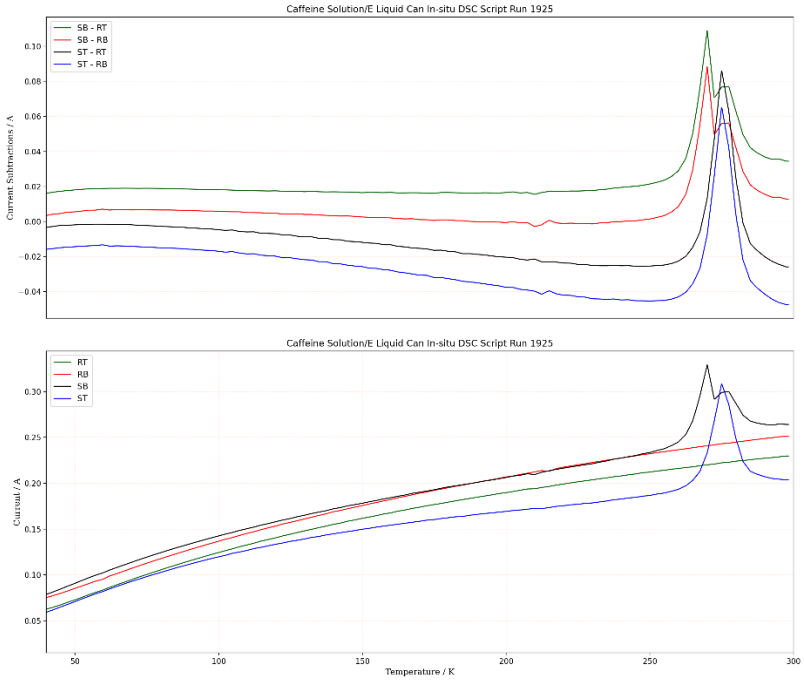

Figure 55: Results from the ex-situ calorimeter setup testing of the new liquid cans containing caffeine solution (2.76 g) with high heater output. The script run was from 20 - 300 K at 5 K/min with a CCR offset of 10 K.

In both Figure 54 and Figure 55, the caffeine solution was shown to melt around 275 K, which corresponds to the melting of frozen water. The peak shoulder seen in the bottom sample heater output (SB) could be due to the settling of any recrystallised caffeine that formed during cooling as the larger caffeine structures would hinder the water from melting

at a consistent temperature down the can. This shoulder was not seen in the commercial DSC test, Figure 11, as the sample size was much smaller for the DSC1 pans than the liquid cans. Therefore, more caffeine would have been present in the in-situ liquid can tests.

By comparing the new and original liquid can designs, it can be concluded that the sensor position around the can has little effect on the results as the same peaks can be seen in both tests. It should be mentioned that the peaks found from the newer design appeared to be slightly broader. The currents outputted by the heaters during the new design run were, also, slightly less than the outputs during the original can run. These differences were not significant and, so, the new cans were not tested further.

Milk

Due to issues with the cooling of the in-situ DSC, which were found during the Empty DSC Sample Can Testing, the recrystallisation of the milk sample could not be tested for. Therefore, only testing for the melting point around 280 K, seen in Figure 12, went ahead.

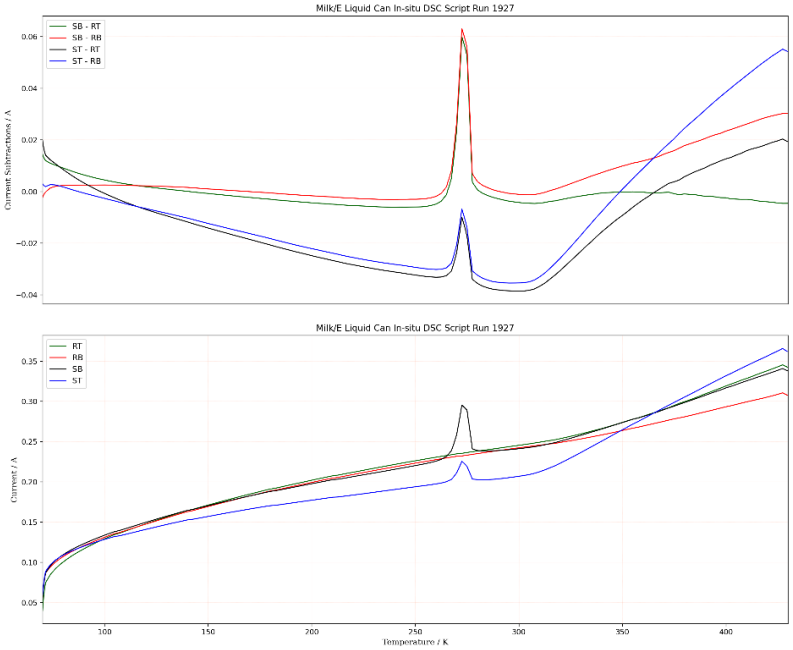

Figure 56: Results from the ex-situ calorimeter setup testing of the original liquid cans containing milk (0.85 g) with high heater output. The script run was from 70 - 430 K at 5 K/min with a CCR offset of 10 K.

The in-situ testing of the original can containing milk, Figure 56, showed a melting peak around 270 K. This peak is at a lower temperature, by around 10 K, than previously seen in the commercial testing of the milk sample. This decrease in temperature could be due to the sample degrading while in storage. However, the liquid can still gave a clear result even with a smaller amount of sample (0.85 g) suggesting the can has a good sensitivity. The SB heater current outputted more than the ST heater as the sample settled to the bottom of the can. This emphasises the need to ensure the can is fully filled without air bubbles to obtain a full signal from the top heater.

Tea Solutions

Tea solutions run with the commercial DSC showed that the tea had small effects on the melting point of the water in the solution. These differences in temperature requires high sensitivity to differentiate and, so, were used to test if the in-situ DSC cans could obtain such high sensitivity. All tests were run in cold setup (maximum temperature is 300 K) to remain well below the boiling temperatures of the solutions.

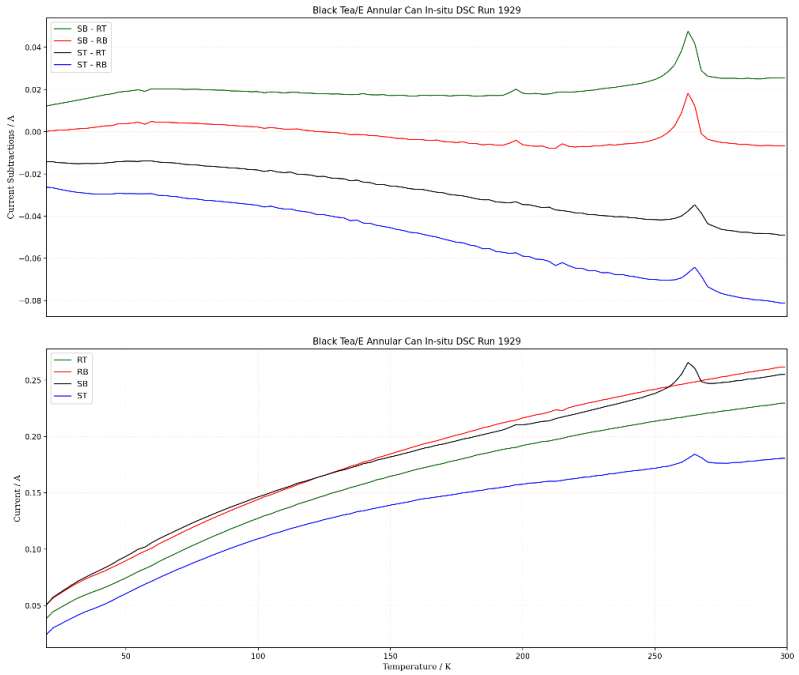

Figure 57: Results from the ex-situ calorimeter setup testing of the original liquid cans containing black tea (0.44 g) with high heater output. The script run was from 20 - 300 K at 5 K/min with a CCR offset of 10 K.

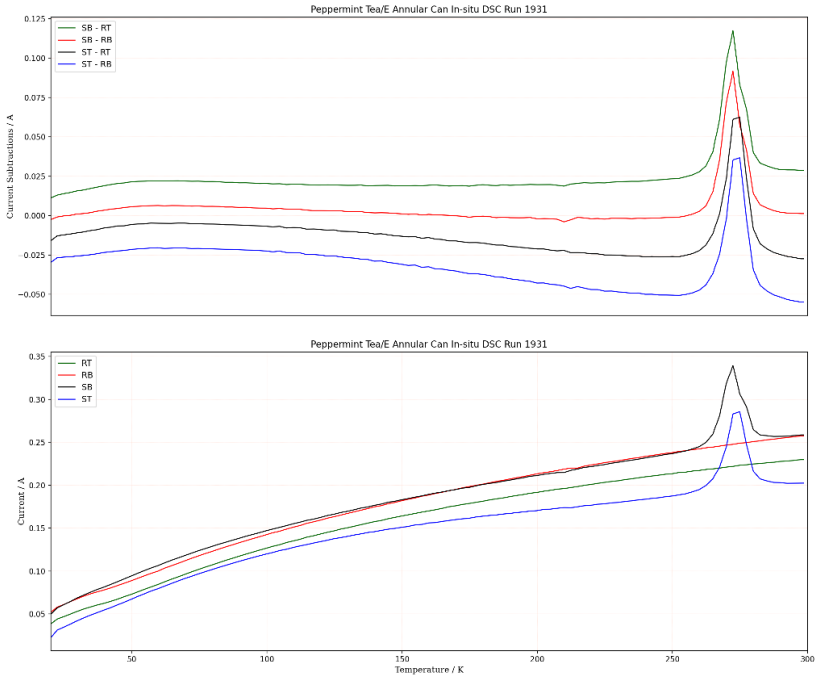

Figure 58: Results from the ex-situ calorimeter setup testing of the original liquid cans containing peppermint tea (1.89 g) with high heater output. The script run was from 20 - 300 K at 5 K/min with a CCR offset of 10 K.

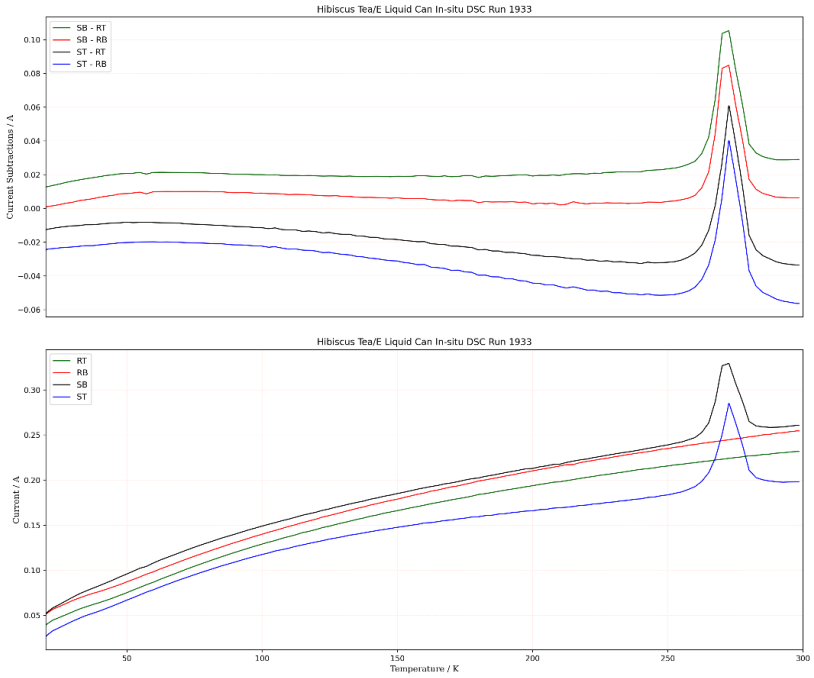

Figure 59: Results from the ex-situ calorimeter setup testing of the original liquid cans containing hibiscus tea (2.36 g) with high heater output. The script run was from 20 - 300 K at 5 K/min with a CCR offset of 10 K.

In the commercial DSC tests, black and hibiscus tea both showed melting points around 284 ± 0.25 K, as shown in Figure 14 and Figure 15, while peppermint tea was observed to melt at 276 ± 0.25 K, in Figure 16. Hibiscus tea in the in-situ test, Figure 59, showed a lower

melting temperature of around 275 K while black tea produced a significantly lower peak temperature closer to 260 K, as shown in Figure 57. The melting temperature of peppermint tea, Figure 58, produced the most similar result to the commercial run, Figure 16, with a peak temperature of around 275 K.

The lowering of melting temperatures seen within the tea results could be as a result of the varying amounts of sample. The expected behaviour of samples under DSC study is to show an increase in peak temperature as sample mass increases due to more thermal energy being required to weaken the increasing number of bonds within the sample. This can be observed between the black and hibiscus teas as the samples were shown in the commercial tests to exhibit the same melting temperature. However, the mass of the black tea within the can was significantly less than the hibiscus tea (0.44 g versus 2.36 g). The lack in mass of sample implies that the sample space inside the liquid can was either contaminated or contained trapped air. Such contamination could include previous samples or solvents from cleaning and could, also, result in the lowering of peak temperature. Therefore, the amount of sample within the liquid can could have a significant effect on the test results and care should be taken when sample loading and cleaning the cans.

Sugar Solutions

Similarly to the tea solutions, sugar solutions were tested to observe the melting point temperature of water in order to benchmark the liquid cans. The slight variance in melting point in the commercial testing was observed with lactose exhibiting the highest temperature.

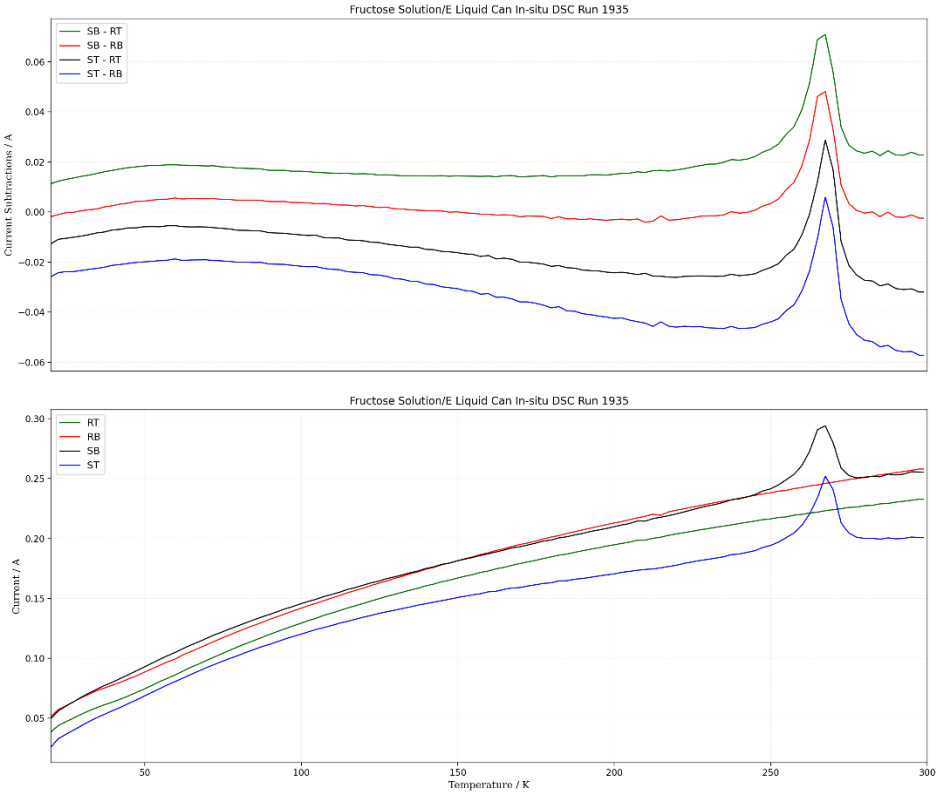

Figure 60: Results from the ex-situ calorimeter setup testing of the original liquid cans containing fructose solution (2.54 g) with high heater output. The script run was from 20 - 300 K at 5 K/min with a CCR offset of 10 K.

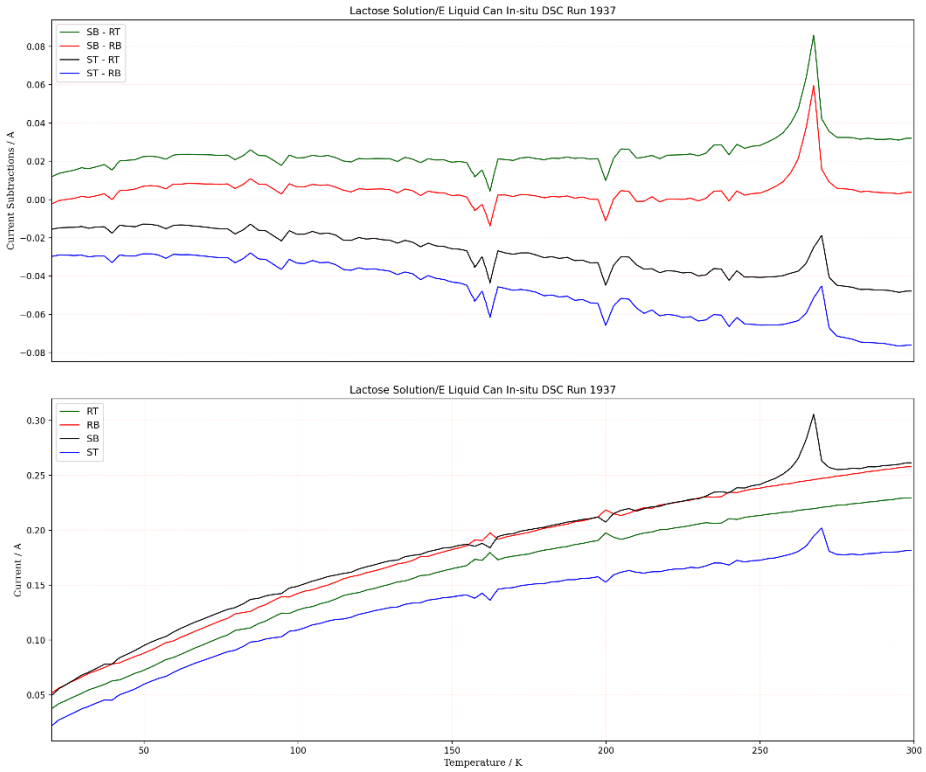

Figure 61: Results from the ex-situ calorimeter setup testing of the original liquid cans containing lactose solution (1.05 g) with high heater output. The script run was from 20 - 300 K at 5 K/min with a CCR offset of 10 K.

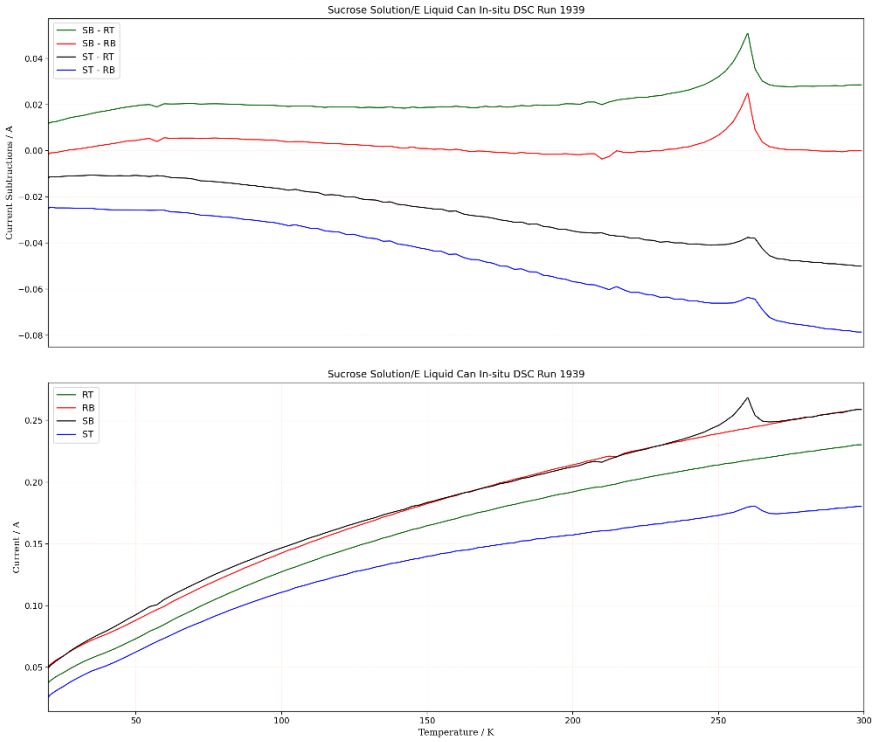

Figure 62: Results from the ex-situ calorimeter setup testing of the original liquid cans containing sucrose solution (1.27 g) with high heater output. The script run was from 20 - 300 K at 5 K/min with a CCR offset of 10 K.

In the commercial testing of the sugar solutions, the melting point of the fructose and sucrose solutions were found to be the same at around 274 ± 1 K, as shown in Figure 17 and Figure 19. In the can tests, the sucrose and fructose solutions produced melts around 255 K and 260 K, respectively. This increase in temperature difference is likely due to the difference in the mass of the samples as less sucrose solution fit into the sample space than the fructose solution due to air becoming trapped in the can. The mass of the lactose solution was similar to the mass of the sucrose solution and showed a similar melting temperature. In the commercial DSC tests, lactose exhibited the highest melting temperature at 278.85 ± 0.25 K, Figure 18. Therefore, all solutions produced lower melting temperatures during the in-situ tests. This could be due to the sugar recrystalising during the slow cooling of the CCR before the heating run starts. Therefore, only the melting of ice was measured as the sugars had less interaction when recrystalised.

12. Conclusions and Outlook

In conclusion, a greater understanding of how the in-situ DSC currently works was gained through troubleshooting the in-situ DSC setup. The warnings and the log plotter function in IBEX were found to be useful when identifying and solving problems as warnings are given to pinpoint the effects of technical issues and the log plotter can be used to view the heater and sensor readings in real time as well as being able to review previous runs. This will allow for any potential technical issues in the future to be fixed with ease. For example, tripping heaters, which are flagged through warnings in IBEX, and incoherent results point towards an electrical issue. Together these two issues suggest a problem with the Lakeshores, as previously found and fixed.

The optimal experimental conditions were found, through the testing of the empty cans and during sample testing, to require CCR offsets of 15 K and 10 K in the hot and cold setups, respectively. The maximum temperature for hot setup runs was required to be limited to 450 K, despite the pt-100 sensors allowing for readings up to 470 K, to sustain the heaters. Meanwhile, the minimum hot setup temperature remained at 70 K and cold setup tests can run at the full sensor range (20 to 300 K). To achieve higher temperatures, a review of different types of heaters could take place for future development. Current testing also obtained that the best characteristics using a rate of 5 K/min with less optimal results gained during slower heating rates, shown in the Empty DSC Sample Can Testing. Future development of the cans should aim to achieve stable baselines for slower rates up to 0.5 K/min, which could require a change of materials.

Testing of the solid in-situ DSC cans showed that transitions within solid materials can be observed with the current setup and highlighted some key features of the cans that could be further developed in the future. As the contact of the sample with the inner cores and wall of the can is restricted by the aluminium sachet, the inner cores of the cans could be edited to allow for a greater amount of sample to be held within the can. The current solution to hold more sample was to use a different style of foil sachet and by using a ‘Tosca-style’ sachet improvements in the results were seen. To further develop the solid cans, the sample loading could be reviewed through the testing of different sample loading methods, including the potential of pressing the powders into a cylindrical shape before placing into the can using a mould. One suggestion for loading the powders, is to use an aluminium foil sachet similar to the ‘Tosca-style’ sachet to create a mould of the sample space and load the sample into the sachet whilst the sachet remains in the can. A key area to review further is the melting of solids within the cans and the potential for sealing the solid can designs.

The liquid can results observed clear phase changes but showed constant dissimilarity to the commercial DSC tests as the peak temperatures were consistently lower, as emphasised in

the testing of Tea Solutions and Sugar Solutions. This was potentially due a difference in pressure within the commercial DSC pans and in-situ DSC cans. Also, air and water regularly became trapped within the sample space, which shows that the cans can be difficult to clean. As the cans are made from aluminium, a user cannot see whether residue remains within the can. Therefore, a method for ensuring the cans are completely clean needs to be reviewed especially for cases where solids are produced within the cans.

In the future, focus should initially be placed on examining the cooling issue for the functionality of the in-situ DSC setup. Currently, cooling produces inconsistent results with some replicating the results of the tripping heaters and all results show consistent anomalous peaks, as shown in Appendix D. Therefore, peaks that occur during the cooling section of the test cannot be observed or are difficult to confirm as a result of the sample. Work with the Cryogenic team has begun, and various tests have been completed, as shown in Appendix D. However, the cause of the anomalous peaks is currently unconfirmed but is thought to be a result of how measurements are taken during the Log Purge, which is the cooling of the system before a run starts. A suggestion is to use the script to set up a run cooling from maximum to minimum temperature using a negative ramping rate (-5 K/min) to test whether this improves the result seen in Figure 83 in Appendix D.

13. Side Project

During periods of downtime, a side project studying the reagents for the production of the thianthrene cation radical tetrafluoroborate was carried out. These reagents were thianthrene and nitrosonium tetrafluoroborate, as shown in Figure 63. Thianthrene has undergone varies studies previously to study the geometric changes that accompany its redox activity. Nitrosonium tetrafluoroborate itself exhibits interesting structural properties and became the focal point of the initial study. Various techniques were used to study both reagents, such as Renishaw-Raman spectroscopy, IR spectroscopy and inelastic neutron spectroscopy as well as DSC and high-resolution neutron diffraction. Results obtained displayed the structural effects of differing temperatures on both reagents with nitrosonium tetrafluoroborate exhibiting interesting behaviour upon cooling. A paper later in the year will be published on this initial study.[26]

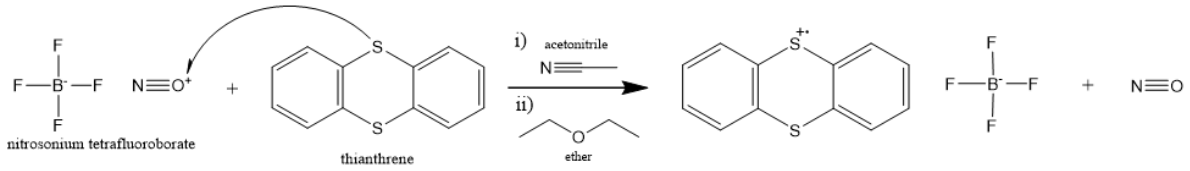

Figure 63: Reaction scheme for the production of thianthrene cation radical tetrafluoroborate from the thianthrene. [26]

Acknowledgements

I would like to thank Dr Mona Sarter, Dr. Victoria Garcia Sakai, and Dr. Ian Silverwood for the opportunity to work on this project with many thanks to Mona for her supervision and advice throughout the year. I would also like to thank the support teams at ISIS for their assistance during the project especially the Cryogenics, Computational and Electronics teams with appreciation to Max Williams from the Electronics team. I also thank the laboratory teams with many thanks to James Taylor for his assistance, training, and support with the commercial DSC tests. Furthermore, many thanks to Dr. Stewart Parker for his

supervision throughout the side project and to Matei Pascariu for his support throughout both projects. Finally, I thank my university supervisor, Dr. Timothy Prior, for his support and advice throughout my placement year.

References

[1] S. Postorino, “Tests and Development of an in situ Calorimeter for IRIS,” Science and Technology Facilities Council, 2018.

[2] J. Ponsonby, “In-situ calorimetry with Quasi-Elastic Neutron Spectroscopy: realising a complimentary dynamic and thermodynamic sample description,” 2019.

[3] C. Twigg, “Ex-Situ Calorimtery ISP 542 Prototype Solid Cell Review,” 2021.

[4] “About,” ISIS Neutron and Muon Source - UKRI, [Online]. Available: https://www.isis.stfc.ac.uk/Pages/About.aspx. [Accessed 04 06 2023].

[5] “ISIS Materials Characterisation Laboratory - UKRI,” Science and Technologies Facilities Council, [Online]. Available: https://www.isis.stfc.ac.uk/Pages/Differential-Scanning-Calorimetry.aspx. [Accessed 04 07 2023].

[6] “ISIS Iris - UKRI,” ISIS, STFC, UKRI, [Online]. Available: https://www.isis.stfc.ac.uk/Pages/iris.aspx. [Accessed 28 10 2022].

[7] V. G. S. S. P. I. S. C. G. J. B. O. K. F. F.-A. D. Fornalski, “Simultaneous thermodynamic and dynamical characterisation using in situ calorimetry with neutron spectroscopy,” *Low,* vol. 45, no. 3, pp. 289-293, 2019.

[8] R. Rushworth, “In-Situ Calorimeter Manual,” 2023.

[9] ISIS Experiment Controls, “ISIS IBEX - UKRI,” Science and Technology Facilities Council, [Online]. Available: https://www.isis.stfc.ac.uk/Pages/IBEX.aspx. [Accessed 04 07 2023].

[10] “Thermal Analysis Software,” Mettler Toledo , [Online]. Available: https://www.mt.com/us/en/home/products/Laboratory_Analytics_Browse/TA_Family_Browse/TA_software_browse.html. [Accessed 05 07 2023].

[11] Mettler Toledo, Thermal Analysis in Practice, Schwerzenbach, Switzerland, 2009.

[12] S. T. Beckett, M. G. Francesconi, P. M. Geary, G. Mackenzie and A. P. E. Maulny, “DSC Study of sucrose melting,” *Carbohydrate Research,* vol. 341, pp. 2591-2599, 2006.

[13] K. Jouppila and Y. H. Roos, “Glass Transitions and Crystallization in Milk Powders,” *Journal of Dairy Science,* vol. 77, no. 10, pp. 2907-2915, 1994.

[14] L. Wu, X. Miao, Z. Shan, Y. Huang, L. Li, X. Pan, Q. Yao, G. Li and C. Wu, “Studies on the spray dried lactose as carrier for dry powder inhalation,” *Asian Journal of Pharmaceutical Sciences,* vol. 9, no. 6, pp. 336-341, 2014.

[15] “PVC Measured by DSC and TGA,” Mettler Toledo, [Online]. Available: https://www.mt.com/in/en/home/supportive_content/matchar_apps/MatChar_HB220.html. [Accessed 16 03 2023].

[16] L. Valentini, S. B. Bon, M.-A. Lopez-Manvhado, L. Mussolin and N. Pugno, “Development of conductive paraffin/graphene films laminated on fluoroelastomers with high strain recovery and anti-corrosive properties,” *Composites Science and Technology,* vol. 149, pp. 254-261, 2017.

[17] Z. Rao and G. Q. Zhang, “Thermal Properties of Paraffin Wax-based Composites Containing Graphite,” *Energy Sources,* vol. 33, no. 7, pp. 587-593, 2011.

[18] “Properties of Solutions,” LibreTexts, [Online]. Available: https://chem.libretexts.org/Bookshelves/Introductory_Chemistry/Basics_of_General_Organic_and_Biological_Chemistry_(Ball_et_al.)/09%3A_Solutions/9.04%3A_Properties_of_Solutions. [Accessed 05 07 2023].

[19] L. Nichols, “Melting Point Theory,” LibreTexts, [Online]. Available: https://chem.libretexts.org/Bookshelves/Organic_Chemistry/Organic_Chemistry_Lab_Techniques_(Nichols)/06%3A_Miscellaneous_Techniques/6.01%3A_Melting_Point/6.1C%3A__Melting_Point_Theory. [Accessed 05 07 2023].

[20] “ICSC: 0078 - Toluene,” 10 2002. [Online]. Available: https://www.ilo.org/dyn/icsc/showcard.display?p_version=2&p_card_id=0078. [Accessed 30 06 2023].

[21] A. O. Owoade, A. Adetutu and O. S. Olorunnisola, “A review of chemical constituents and pharmacological properties of Hibiscus sabdariffa L.,” *International Journal of Current Research in Biosciences and Plant Biology,* vol. 6, no. 4, pp. 42-51, 2019.

[22] B. L. Koop, M. Nascimento da Silva , F. Diniz da Silva, K. Thayres dos Santos Lima, L. S. Soares, C. Jose de Andrade, G. A. Valencia and A. R. Monteiro, “Flavonoids, anthocyanins, betalains, curcumin, and carotenoids: Sources, classification and enhanced stabilization by encapsulation and adsorption,” *Food Research Intenational,* vol. 153, 2022.

[23] “Caffeine in Tea - Your Questions Answered,” Twinings, [Online]. Available: https://twinings.co.uk/blogs/news/caffeine-in-tea-your-questions-answered. [Accessed 05 07 2023].

[24] “ICSC 0057 - METHANOL - International Programme on Chemical Safety,” [Online]. Available: https://inchem.org/documents/icsc/icsc/eics0057.htm. [Accessed 08 07 2023].

[25] “Fructose- American Chemical Society,” American Chemical Society, 28 08 2017. [Online]. Available: https://www.acs.org/molecule-of-the-week/archive/f/fructose.html. [Accessed 07 07 2023].

[26] R. Rushworth, M. Pascariu and S. Parker, “A Study on the Production of the Thianthrene Cation Radical Tetrafluoroborate”.

[27] K. A. C. R. B. P. J. W. M. W. Z. G. Simperier A, “Glass Transition Temperature of Glucose, Sucrose, and Trehalose: An Experimental and in Silico Study,” *The Journal of Physical Chemistry,* vol. 110, no. 39, pp. 19678-19684, 2006.

[28] V. Truong, B. R. Bhandari, T. Howes and B. Adhikari, “Glass transition behaviour of fructose,” *International Journal of Food Science and Technology,* vol. 39, no. 5, pp. 569-578, 2004.

[29] A. Gombas, P. Szabo-Revesz, M. Kata and G. Regdon, “Quantitative Determination of Crystallinity of α-Lactose Monohydrate by DSC,” *Journal of Thermal Analysis and Calorimetry,* no. 68, pp. 503-510, 2002.

Appendix A – Extract from In-Situ DSC Manual

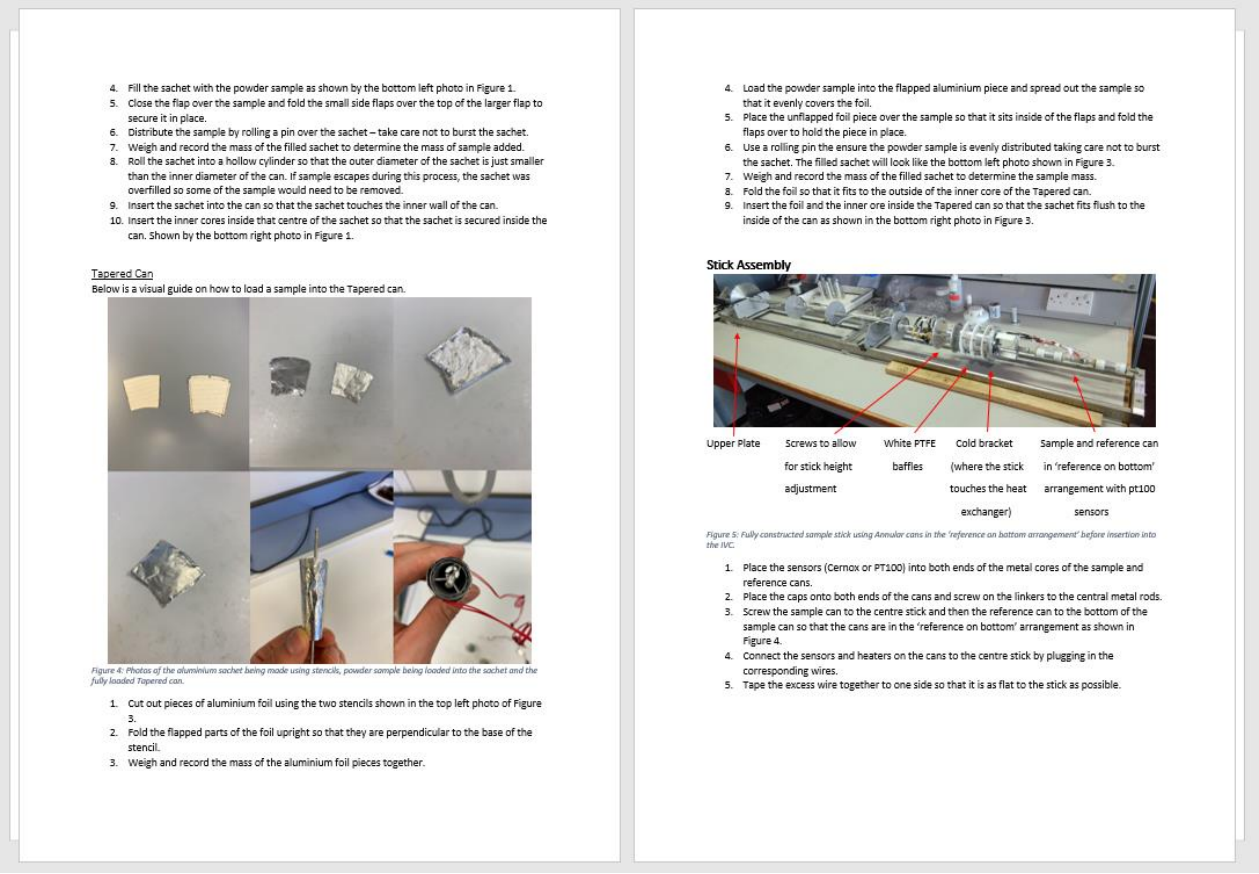

4. Fill the sachet with the powder sample as shown by the bottom left photo in Figure 1.
5. Close the flap over the sample and fold the small side flaps over the top of the larger flap to secure it in place.
6. Distribute the sample by rolling a pin over the sachet – take care not to burst the sachet.
7. Weigh and record the mass of the filled sachet to determine the mass of sample added.
8. Roll the sachet into a hollow cylinder so that the outer diameter of the sachet is just smaller than the inner diameter of the can. If sample escapes during this process, the sachet was overfilled so some of the sample would need to be removed.
9. Insert the sachet into the can so that the sachet touches the inner wall of the can.
10. Insert the inner cores inside that centre of the sachet so that the sachet is secured inside the can. Shown by the bottom right photo in Figure 1.

Tapered Can

Below is a visual guide on how to load a sample into the Tapered can.

Figure 4: Photos of the aluminium sachet being made using stencils, powder sample being loaded into the sachet and the fully loaded Tapered can.

1. Cut out pieces of aluminium foil using the two stencils shown in the top left photo of Figure 3.
2. Fold the flapped parts of the foil upright so that they are perpendicular to the base of the stencil.
3. Weigh and record the mass of the aluminium foil pieces together.
4. Load the powder sample into the flapped aluminium piece and spread out the sample so that it evenly covers the foil.
5. Place the unflapped foil piece over the sample so that it sits inside of the flaps and fold the flaps over to hold the piece in place.
6. Use a rolling pin the ensure the powder sample is evenly distributed taking care not to burst the sachet. The filled sachet will look like the bottom left photo shown in Figure 3.
7. Weigh and record the mass of the filled sachet to determine the sample mass.
8. Fold the foil so that it fits to the outside of the inner core of the Tapered can.
9. Insert the foil and the inner ore inside the Tapered can so that the sachet fits flush to the inside of the can as shown in the bottom right photo in Figure 3.

Stick Assembly

Upper Plate | Screws to allow for stick height adjustment | White PTFE baffles | Cold bracket (where the stick touches the heat exchanger) | Sample and reference can in ‘reference on bottom’ arrangement with pt100 sensors

Figure 5: Fully constructed sample stick using Aemular cans in the ‘reference on bottom arrangement’ before insertion into the IVC.

1. Place the sensors (Cernox or PT100) into both ends of the metal cores of the sample and reference cans.
2. Place the caps onto both ends of the cans and screw on the linkers to the central metal rods.
3. Screw the sample can to the centre stick and then the reference can to the bottom of the sample can so that the cans are in the ‘reference on bottom’ arrangement as shown in Figure 4.
4. Connect the sensors and heaters on the cans to the centre stick by plugging in the corresponding wires.
5. Tape the excess wire together to one side so that it is as flat to the stick as possible.

Figure 64: An extract from the In-Situ DSC Manual, which was written after the Powder DSC Can Testing, showing instructions on the loading of the tapered can and the assembly of the cans onto the sample stick.

Appendix B – Commercial DSC Heat-Cool Cycles

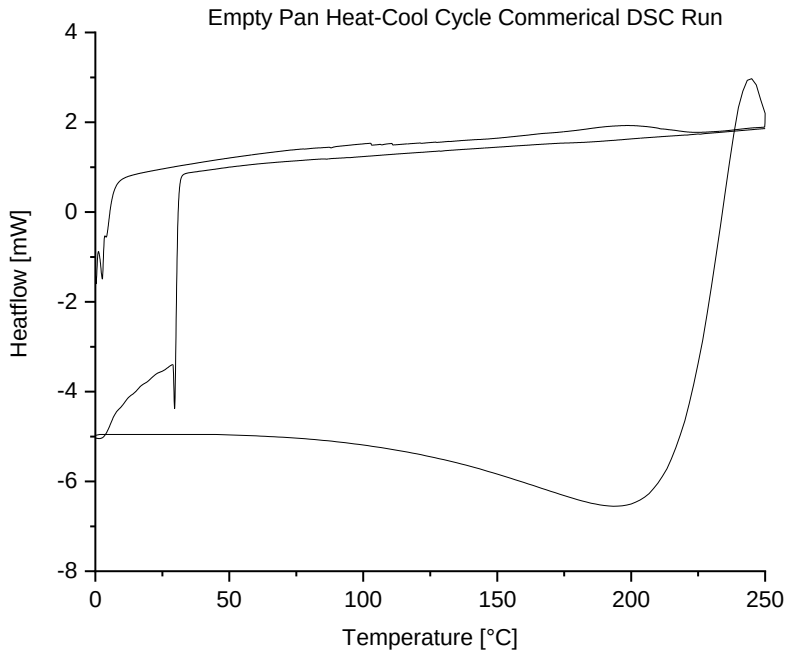

Figure 65: Commercial DSC results for an empty sample pan using the Mettler Toledo DSC1. The first dynamic segment was set to a temperature range of 273 to 723 K with a ramping rate of 5 K/min. The second dynamic segment was set to a temperature range of 723 to 273 K at a rate of 100 K/min. The last dynamic segment was set to a temperature range of 273 to 273 K at 5 K /min.

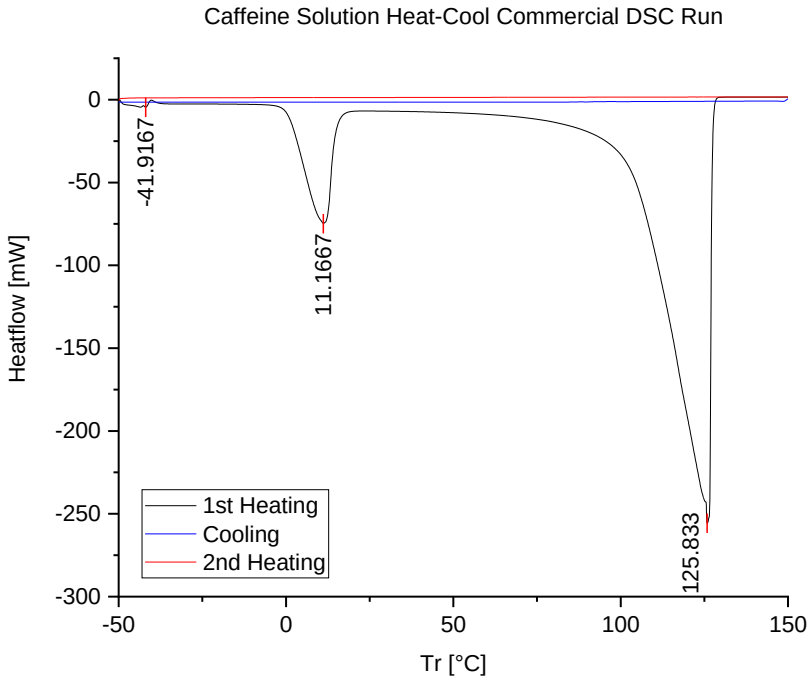

Figure 66: Commercial DSC1 caffeine solution results from 223 to 423 K using a rate of 5 K/min showing a melt at 284.17 ± 0.25 K and boiling at 398.83 ± 0.25 K .

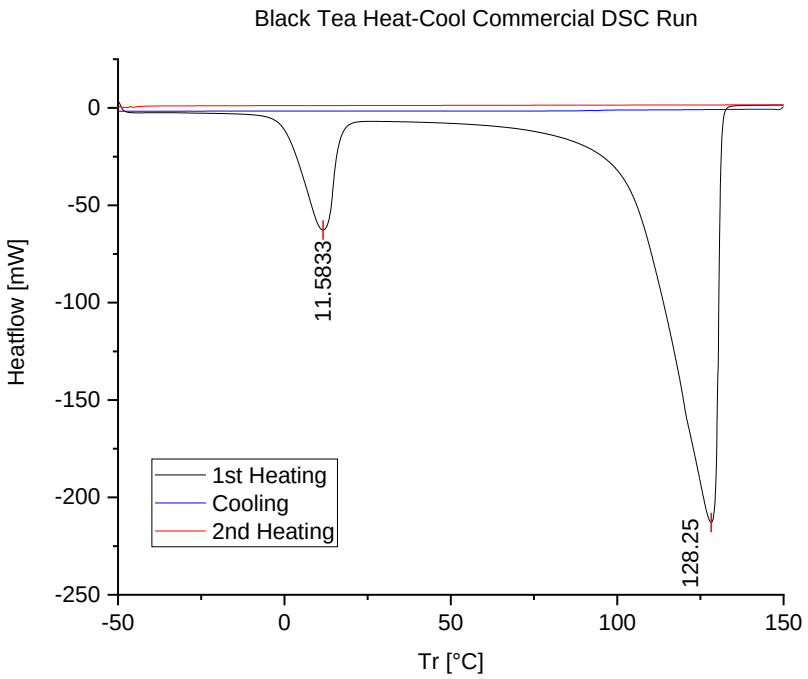

Figure 67: Commercial DSC black tea solution results using the Mettler Toledo DSC1. Data were collected in the temperature range 223 to 423 K using a heating rate of 5 K/min and shows water melting at 284.58 ± 0.25 K and boiling at 401.25 ± 0.25 K .

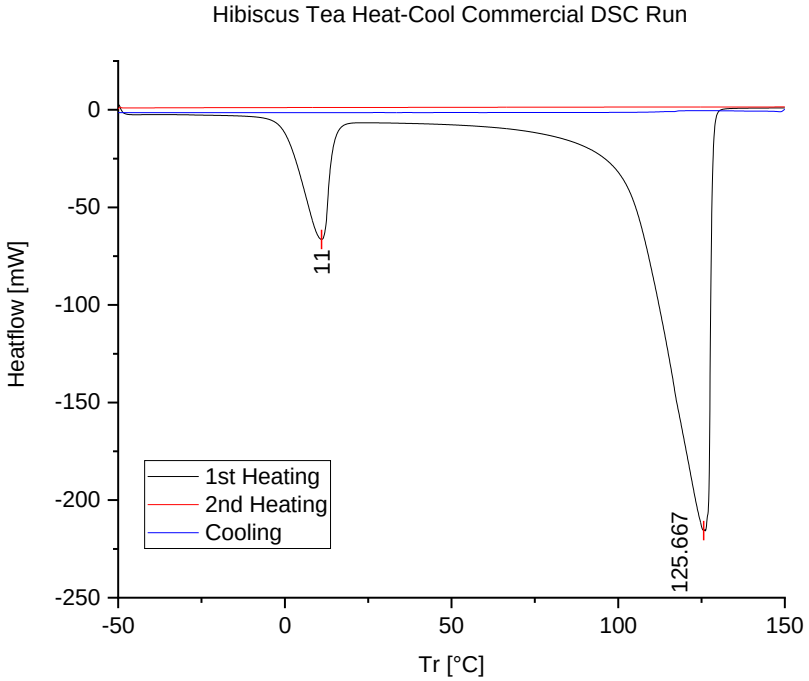

Figure 68: Commercial DSC hibiscus tea solution results using the Mettler Toledo DSC1. Data were collected in the temperature range 223 to 423 K using a heating rate of 5 K/min and shows water melting at 284.00 ± 0.25 K and boiling at 398.67 ± 0.25 K .

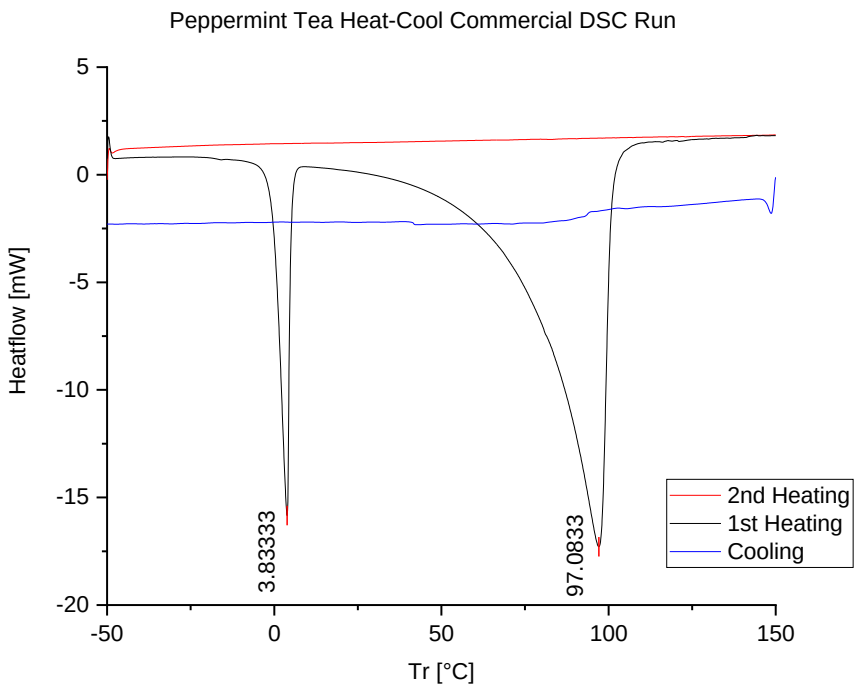

Figure 69: Commercial DSC peppermint tea solution results using the Mettler Toledo DSC1. Data were collected in the temperature range 223 to 423 K using a heating rate of 5 K/min and shows water melting at 276.83 ± 0.25 K and boiling at 370.08 ± 0.25 K.

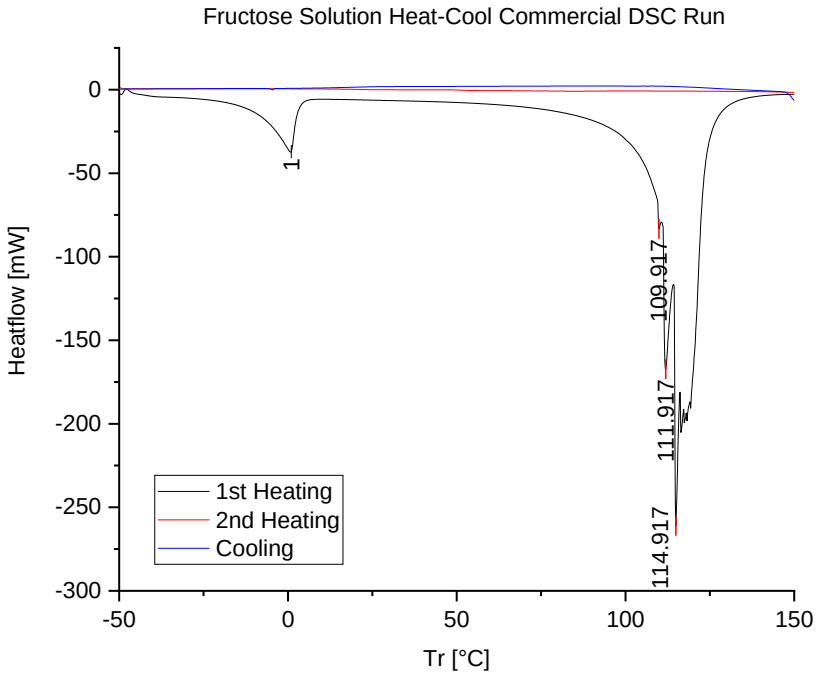

Figure 70: Commercial DSC fructose solution results using the Mettler Toledo DSC1. Data were collected in the temperature range 223 to 423 K using a heating rate of 5 K/min and shows water melting at 274.00 ± 0.25 K and boiling at 382.00 ± 0.25 K . Extra peaks are caused by melting fructose around 388 K.

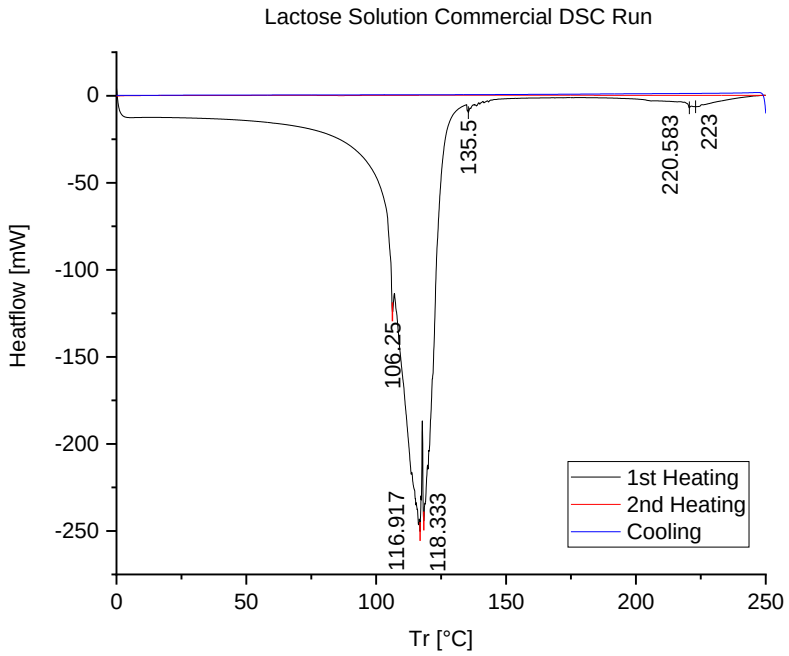

Figure 71: Commercial DSC lactose solution results using the Mettler Toledo DSC1. Data were collected in the temperature range 223 to 423 K using a heating rate of 5 K/min and shows water melting at 278.75 ± 0.25 K and boiling around 394.50 ± 0.25 K . Extra peaks are caused by lactose melting at 402.00 ± 0.25 K.

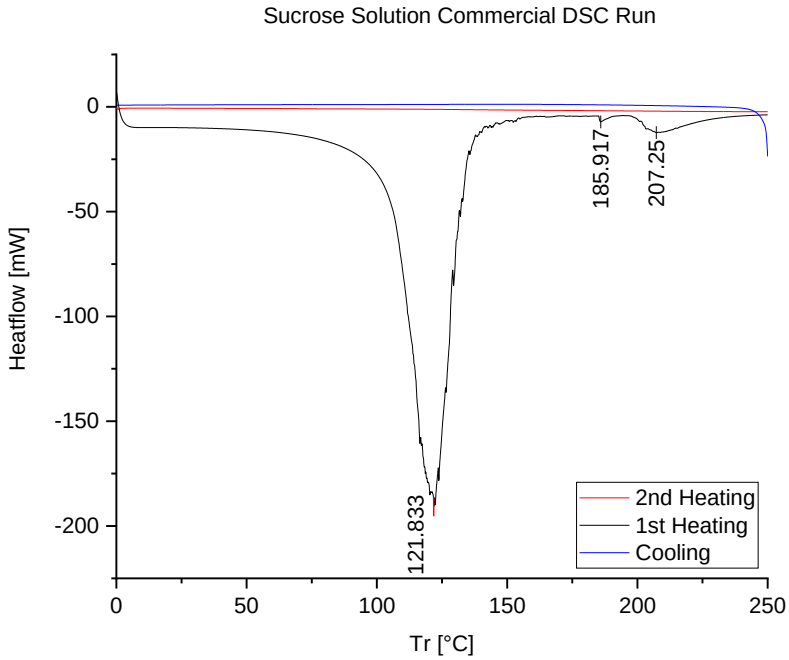

Figure 72: Commercial DSC sucrose solution results using the Mettler Toledo DSC1. Data were collected in the temperature range 223 to 423 K using a heating rate of 5 K/min and shows water melting at 273.83 ± 0.25 K and boiling around 428.83 ± 0.25 K . Extra peaks are caused by melting sucrose from 395.917 to 404.250 K.

Appendix C – Empty Tapered Can Results with O-ring Seal

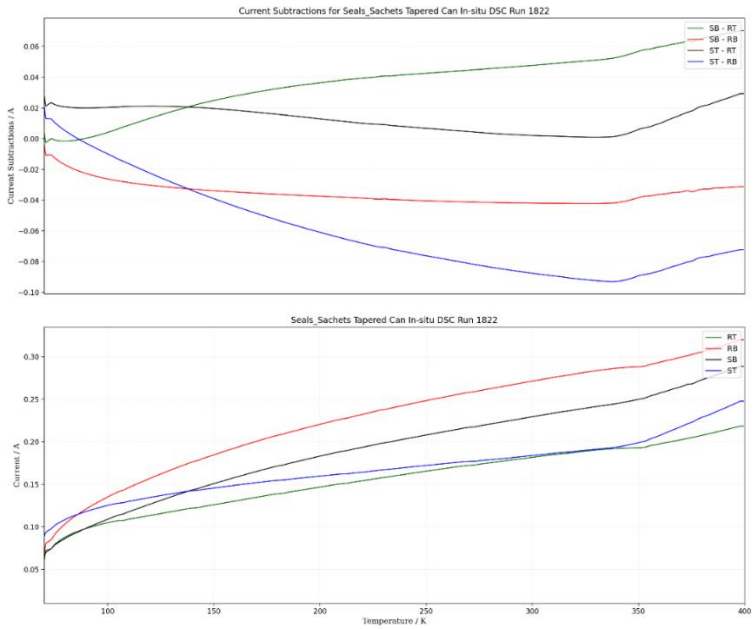

Figure 73: Results from the ex-situ calorimeter setup testing of the tapered cans containing just seals and empty sachets with the wider side down and using high heater output. The run was from 70 - 400 K at 5 K/min with a CCR offset of 15 K.

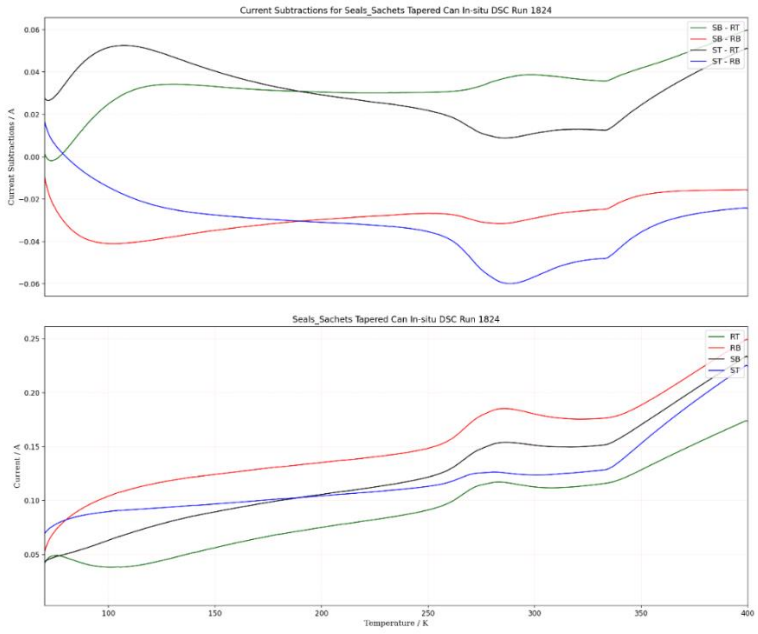

Figure 74: Results from the ex-situ calorimeter setup testing of the tapered cans containing just seals and empty sachets with the wider side down and using high heater output. The run was from 70 - 400 K at 1 K/min with a CCR offset of 15 K.

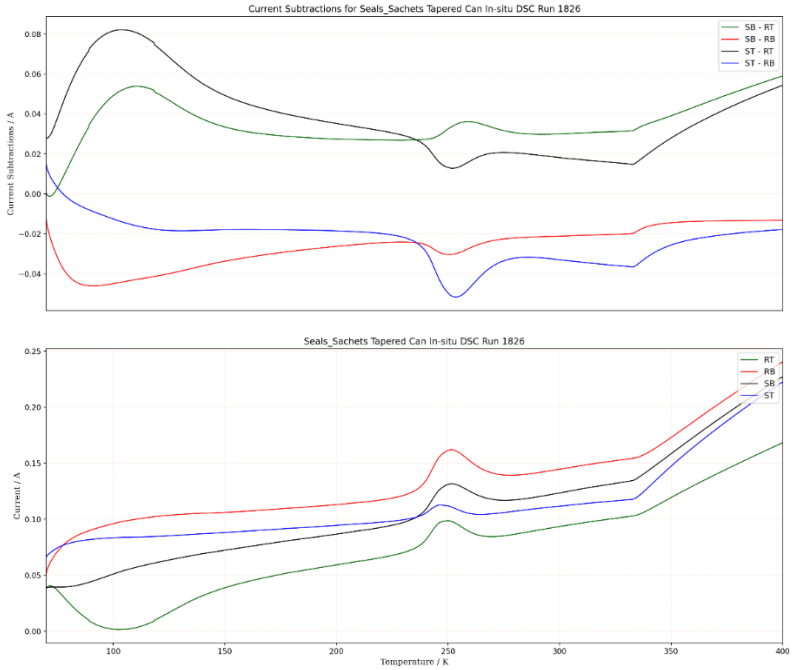

Figure 75: Results from the ex-situ calorimeter setup testing of the tapered cans containing just seals and empty sachets with the wider side down and using high heater output. The run was from 70 - 400 K at 0.5 K/min with a CCR offset of 15 K.

Appendix D – Log Purges

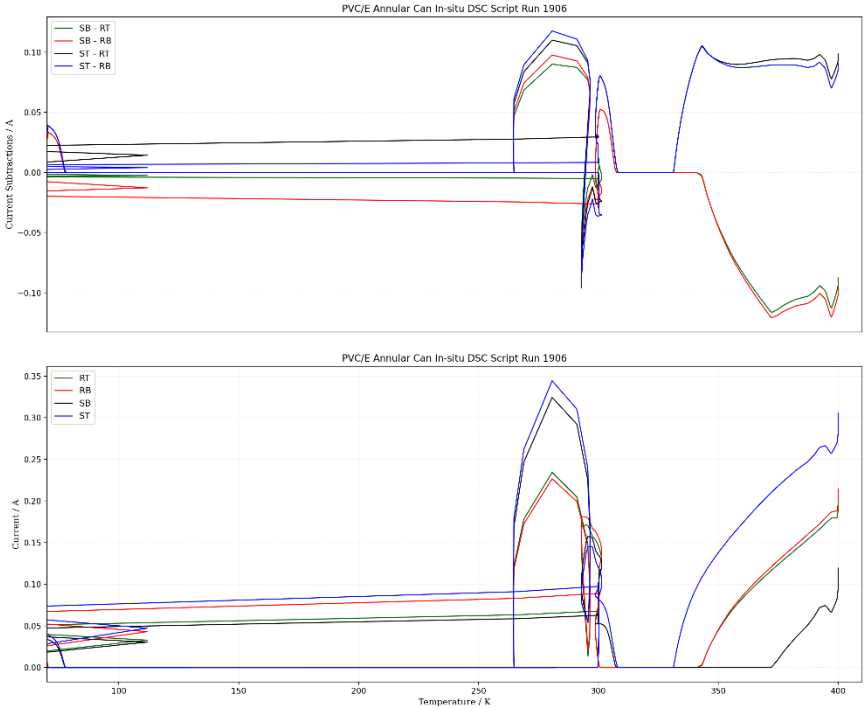

Figure 76: Results from the ex-situ calorimeter setup testing of the annular cans containing PVC after moving the heaters to the centre of the can. The log purge was from 400 - 70 K at 5 K/min with a CCR offset of 10 K and high heater output.

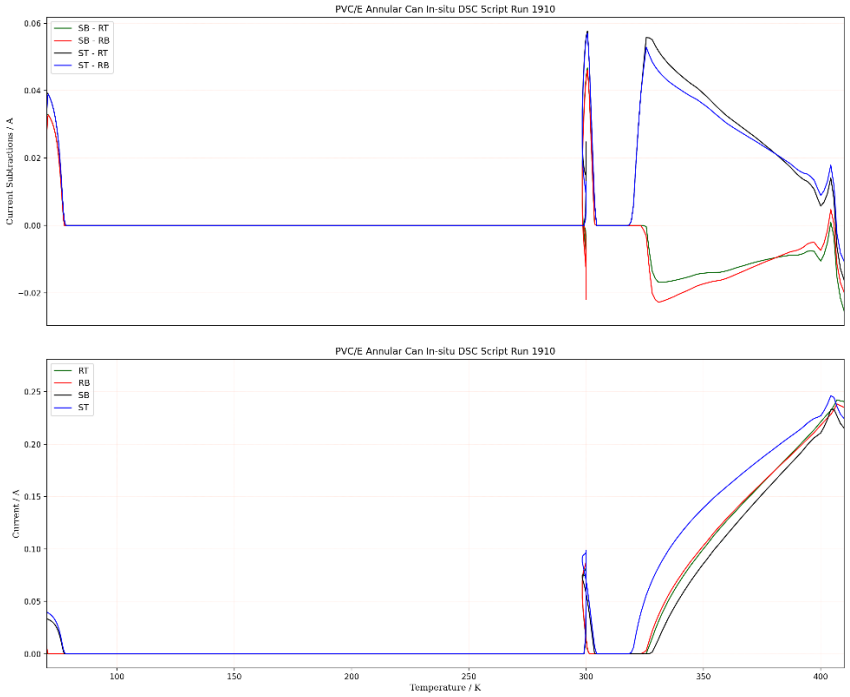

Figure 77: Results from the ex-situ calorimeter setup testing of the annular cans containing PVC after moving the heaters to the centre of the can. The log purge was from 410 - 70 K at 5 K/min with a CCR offset of 10 K and high heater output. The wait time ('g.waitfor (minutes='), as seen in Appendix E, was changed from 20 to 2 minutes. However, this had no effect when compared to the previous log purge, Figure 47.

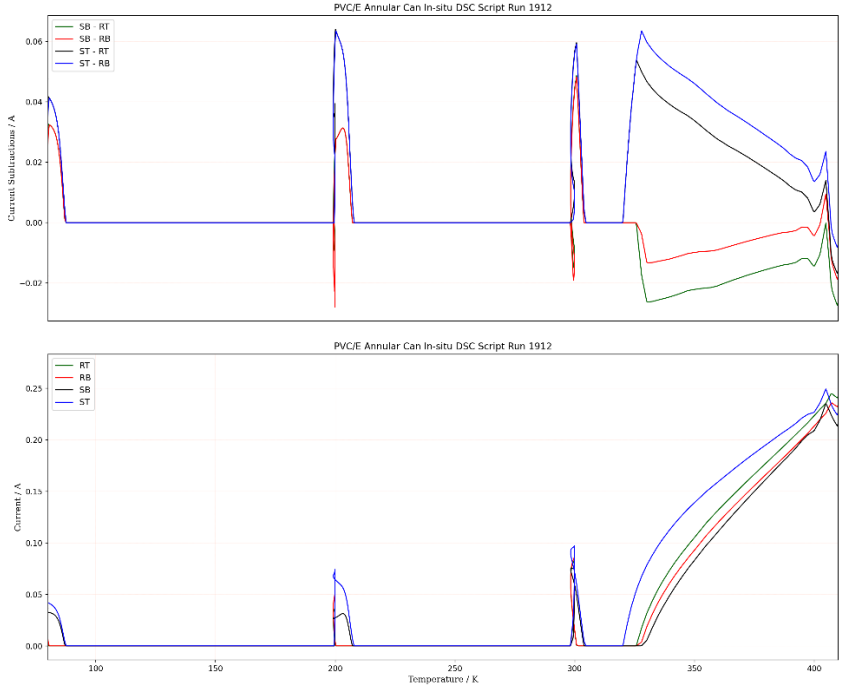

Figure 78: Results from the ex-situ calorimeter setup testing of the annular cans containing PVC after moving the heaters to the centre of the can. The log purge was from 410 - 70 K at 5 K/min with a CCR offset of 10 K and high heater output. The heater temperature ('setall_temp (300, 290)' and 'waitall_temp (300, 290, 2)'), as seen in Appendix E, was changed from 300 to 200 K. However, this produced an additional peak around 200 K.

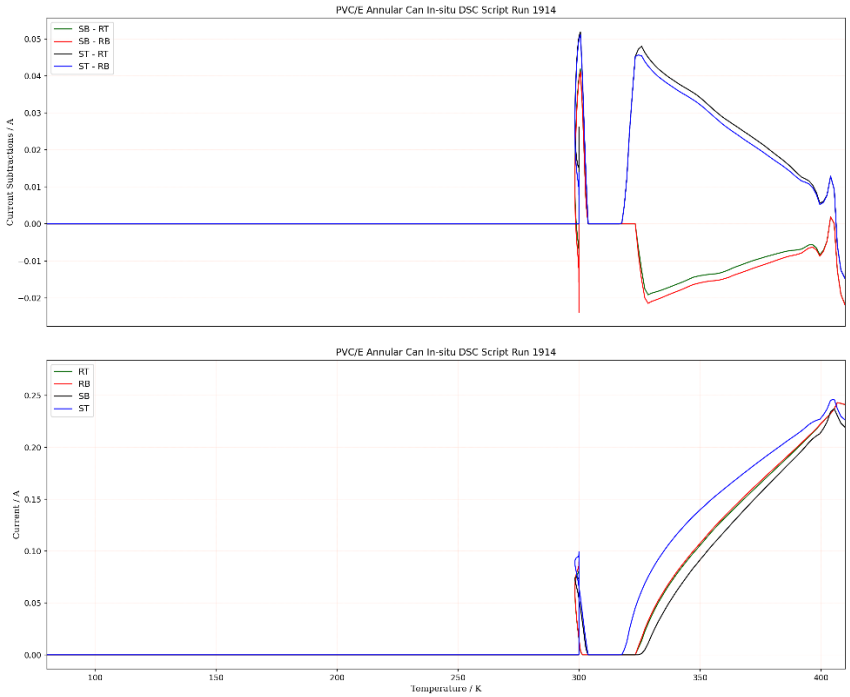

Figure 79: Results from the ex-situ calorimeter setup testing of the annular cans containing PVC after moving the heaters to the centre of the can. The log purge was from 410 - 70 K at 5 K/min with a CCR offset of 10 K and high heater output. The heater temperature was set back to 300 K and CCR temperature ('setall_temp (300, 290)' and 'waitall_temp (300, 290, 2)'), as seen in Appendix E, was changed from 290 to 250 K. However, this again had no effect. The peak at 70 K is no longer present but this cannot be linked to any adaptions of the script.

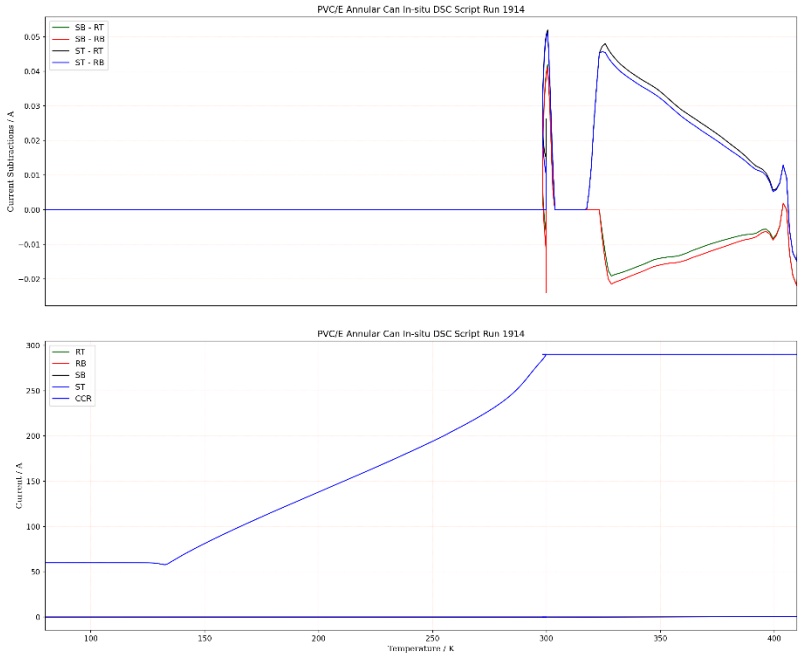

Figure 80: Result from changing the heater temperature from 400 K to 410 K, Figure 79, with the CCR plotted to show the CCR cooling.

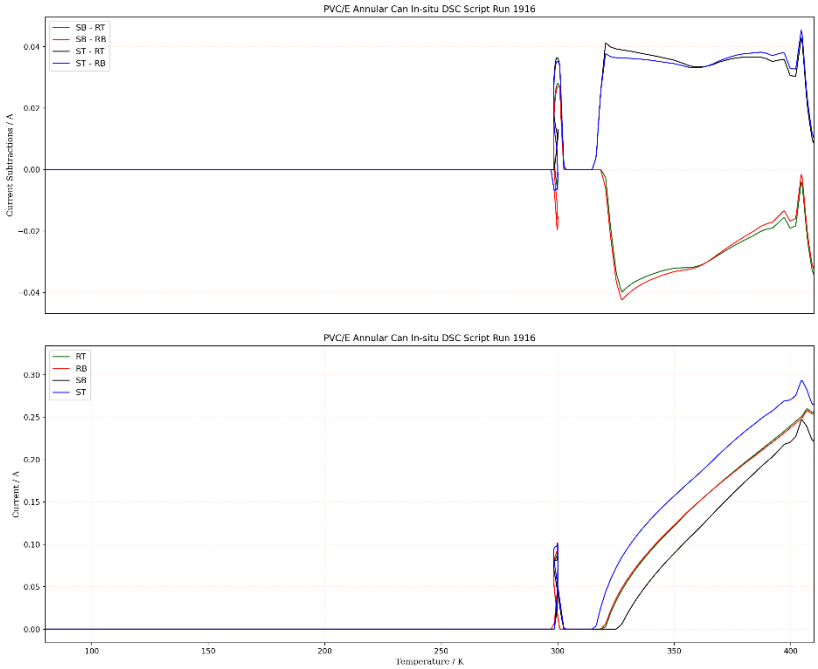

Figure 81: Results from the ex-situ calorimeter setup testing of the annular cans containing PVC after moving the heaters to the centre of the can. The log purge was from 410 - 70 K at 5 K/min with a CCR offset of 10 K and high heater output. The wait time ('g.waitfor (minutes='), as seen *in Appendix E, was changed from 20 to 40 minutes and the cooling rate was increased from 5 to 0.5 K/min. However, this had little effect.*

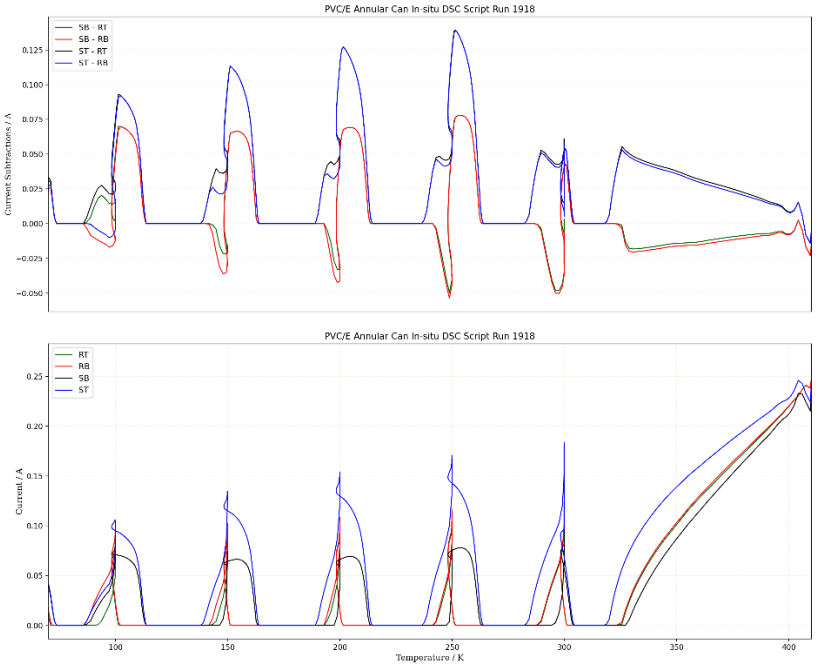

Figure 82: Results from the ex-situ calorimeter setup testing of the annular cans containing PVC after moving the heaters to the centre of the can. The log purge was from 410 - 70 K at 5 K/min with a CCR offset of 10 K and high heater output. The heater temperature ('setall_temp (300, 290)' and 'waitall_temp (300, 290, 2)'), as seen *in Appendix E, was set to temperatures decreasing by 50 K and the CCR was set to be 50 K cooler than the heaters. However, this produced peaks at each set temperature. Notably, the height of each peak decreases as the temperature decreases.*

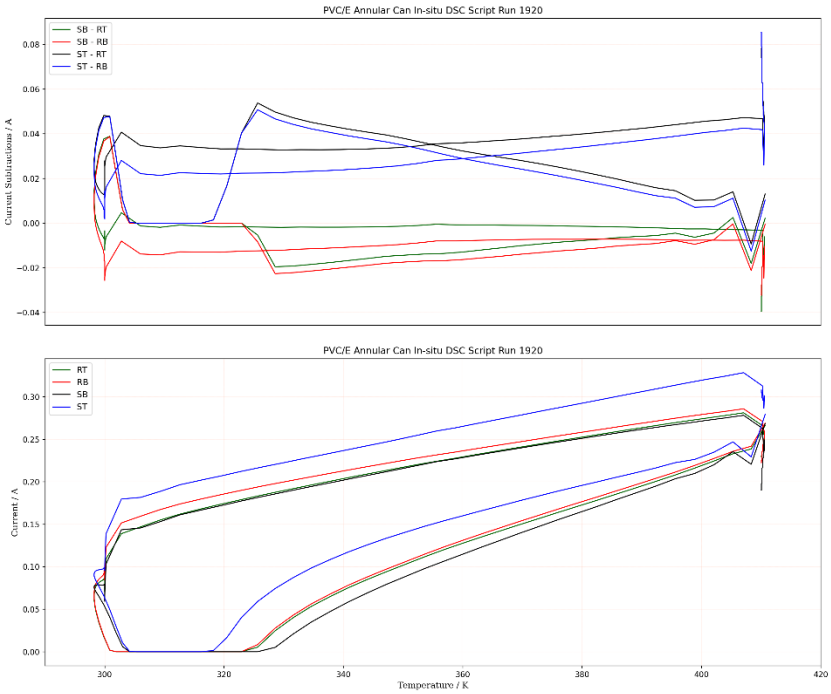

Figure 83: Results from the ex-situ calorimeter setup testing of the annular cans containing PVC after moving the heaters to the centre of the can. The log purge was from 410 - 70 K at 5 K/min with a CCR offset of 10 K and high heater output. The heater temperatures ('setall_temp (300, 290)' and 'waitall_temp (300, 290, 2)'), as seen in Appendix E, were swapped so that 300 K was set to 40K and vice versa. This resulted in no peaks but inconclusive data.

Appendix E – Scripting

```
    g.begin()
    g.change(title="%s %s K/min" % (sample_name1, rate1))
    while g.cget('Sample_top')['value'] < temp1:
        sleep(1)
    setall_ramp(rate2, ccrrate2)
    setall_temp(temp2, ccrtemp2)
    while g.cget('Sample_top')['value'] < temp2:
        sleep(1)

    g.end()

def prelim_checks():
    setall_ramp(10,10)


def go(Heater_rate,Ccr_rate,Heater_output):
    setall_heater(Heater_output)

    #Toluene/Empty / Liquid can (5)

    setall_ramp(5, 5)
    setall_temp(300, 290)
    waitall_temp(300, 290, 2)
    g.waitfor(minutes=20)

    # Set all can heater temperatures to same, CCR temp not optional
    setall_ramp(100, 100)
    setall_temp(40,30)

    # Wait for all temperatures to be in range, (cans, CCR, range +/-)
    waitall_temp(40, 30, 2)

    #inst.IEG('Pump')
    g.waitfor(minutes=40)

    # Run to temperature, heating rate (ccrtemp + ccr rate)
    smplnm="Toluene/Liquid can/He/Pt100/Ref on bot/"
    calorrun(smplnm, temp=300, ccrtemp=290, rate=Heater_rate, ccrrate=Ccr_rate,Heater_output=Heater_output)

    setall_ramp(5,5)
    setall_temp(300,290)
#go(1,1,'Medium')
#go(5,5,'Medium')
#go(10,10,'Medium')
#go(1,1,'High')
go(5,5,'High')
go(1,1,'High')
```

Figure 84: The script, 'Joel_High_Temp.py', used to run tests with the in-situ DSC. Here the experimental parameters for the toluene run are shown.